AN INVESTIGATION OF HIGH VELOCITY FLASHING FLOW IN A STRAIGHT TUBE

by

JOHN WILSON MURDOCK

S.B., MASSACHUSETTS INSTITUTE OF TECHNOLOGY
(1964)

S.M., MASSACHUSETTS INSTITUTE OF TECHNOLOGY
(1964)

MECH. ENGR., MASSACHUSETTS INSTITUTE OF TECHNOLOGY
(1965)

SUBMITTED IN PARTIAL FULFILLMENT

OF THE REQUIREMENTS FOR THE

DEGREE OF

DOCTOR OF SCIENCE

at the

MASSACHUSETTS INSTITUTE OF TECHNOLOGY

JANUARY, 1967

Signature of Author .....
Department of Mechanical Engineering, January 9, 1967

Certified by .....
Thesis Supervisor

Accepted By .....
Chairman, Departmental Committee on Graduate Students

ABSTRACT

AN INVESTIGATION OF HIGH VELOCITY FLASHING FLOW

IN A STRAIGHT TUBE

by John Wilson Murdock

Submitted to the Department of Mechanical Engineering
January 1967, in partial fulfillment of the requirements
for the degree of Doctor of Science

A study of high-velocity flashing flow in a straight tube has been made in order to obtain further understanding of this two-phase flow and also the subsequent choking which occurs if the downstream pressure is low enough.

A one-dimensional slip model which includes non-equilibrium effects is proposed. This model predicts the choking pressure with the upstream single-phase flow conditions as the only inputs. The model is extended to predict the pressure distribution in the two-phase region in terms of an interphase heat transfer coefficient.

The experimental data were obtained using Freon 114 ($Cl_2F_4C_2$) as a working fluid in a closed flow loop. The test section was a 0.259 inch diameter stainless steel section with a 90° acrylic plastic sector inserted for viewing the two-phase flow. The two-phase flow region was about 1/4 inch long under choked conditions with liquid velocities at the flash point being about 200 ft/sec.

Thesis Supervisor

George A. Brown
Associate Professor of Mechanical Engineering

ACKNOWLEDGEMENTS

This thesis was supervised by Professor George A. Brown. I wish to thank him for his help and encouragement throughout the duration of this project.

Professors A. H. Shapiro and S. W. Gouse served on the thesis committee. I wish to thank them both for their valuable suggestions.

I wish to thank my wife, Sandra, for her support and encouragement. She typed the rough draft and did much of the proof reading.

This work was done in part at the Computation Center at the Massachusetts Institute of Technology.

The research program was supported by the Massachusetts Institute of Technology Solar Energy Committee.

TABLE OF CONTENTS

LIST OF FIGURES

List of Figures (continued)

LIST OF TABLES

NOMENCLATURE

A	Area
c	Specific heat
C_p	Pressure coefficient
D	Tube diameter
G	Mass flow per unit area
h	With subscript, specific enthalpy; without subscript, heat transfer coefficient
h^o	Total specific enthalpy
k	Thermal conductivity
K	Slip ratio (Vapor velocity divided by liquid velocity)
L	Tube length
Nu	Nusselt number
P	Pressure
Pr	Prandtl Number
q	Heat flow rate
r	Radial independent variable
R	Bubble radius, Liquid core radius with subscript ℓ
Rey	Reynolds Number
s	Specific entropy
t	Temperature (°F), Time
T	Absolute Temperature
v	Radial velocity, Specific volume
V	Axial Velocity
$\overline{V}$	Volume
x	Axial position in flow direction
X	Mass flow fraction

Nomenclature (continued)

y	Axial position opposite flow direction
α	Thermal diffusivity
γ	Temperature difference defined by Equation A-13
δ	Thermal boundary layer thickness
μ	Viscosity
ν	Kinematic viscosity
ρ	Density
σ	Surface tension

Subscripts

c	Choked condition
eff	Effective value
fg	Change from vapor to liquid state
g	Gas phase
h	Refers to heat transfer area
i	Refers to artificial initial pressure
ℓ	Liquid phase
o	Reference value
p	Constant pressure
rel	Refers to relative velocity
s	Saturation condition
∞	Reference value
1-16	Refers to pressure tap number

Chapter I

INTRODUCTION

The condensing ejector is a device which has been the object of considerable research in the recent past. The condensing ejector is essentially a two-phase jet pump in which one of the entering streams is a liquid and the other a vapor. Both streams are accelerated in separate nozzle passages to a lower pressure at the entrance to a mixing section. After the streams are mixed, the flow enters a diffuser to recover the dynamic pressure. Since the thermodynamic availability of the inlet vapor stream is much higher than that of the inlet liquid stream, it is possible to produce a significant pressure rise across the condensing ejector. In fact, operation is possible where the exit pressure is higher than either inlet stagnation pressure. Conditions also exist for which a temperature rise occurs across the device with an outlet state whose temperature is higher than either inlet stagnation temperature.

Because of these somewhat unusual characteristics---at least for a no moving parts device---the condensing ejector has been proposed for use in various thermodynamic cycles. A specific example is in the field of desalination of water. One of the standard methods for converting salt water to fresh water is the vapor compression distillation process in which fresh water vapor is put through a compressor to increase its temperature and pressure. The vapor is then circulated through a heat exchanger in which heat is transferred

back to a boiling mass of salt water in a regenerative system. A new system has been proposed in which the condensing ejector substitutes for the vapor compressor. A second type of desalination system using the condensing ejector is based upon a direct contact freezing configuration where the condensing ejector replaces the vapor compressor in a refrigeration system. The attractiveness of the condensing ejector systems rests on the fact that the overall desalination process can be tailored to receive either a heat or a work input. Of particular interest to the sponsors of the project, the M.I.T. Solar Energy Committee, is the fact that this heat input could be a solar energy input.

In the operation of the condensing ejector both a liquid and a vapor stream are accelerated through appropriate nozzles into the mixing section. It would be desirable to match pressure, velocity, and temperature simultaneously, if possible, in order to minimize thermodynamic irreversibilities. Under many of the proposed operating conditions this match requires the liquid to be accelerated into the two-phase region. This acceleration requires a convergent-divergent nozzle. This nozzle flow process is qualitatively very similar to gas flow in a convergent-divergent nozzle in that at low enough back pressures choking occurs at the throat and shock-like phenomena are possible in the divergent section. Although adequate models exist for the prediction of gas nozzle flows, none are available for predicting the performance of a two-phase nozzle or even for giving a completely satisfactory explanation of the two-phase choking process. This investigation began with the aim of

studying the acceleration of a high velocity flashing liquid in a convergent-divergent nozzle. Some of the specific problem areas were the initial nucleation of the vapor phase, the mechanism for the choking of the flow, and the expansion of the two-phase flow in the divergent section. Consideration of all these problems was not possible in a single investigation. The scope was eventually narrowed down to a study primarily of the mechanism of choking in the limiting case of a convergent nozzle -- that is a straight tube.

Initial Studies on Nozzles

Preliminary studies of the nozzle flow process were made with water as a working fluid using a transparent plastic, convergent-divergent nozzle. This nozzle had straight cones for convergent and divergent passages with a rounded throat between the two passages. (See Figure 1) The nozzle throat had a nominal diameter of 1/4 inch. A typical upstream liquid stagnation pressure was 500 psia. Using Bernoulli's equation and assuming saturation pressure at the point of flashing gives 250 ft/sec as a typical liquid velocity. Assuming that flashing takes place very near the throat (which is a very good assumption at these high liquid velocities), the flow rate may be calculated to be about 50 gal/min. These numbers are representative of the conditions throughout this entire investigation.

Studies with water showed that flashing first occurred less than a tenth of an inch upstream of the geometric throat. Choking did take place and shock-like phenomena were present in the divergent section at high enough back pressures. Downstream of the shock

region the flow was single-phase liquid at stagnation pressures of the order of 50 psia compared to the 500 psia upstream. The pressure dropped from the throat pressure in the divergent section. Thus the tests on water showed all the qualitative features that were expected from this type of convergent-divergent nozzle. The water nozzle did have some difficiencies from an experimental standpoint. The maximum and minimum water temperature was fixed by the steam and city water available in the laboratory. Thus the maximum water stagnation temperature is about 200°F. This means that all the pressures in the two-phase region are subatmospheric. Secondly and perhaps more important, the slope of the saturation line in this region is such that small pressure changes imply large temperature changes. Thus pressure measurements are difficult to make and a high degree of accuracy is required as a consequence. The amount of liquid superheat at the point where flashing first occurs may be determined from a measured pressure distribution and a visual observation of the flash point. This is difficult to do if dP/dT is small.

To get around these difficulties it is possible to use water at higher temperatures or use a different fluid at the same temperature. To avoid the expense of a large boiler, Freon 114 ($F_4Cl_2C_2$) was adopted as a working fluid. Early tests run with the Freon 114 showed the same general characteristics as that of water, that is choking, flashing just upstream of the throat, and the appearance of a shock-like phenomena in the divergent section. A crucial experimental parameter needed to understand choking is the throat pressure. The rather abrupt throat in the first nozzle (see Figure 1) gave rise to

some questions about the accuracy of the measurements. The rapid area change in this region could result in non one-dimensional flow effects due to streamline curvature. The pressure gradient is very high due to the rapid acceleration of the pure liquid phase and is even higher due to the two-phase choking. To eliminate the uncertainty associated with positioning a pressure tap exactly at the throat and the uncertainty resulting from an expected finite pressure change in a distance the order of the pressure tap diameter (0.040 inches), a nozzle with a much longer throat region was constructed from acrylic plastic. (See Figure 1).

When experiments were performed with this nozzle the measured throat pressure was found to be as much as 15 psi above the saturation pressure corresponding to the upstream temperature. Visual observations of these flows showed the two-phase region started about 1/4 inch upstream of the throat. It is impossible for a liquid undergoing a pressure drop at very nearly constant temperature to flash until the saturation pressure is reached. (The flashing may occur at a pressure below the saturation pressure, however.) Variation of the pressure tap hole size tended to confirm that a pressure measuring error existed and that this was associated with the pressure tap geometry. Some typical results for the second nozzle are given in the following table for Freon 114.

Table 1

Nozzle Throat Pressure Measurements With Different Size Pressure Taps

Pressure Tap Diameter (Inches)					Saturation Pressure
0.040	0.0292	0.020	0.0125✓	0.0125✓	
44.9*	29.9	20.6	33.7	34.1	40.3
54.8	40.1	30.2	43.9	44.5	37.6
64.0	48.9	38.0	52.8	53.9	47.8

*All pressures in psig

✓Both taps at throat location

The above results were somewhat discouraging in that there seemed to be no way to determine which pressure reading was the "correct" one. However, the highest pressure (0.040" tap) can be ruled out as impossible for the reasons cited above. The nozzle was run at a high enough pressure to maintain single-phase flow throughout the nozzle and the pressure differences between the various size taps remained about the same as shown in Table 1. Thus it was concluded that the pressure error was due primarily to geometric effects and not to flow regime. Shaw (1)* made a careful study of pressure tap error in straight tubes with fully developed turbulent flow and found the measured

---

*Numbers in parentheses refer to items in the Bibliography

pressure to be above the true pressures in practically all cases. This is in agreement with the 0.040" pressure tap in the nozzle, which was known to have a positive error. (A positive error exists when the measured pressure is greater than the true pressure.) Assuming all the taps in the above table have positive errors, then the 0.020" tap is best but still has an unknown error. Because of this problem it seemed necessary to go to a geometry in which the pressure error could be calibrated at least in the single-phase region or nothing at all could be learned about the two-phase flow. The eventual solution was to consider the choking problem in a long straight tube. Pressure taps in a straight tube may be calibrated by running tests in the single-phase region, measuring the back pressure, and using the fully developed turbulent flow pressure drop to determine the true pressure at some upstream point. The single-phase pressure tap calibration and subsequent experimental and theoretical study of two-phase flow in a straight tube turned out to be sufficiently complicated to necessitate leaving a study of the overall two-phase nozzle flow as future work.

Chapter 2

THEORETICAL MODEL FOR TWO-PHASE CHOKING IN A STRAIGHT TUBE

Consider the problem of the fully developed flow of a liquid in a straight tube. The pressure decreases along the tube due to the effects of wall friction. If the back pressure is lowered then eventually the saturation pressure of the liquid will be reached at the exit plane of the tube. A further decrease in the back pressure will produce nucleation of vapor bubbles at or below the saturation pressure at some point near the end of the tube and a two-phase flow will then exist between the nucleation point and the tube exit plane. Downstream of the nucleation point the pressure drops and the back pressure and the pressure in the tube exit plane are equal. Although the back pressure can be lowered indefinitely a finite pressure limit at the tube exit occurs below which no steady flow situation is possible and for which the tube pressure distribution will be independent of the back pressure. This pressure limit is the choking or the critical pressure. The following analysis contains a model of the two-phase region and produces predictions regarding the choking processes.

Slip Model for Two-Phase Flow Regime

The analysis for this flow is developed from a "slip model" which contains the following assumptions:

1. The flow is steady.

2. The flow is one dimensional in the sense that any property may be represented by its average value at a given cross-section.

3. The velocities of the two phases may not be equal. (Hence, "slip model".)

4. The temperature of the gas phase is the equilibrium saturation temperature corresponding to the pressure.

5. The liquid temperature is, in general, not the equilibrium saturation temperature at that pressure.

6. The pressures in the liquid and gas phases are equal; i.e., surface tension is negligible.

7. The two-phase mixture is accelerated in such a short distance that the pressure forces are balanced primarily by the inertia forces. Friction forces at the wall and between the phases are negligible.

8. Liquid phase density is constant.

9. The specific heat of the liquid is constant.

10. The two-phase flow is adiabatic in the sense that there is no heat transfer to the tube wall.

For the flow under study it has been observed that the vapor phase forms at and remains near the wall with the major portion of the tube being a central core of liquid. The thin annular region surrounding this central liquid core contains the vapor phase,

either as a pure vapor or as a high quality two-phase mixture.

Consider first the validity of the one dimensional assumption in the liquid. A typical diameter Reynolds number for the Freon 114 flow considered here is 10^6. Using the universal velocity distribution in turbulent flow from Rohsenow and Choi (2), the thickness of the so-called laminar sublayer and of the buffer layer may be calculated. For a tube with a 1/4 inch diameter, the thickness of the laminar sublayer is found to be 2.5×10^{-5} inches and the buffer layer thickness is 1.5×10^{-4} inches. Thus the one-dimensional assumption for the liquid velocity is very good in the single-phase region. This uniform velocity profile should be retained in the two-phase region in the central liquid core which contains almost all the liquid. The specific models considered in Appendices A and B show that the liquid temperature gradients are confined to thin thermal boundary layers. (Appendix A considers the growth of discrete bubbles while Appendix B assumes that the flow consists of a liquid core surrounded by a pure vapor annulus.) The existance of these thin thermal boundary layers justifies assuming a one dimensional temperature profile in the liquid. The validity of the one dimensional assumption in the vapor is related to some of the other assumptions and will be discussed in connection with these assumptions.

The third assumption is generally accepted as necessary in two-phase flow under the influence of a pressure gradient. The "slip" is caused by a pressure gradient acting on phases with very different densities. Of course the amount of "slip" is controlled by

the relative magnitudes of the various forces acting on the vapor phase. (See Assumption #7.)

The fourth and fifth assumptions are related and are based, to some extent, on studies of the growth of a single stationary bubble in a superheated liquid. This problem has been studied theoretically in Appendix A and by Plesset and Zwick (3), Forster and Zuber (4), and Scriven (5) and experimentally by Dergarabedian (6). All solutions are obtained by assuming that the vapor bubble is at the equilibrium temperature corresponding to the pressure and is growing in a non-equilibrium (superheated) liquid. The theoretical solutions are similar and in good agreement with Dergarabedian's data. These data were obtained under constant pressure conditions and therefore constant saturation temperature conditions. The two-phase flow considered here has variable pressure and saturation temperature. To maintain a volume of gas at the saturation temperature as it expands to a lower pressure would require an infinite thermal conductivity. Thus the assumption which states that the gas is at the saturation temperature can never be exactly correct. It is necessary to know the gas temperature in order to calculate the gas enthalpy. The important enthalpy change is the final gas enthalpy minus the initial liquid enthalpy and the largest part of this change is the enthalpy of vaporization, h_{fg}. Thus it is concluded that small deviations of the gas temperature from the saturation temperature are negligible in the calculation of this enthalpy change. If the

average gas temperature were 10°F. above the saturation temperature the error in the enthalpy calculation would be about 1.5 Btu/lb. This should be compared to the enthalpy of vaporization of Freon 114, which is about 50 Btu/lb. It is very unlikely that the average temperature could be more than 10°F above the local saturation temperature, because of heat transfer effects and because the vapor being produced is at the local saturation temperature. These calculations justify the assumption that the gas phase has a one dimensional temperature profile and that this temperature is the local saturation temperature. Although this assumption is not strictly true the errors introduced by it are small.

The assumption which states that the liquid temperature is not the equilibrium saturation temperature may be further justified by the well known fact that a liquid which flashes while flowing in a tube often does not nucleate vapor bubbles until the pressure is significantly below the saturation pressure. Thus the liquid may start at the beginning of the two-phase region in a non-equilibrium state and if so, it would take a finite distance to get back to equilibrium, if in fact this occurs at all.

The sixth assumption is also based largely on bubble growth studies. Surface tension forces are important only when very small bubbles are present. This effect should be negligible when there is a sufficient amount of vapor present to affect the dynamics of the flow.

The seventh assumption is based on the observed fact that the

length of the two-phase flow in this investigation is small (about 1/4 inch in a 1/4 inch diameter tube). Futhermore, the pressure gradient is very high in this region with a pressure drop of 50 psi or more in 1/4 inch. To justify the neglect of shear forces, various models must be considered to insure that both wall shear and interphase shear are negligible regardless of the distribution of phases. Various possibilities will be considered separately and the corresponding shear forces will be shown to be negligible.

One possibility is to assume that the liquid remains in contact with the tube wall and that the shear stress is the same as that in the fully developed single phase region. A typical value for this shear stress is 1 psi. The total shear force on a control volume consisting of the two-phase region is therefore about 0.2 lb. The total pressure force is 3 lb. The pressure force is more than an order of magnitude greater than the shear force and therefore this shear force may be neglected. This model for the shear stress is considered in greater detail at the end of this chapter and it is conclusively shown that this shear force is negligible except in a small region at the start of the two-phase region.

If the shear force between the phases can be shown to be negligible assuming that the vapor phase is composed of small bubbles, then it should also be negligible for other distributions of the vapor phase which necessarily have a smaller surface area between the phases. Consider a vapor bubble of a fixed size moving with respect to a liquid and acted upon by a drag force and a force due to the pressure gradient in

the liquid. Chao (7) has studied the problem of drag on a vapor bubble in a liquid from a theoretical point of view and compared his results with available data. His results indicate that the drag may be approximated by the Stokes drag ($D = 6\pi R\mu V_{rel}$) up to a Reynolds number of about 4×10^2. Above this Reynolds number the bubbles deform and the drag coefficient rises rapidly to about unity.

For the two-phase flow under consideration a typical void fraction is 0.03. If this vapor were distributed in an annulus around the liquid the thickness of the annulus would be about 0.003 inches. If the vapor is actually made up of discrete bubbles in this annular region, it is assumed that a characteristic bubble size would be the 0.003 inches calculated above. A typical pressure gradient at the start of the two-phase region is 16 psi/inch. The Stokes drag force is at least an order of magnitude less than the pressure force for relative velocities less than 20 ft/sec. For relative velocities greater than 20 ft/sec, the Stokes drag approximation is no longer correct. The pressure gradient also changes in the two-phase region and in fact increases to infinity at the choking point. From the model presented later on in this Chapter, it is found that when the relative velocity of the phases has reached 20 ft/sec a typical pressure gradient is 150 psi/inch. At this point the force on the bubble due to drag, assuming a drag coefficient of unity, is about the same order of magnitude as the pressure force. The pressure gradient increases much more rapidly than the bubble drag and the drag force quickly becomes negligible. Thus over almost the

entire length of the two-phase flow region the drag force is negligible compared to the pressure force. On the basis of these calculations it is concluded that the shear drag between the phases is negligible regardless of the distribution of the vapor phase. It may also be concluded that the vapor velocity may be characterized as one dimensional even though there are discrete bubbles in the flow.

One more possible shear force must be considered. This is vapor shear at the wall. Assuming that the vapor forms an annulus surrounding the liquid, a Reynolds number may be calculated and the wall shear force estimated. Using the thickness of 0.003 inches obtained above gives a Reynolds number of 19,000. The wall shear is therefore about 0.1 psi. This is negligible compared to the pressure forces. The buffer layer thickness is about 5% of the thickness of the region. There will also be a thin boundary layer at the liquid-vapor interface if the velocity of the vapor coming off this layer is small. Order of magnitude calculations show this velocity to be about 1 ft/sec. This is less than 1% of a typical tangential velocity, which is, according to Schlichting (8), sufficiently small for the boundary layer approximations to be satisfactory. Thus it is concluded that for a model in which the vapor is in an annulus around the liquid, the vapor velocity is one dimensional and the wall shear force is negligible compared to the pressure force.

Over the range of temperature and pressure variation of the two-phase flow process the liquid density and specific heat change very slightly.

The assumption of no heat transfer through the tube wall may be easily justified by calculating the total heat transfer coefficient through the test section. The test section is stainless steel and has an outside diameter of 3 inches and an inside diameter of 1/4 inches. The resistance to heat transfer is the sum of the film resistance inside the tube, the conduction resistance of the tube, and the natural convection film resistance on the outside of the tube. The internal film resistance was neglected and the other two resistances summed to give a total heat transfer coefficient of 20 Btu/hr ft^2°F. Assuming a temperature difference of 50°F and a flow of 8 lb/sec of Freon 114 gives a typical liquid temperature change of 2×10^{-4} °F. in a 1/4 inch. This is a length comparable to the length of the two-phase region and the small heat transfer is obviously negligible.

Making use of the above assumptions the following equations may be obtained.

The area equation is

$$A_g + A_\ell = A \tag{1}$$

where A is the cross-sectional area of the tube.

The continuity equation is

$$\rho_g V_g A_g + \rho_\ell V_\ell A_\ell = \rho_\ell V_o A \tag{2}$$

where V_o is the velocity upstream in the pure liquid phase.

The two-phase flow may be idealized as annular flow to aid in the derivation of the liquid momentum equation. Using the control volume defined in Figure 2 the liquid momentum equation may be obtained. Note

that the control surface is placed just inside the liquid-vapor interface.

$$PA_\ell - PA_\ell - d(PA_\ell) + PdA_\ell = -\rho_\ell V_\ell^2 A_\ell + \rho_\ell V_\ell^2 A_\ell + d(\rho_\ell V_\ell^2 A_\ell)$$

$$-V_\ell d(\rho_\ell V_\ell A_\ell) = -A_\ell dP = \rho_\ell V_\ell A_\ell dV_\ell \tag{3}$$

This may be integrated to give

$$P_o - P = \rho_\ell \left[\frac{V_\ell^2}{2} - \frac{V_o^2}{2}\right] \tag{4}$$

P_o is the pressure at which nucleation first occurs, i.e. the pressure at the start of the two-phase region.

The total momentum equation is

$$-AdP = d\left[\rho_g V_g^2 A_g\right] + d\left[\rho_\ell V_\ell^2 A_\ell\right] \tag{5}$$

which may be integrated to give:

$$P_o - P = \rho_g V_g^2 \frac{A_g}{A} + \rho_\ell V_\ell^2 \frac{A_\ell}{A} - \rho_\ell V_o^2 \tag{6}$$

The total energy equation is

$$0 = \rho_g V_g A_g \left[h_g(P) - h_g(P_s) + h_{fg} + \frac{P_s - P_o}{\rho_\ell} + \frac{V_g^2 - V_o^2}{2}\right] + \rho_\ell V_\ell A_\ell \left[c_\ell (T_\ell - T_o) + \frac{P - P_o}{\rho_\ell} + \frac{V_\ell^2 - V_o^2}{2}\right] \tag{7}$$

Where $h_g(P)$ is the specific enthalpy of the gas phase at some pressure P on the saturation line and h_{fg} is the specific enthalpy of vaporization evaluated at the pressure P_s.

To complete the above set of equations [Equations (1), (2), (4), (6), and (7)] it is possible to write a second energy equation.

This equation includes a heat transfer term containing the distance along the tube, x. Since none of the other equations given above involve x, they can be solved with pressure (for example) as the independent variable. All that is required for this solution is a set of tables or functions giving the appropriate values of the thermodynamic properties. These equations have the advantage that all the differential equations can be integrated exactly.

To determine the critical pressure a maximum entropy flux criterion may be used. As will be shown later, this is not the only criterion possible. There are other possibilities which are easier to understand physically and also much easier to calculate than the entropy method. Care is required in calculating the entropy changes because the process is very nearly reversible. The average specific entropy, s, is defined as:

$$\rho_\ell V_o A s = \rho_g V_g A_g s_g + \rho_\ell V_\ell A_\ell s_\ell \qquad (8)$$

Although all the quantities on the right hand side of Equation (8) are known when the previous equations have been solved simultaneously, just substituting values into the equation may produce large errors. The two terms on the right side of Equation (8) are very nearly equal and are of opposite sign. Substantial errors were obtained when these calculations were performed on the digital computer which uses about 8 significant figures. It is possible to reduce this problem to a large extent by dividing Equation (7) by T_o and subtracting the result (which equals zero) from Equation (8). Algebraic simplification and cancellation of equal terms yields an expression which

is better suited for numerical calculations.

This entropy flux must increase continuously for this irreversible adiabatic two-phase flow. The slip model indicates that the entropy flux does increase for a time as the pressure is dropped into the two-phase region but eventually reaches a maximum and then starts to drop. This entropy decrease violates the Second Law. Therefore the point of maximum entropy defines the critical pressure for the flow. This behavior is shown for a typical case for Freon 114 in Figure 3. For this case, $P_o = P_s = 69.6$ psia, $V_o = 180$ ft/sec, and s is arbitararily defined as zero at the point where the two-phase flow starts. This curve defines a critical pressure of 22.5 psia. Note that unless otherwise specified all results refer to Freon 114.

The behavior of the entropy is closely related to that of the liquid temperature. As the pressure is dropped, the liquid temperature starts to drop but not nearly as rapidly as the vapor temperature. The liquid temperature goes through a minimum at the point of maximum entropy. Thus, the process which is not allowed by the Second Law is that process in which the liquid temperature rises while in contact with a colder gas. This is a physical explanation of the violation of the Second Law. The liquid and vapor temperatures are plotted in Figure 4. The change in the liquid temperature is plotted in Figure 5 on an expanded scale in order to more clearly show the minimum liquid temperature at the critical pressure.

To complete the picture, Figure 6 shows the velocity of both phases and Figure 7 shows the void fraction as a function of pressure.

The state equations for the saturation line, the enthalpy of the saturated vapor, the entropy of the saturated vapor, the density of the saturated vapor, the enthalpy of vaporization, and the density of the saturated liquid used in the above and following calculations were obtained from bulletins published by the E.I. du Pont de Nemours and Company. (9, 10)

Typical Theoretical Predictions

Given a fluid and thus given the form of the state equations, the above model requires the specification of only three independent quantities to determine the critical pressure. These three quantities are the saturation pressure of the liquid phase at the flash point, P_s (or its equivalent the liquid temperature, T_o), the pressure at which the flashing first begins, P_o, and the velocity of the liquid phase at the flash point, V_o, (or equivalently the dynamic pressure, $\rho_\ell V_o^2/2$).

It is interesting to consider the effects of these parameters on the critical pressure. Consider first variations in the pressure at which flashing occurs, P_o. This pressure is assumed to be less than or equal to the saturation pressure, P_s. Bergles and Rohsenow (11) consider the problem of inception of boiling of a liquid flowing in a straight tube with heat addition. They obtain an expression which predicts the conditions required to initiate boiling. The result which they obtain is dependent on surface tension, heat transfer rate to the fluid, and cavity size in the solid surface. In the present case the flow is adiabatic; thus the heat transfer at the wall is zero. In this simpler case it is therefore assumed that bubble nucleation at the wall can

first occur at the point where the following equality is valid.

$$P_S - P_o = \frac{2\sigma}{r} \qquad (9)$$

Where σ is the surface tension and r a typical radius of a surface cavity. The surface tension of the Freon 114 is given by the following expression (12)

$$\sigma = (9.84 - 0.0378t) \times 10^{-5} \text{ lbf/in} \qquad (10)$$

Where t is the temperature in degrees Fahrenheit. Thus at 127°F which is the liquid temperature of the sample case considered above, $\sigma = 5.04 \times 10^{-5}$ lbf/in. A honed or lapped tube will typically have an RMS roughness height of 10 microinches. Assuming that this dimension is also typical of the cavity size and using Equation (9) gives $P_s - P_o = 10$ psi. This is the value for a very carefully machined surface and most any other machining process reduces this pressure difference.

On the basis of these rough calculations, the variation of the critical pressure with P_o was considered over a 10 psi range. The results are summarized in Table 2.

TABLE 2

Variation of Critical Pressure with Nucleation Pressure

Saturation Pressure, P_s = 69.6 psia

Single-Phase Velocity, V_o = 180 ft/sec

Nucleation Pressure P_o psia	Critical Pressure P_c psia	Critical Pressure Ratio P_c/P_o
69.6	22.5	0.323
67.6	21.8	0.322
65.6	21.1	0.321
63.6	20.4	0.320
61.6	19.7	0.319
59.6	19.0	0.318

The critical pressure ratio based on the nucleation pressure, P_o, is constant within 1.5% over a 10 psi range of P_o. Thus for all practical purposes the ratio P_c/P_o is not a function of P_o but only of the velocity, V_o, and the saturation pressure, P_s.

Figure 8 shows the variation of this critical pressure ratio with changes in saturation pressure, with the liquid phase dynamic pressure held constant. This curve is very nearly identical to one which would be obtained by holding the velocity, V_o constant, because of the relatively small changes in the liquid density with temperature. The critical pressure ratio is seen to increase almost linearly with saturation pressure.

Figures 9 and 10 are typical curves showing the variation of the critical pressure ratio with the third independent parameter. These figures are the same except for the fact that in Figure 9 the critical pressure ratio is plotted versus the liquid dynamic pressure, $\rho_\ell V_o^2/2$, and in Figure 10 versus the liquid velocity, V_o. It should be noted that some of the assumptions introduced into the model are not correct at low liquid velocities. In particular, the assumption in which the friction forces were neglected in comparison to the inertia forces becomes questionable because the length of the two-phase region increases substantially as the velocity decreases.

Thus the results given in Figures 9 and 10 are, at velocities below about 150 ft/sec, only results given by a mathematical model which may or may not correspond to physical reality. Some remarks on this limiting value will be made later. At the higher velocities the assumptions which have been made are better, as the predictions at high velocities are presumed to be correct on the basis of the data presented later in this report.

Despite the questions about the validity of the model at low velocities, it is interesting to look at the predictions for this limiting case. It is to be expected that at very low velocities the critical pressure ratio will approach unity. This may be seen by considering Equations (1) through (7). The energy equation, Equation (7), is the only equation involving the local liquid temperature, T_ℓ. Thus the other equations may be solved simultaneously for all other quantities first, and then the energy equation is used to find the

liquid temperature. At low enough liquid phase velocity, V_o, this temperature change is positive. This change is impossible and therefore choking occurs. The critical pressure does in fact go to unity at low velocity in Figures 9 and 10 but it seems to do so discontinuously. In Figure 10 when V_o was lowered from 18.6 to 18.4 the critical pressure ratio jumped from 0.439 to 0.965. This would be an interesting region to investigate experimentally to see if this discontinuous phenomenon is really present.

Thermodynamic Property Approximations

In the above results the properties of the Freon 114 were calculated from rather complicated state equations. In the early stages of this investigation some approximations were made in order to simplify the calculation procedure. These approximate results turned out to be in good agreement with the results obtained by using the more complicated state equations. The approximations are outlined here, results of some sample calculations are presented, and a comparison is made with the earlier results in order to show the usefulness of these simplifications.

In addition to the assumptions listed at the beginning of this chapter, the following assumptions were made. The gas phase is assumed to obey the perfect gas law with a constant specific heat. The enthalpy of vaporization, h_{fg}, was assumed to be constant. The liquid specific volume is negligible in comparison with the specific volume of the vapor. As a result of the final assumption the Clapeyron equation may be written in the following form.

$$\rho_g \, h_{fg} = T_g \frac{dP}{dT_g} \tag{11}$$

Combining the above expression with the perfect gas law under the assumption of constant h_{fg} gives a simple equation which may be integrated directly. The result of the integration is an approximate analytic equation for the saturation line in terms of pressure and temperature.

It should be pointed out that the assumptions made above are not entirely self-consistant from a thermodynamic point of view. The assumptions of incompressible liquid, constant liquid specific heat, perfect gas, constant gas specific heat, and constant enthalpy of vaporization can be shown to be inconsistant by considering the following cycle. Saturated liquid is evaporated to vapor at T_1 and then cooled to T_2 along the saturation line. The vapor at T_2 is condensed to liquid at T_2 and the liquid heated to temperature T_1 along the saturation line. The total enthalpy change around this cycle is not quite zero, given the above assumptions.

Despite this inconsistency the approximations were good enough to give results in good agreement with the results obtained with the more exact and much more complicated state equations. The expression used for the gas enthalpy change was

$$h_g = c_{pg} \, (T_g - T_o) + h_{fg} + \frac{P_s - P_o}{\rho_\ell} \tag{12}$$

The corresponding entropy expression is

$$S_g = c_{pg} \, \ln \left[T_g / T_o \right] + \frac{h_{fg}}{T_g} \tag{13}$$

Where c_{pg} and h_{fg} are the values of these properties at P_s and T_o

and are assumed to be constant.

A variety of calculations were made to compare the results of the approximate calculations with those obtained by using the more exact state equations. In no case did the critical pressure predicted by the two methods differ by more than 3%. The other quantities differed by larger percentages and Table 3 summarizes the results of a typical calculation at the critical pressure.

TABLE 3

Comparison of Results at the Critical Pressure Using Approximate Thermodynamic Properties and Using the Best Available State Equations

$$P_s = P_o = 69.6 \text{ psi } \rho_\ell V_o^2/2 = 297 \text{ psi}$$

	"Exact Theory"	"Approximate Theory"
Critical Pressure, P_c, psia	22.5	22.6
Average Entropy, s, $\frac{\text{Btu}}{\#^\circ\text{R}}$	6.17×10^{-6}	6.39×10^{-6}
Liquid Temperature, T_ℓ, °F	126.701	126.691
Vapor Temperature, T_g, °F	59.73	57.45
Liquid Velocity, V_ℓ, ft/sec	193	194
Vapor Velocity, V_g, ft/sec	498	482
Void Fraction, A_g/A	0.0725	0.0724

Note that the results given in Table 3 for the "Exact Theory" are the same as those plotted in detail in Figures 3 through 7.

Theoretical Predictions for Water

Since the approximations to the thermodynamic properties considered in the previous section worked so well in comparison to the more exact model for Freon 114, the conclusion was reached that it would be useful to present results using these approximations for a much more common fluid, water. Although no experimental work was carried out in this project using water, predictions for this fluid are included in order to better relate this work to the large amount of work that has been done and is being done in the field of two-phase flow using steam and water.

The results for water are presented in the same manner as were the results for Freon 114. That is, the variation of the critical pressure with the three separate initial conditions of the mathematical model is considered.

Looking first at the variation of the critical pressure with the pressure at the start of the two-phase flow, P_o, it is again found that the ratio P_c/P_o remains constant to within the accuracy of the calculations. Typical results are summarized in Table 4.

TABLE 4

Variation of Critical Pressure With

Nucleation Pressure for Water

Saturation Pressure P_s = 70 psia

Single-Phase Velocity V_o = 221 ft/sec

Nucleation Pressure P_o psia	Critical Pressure P_c psia	Critical Pressure Ratio P_c/P_o
70	17	0.24
68	17	0.25
66	16	0.24
64	16	0.25
62	15	0.24
60	15	0.25

The variation of the critical pressure ratio with saturation pressure shows a much smaller variation for the water than that observed for the Freon 114. The Freon 114 critical pressure ratio changed by about 40% over the saturation pressure range considered in Figure 8, while the water ratio changed by only about 4% over a similar pressure range. In both cases the critical pressure ratio increased with increasing saturation pressure (or liquid temperature). Some typical results for water are summarized in Table 5.

TABLE 5

Variation of Critical Pressure with Initial Saturation Pressure for Water

$P_s = P_o$ $\rho_\ell V_o^2/2 = 300$ psi

Saturation Pressure	Initial Liquid Velocity	Critical Pressure	Critical Pressure Ratio
P_s psia	V_o ft/sec	P_c psia	P_c/P_o
10	215	2.4	0.24
40	218	9.8	0.25
70	221	17	0.24
120	223	30	0.25
170	225	44	0.26
220	227	58	0.26

Thus it is concluded from the above calculations, that to a very good approximation the critical pressure ratio may be considered to be a function only of the upstream liquid velocity. Figure 11 shows a curve giving the variation of the critical pressure ratio, P_c/P_o, versus the liquid velocity, V_o. The shape of the curve is very similar to Figure 10 which displays essentially the same information for the Freon 114. Again it must be stressed that the assumptions upon which this theory is based are not necessarily valid at the low velocity end of the curve.

Slip Model with Length Variable Included

The above model has a disadvantage in that it does not contain a relation giving pressure versus length as the pressure drops from conditions at or near the saturation pressure to the critical pressure. The length variable appears in a rate equation governing the heat flow from the liquid to the liquid-vapor interface. The length variable would also appear in wall and interfacial shear terms if they were included. In the following development, a constant wall shear is included for two reasons: (1) the assumption of negligible wall friction can be investigated by putting into the equations a zero wall friction term and one of the correct order of magnitude in order to check the difference. (2) the two-phase flow region can be connected to the single phase region without a discontinuity in the pressure gradient by assuming the wall shear in the two-phase region is the wall shear for fully developed turbulent single-phase flow.

Making this addition, Equation (4) becomes

$$P_o - P = \frac{\rho_\ell}{2} (V_\ell^2 - V_o^2) + \frac{4 \tau x}{D} \qquad (14)$$

$4 \tau x/D$ represents a wall shear stress term which is assumed, for the reasons stated above, to be acting on the liquid phase. The interfacial shear stress is still zero. x is the axial distance from the start of the two-phase region and it has been assumed that $A_\ell \cong A$.

Equation (6) becomes

$$P_o - P = \rho_g V_g^2 \frac{A_g}{A} + \rho_\ell \left[V_\ell^2 \frac{A_\ell}{A} - V_o^2 \right] + \frac{4 \tau x}{D} \qquad (15)$$

It is now necessary to derive an energy flow equation for the liquid phase using the idealized control volume shown in Figure 2. Before writing an equation it is convenient to consider the physics of the problem. Under investigation is a two-phase flow problem in which a vapor phase is being rapidly formed and is strongly affecting the flow. It is desireable to characterize this vapor formation with an appropriate rate equation. To form the vapor, heat must be transferred to the liquid-vapor interface to evaporate the liquid. Referring to Figure 2, it is obvious that heat may be transferred to this interface from both the liquid and vapor side. If one of these heat transfer rates is much larger than the other, then it will be the process which is controlling and is the appropriate one to consider. For the problems considered here the vapor mass flow fraction is around 4×10^{-4}. The total vapor enthalpy flux is therefore so small that it is impossible to transfer a significant quantity of heat from the vapor phase. The heat transfer from the liquid is thus the important physical parameter and any calculations must consider this heat transfer. To calculate this heat transfer rate a control volume must be drawn such that the heat flows across its boundaries. The appropriate control volume is that shown in Figure 2, which lies on the liquid side at the liquid-vapor interface. The energy flow equation for this control volume is

$$dq = \rho_\ell V_\ell A_\ell h^o_\ell - \rho_\ell V_\ell A_\ell h^o_\ell - d(\rho_\ell V_\ell A_\ell h^o_\ell) + h^o_\ell d(\rho_\ell V_\ell A_\ell)$$

$$= - \rho_\ell V_\ell A_\ell dh^o_\ell \qquad (16)$$

Where h^o_ℓ is the total, liquid, specific enthalpy.

Equation (16) may be combined with the total energy equation, Equation (7) to give

$$dq = (h^o_g - h^o_\ell)\ d\ (\rho_g V_g A_g) + \rho_g V_g A_g dh^o_g \qquad (17)$$

The first term on the right hand side of Equation (17) is the dominant one and clearly shows that the heat transfer dq is providing the energy to evaporate the liquid.

Equation (16) may be rewritten to give

$$h(T_\ell - T_g) \frac{dA_h}{dx}\ dx = - (c_\ell d\ T_\ell + \frac{dP}{\rho_\ell} + V_\ell dV_\ell)\rho_\ell V_\ell A_\ell \qquad (18)$$

where h is an effective heat-transfer coefficient based on the area of the phase boundary A_h. Both these parameters are probably obtainable only in an empirical or semi-empirical fashion. For this reason, it is convenient to combine the two quantities leaving only one parameter to be experimentally determined.

If A_h is based on the tube wall area then

$$A_h = \pi D x \qquad (19)$$

Then Equation (18) becomes

$$h\ (T_\ell - T_g)\ \pi D\ dx = -\rho_\ell V_\ell A_\ell (c_\ell dT_\ell + \frac{dP}{\rho_\ell} + V_\ell dV_\ell) \qquad (20)$$

Given the value of h and using the previously introduced set of equations [Equations (1), (2), (7), (14), and (15)], Equation (20)

may be integrated numerically on the digital computer. This results in a pressure versus length curve. The integration may be performed for various functional behaviors of h and the results compared with experimental data. As will be shown in the following chapter, a constant value of h can give a good fit with the data. Figure 12 shows the results of numerically integrating Equation (20) using the well-known Runge-Kutta formula. (See Crandall (13) for a discussion of numerical techniques.) The initial conditions are the same as those used to obtain Figures 3 through 7. The coordinate y is the negative of x and is the distance along the tube measured upstream from the end. The value of τ used is that in the liquid region, assuming fully-developed turbulent flow in a smooth walled tube. This assumption makes the slope of the pressure versus length curve continuous at the boundary between the single-phase and two-phase region.

Also shown in Figure 12 is the solution for the case in which $\tau = 0$. The two curves are seen to be less than one psi apart over the whole range. The two curves do predict a quite different total length of the two-phase region but, as may be seen from Figure 12, this is due largely to a difference in slope at the saturation pressure end of the curve. This is the region of the two-phase flow curve in which the assumed wall shear is most nearly correct and also the only region where the shear has a significant effect. All other quantities except the entropy calculated from the two models are in agreement to within less than 5% at the choking point. The entropy change is significantly changed by the introduction of an additional irreversible process, wall shear. When $\tau = 0$ the maximum entropy is

0.618×10^{-5} Btu/#°R, while when $\tau = 0.791$ psi the maximum is 1.44×10^{-5} Btu/#°R. The most important fact is not that the magnitude of the entropy in these two cases is different but that in both cases the entropy reaches a maximum value at the same pressure (still considering pressure to be the independent variable). The curves in Figure 12 approach the critical pressures predicted from the slip-model maximum entropy criterion as y goes to zero.

It is interesting to consider the behavior of the mathematical model at the choking point. As has already been shown, with pressure as the independent variable the entropy reaches a maximum and the liquid temperature reaches a minimum value at the choking point. Combining Equation (20) with Equation (14) gives

$$h\,(T_\ell - T_g)\,\pi D dx = -\rho_\ell V_\ell A_\ell \left(c_\ell dT_\ell - \frac{4\tau}{\rho_\ell}\,\frac{dx}{D}\right) \tag{21}$$

From this it may be seen that if T_ℓ has a minimum, then the variable x must reach a maximum at the choking point. Again it is seen that a continuation of the solution beyond this point is impossible. If instead of pressure the length dimension x is considered to be the independent variable then it is clear that the derivatives with respect to x of the pressure, liquid velocity, vapor velocity, void fraction, etc. become infinite at the point of choking. This is very analogous to the situation which occurs when considering the one-dimensional flow of a perfect gas at the choking point.

Chapter 3

EXPERIMENTAL INVESTIGATION OF TWO-PHASE STRAIGHT TUBE CHOKING

Description of Apparatus

A schematic of the test apparatus used for this project is shown in Figure 13. The test section was mounted with the flow downward. Various interchangeable test sections were machined from 3 inch round stock 12 inches in length. Pressures were measured on carefully calibrated (1/4% and 1/10% of full scale accuracy) test gauges with 8 1/2 inch diameter dials. The flow downstream of the test section expanded into a 4 inch line to prevent any two-phase choking effects. Accurate control of the back pressure at the test section was provided by two valves in parallel. The two-phase flow was separated by gravity with the vapor phase flowing vertically upward to the condenser. City water was used on the tube side of the condenser to liquify the Freon 114.

The two liquid streams rejoin and are pumped by a centrifugal pump requiring a very low head at the inlet. The centrifugal pump increases the stagnation pressure of the liquid by about 100 psi. The liquid is then heated in the heat exchanger with condensing steam on the shell side. The liquid is then pumped by a positive-displacement piston pump having a maximum flow rate of 50 gal/min and a maximum output pressure of 800 psig. A 2 1/2 gallon accumulator was placed on each side of the piston pump to damp out the fluctuations produced by this pump.

A 5 micron filter removes particles from the flow which might serve as nucleation sites. The flow rate was measured using a calibrated orifice plate flow meter with a flow straightener and a reamed and honed tube upstream of the orifice plate. The temperature of the liquid was measured using a calibrated Copper-Constantan thermocouple. A flow straightener, followed by a pipe with an L/D ratio of 30, produced fully developed turbulent flow at the entrance to the test section under all conditions. The flow entered the test section in 1 1/2 inch (inside diameter of 1.635 inches) stainless steel pipe. Copper or stainless steel pipe and fittings were used in the flow loop wherever possible in order to minimize the rust particles in the flow. The loop was connected to a vacuum system so that the air could be removed from the system before it was filled with Freon 114.

Pressure Tap Error

Preliminary tests with nozzles indicated that at the velocities of interest in this investigation pressure measurement errors were a significant problem. These errors were so large (around 10% of the dynamic pressure) that it seemed necessary to devise a method for individually calibrating each pressure tap before actual two-phase flow tests were made. The following pressure tap calibration technique was used for straight tube test sections. The test loop was broken open between the centrifugal pump and the heat exchanger and connected to the city water main. (See Figure 13.) Water was pumped through the test section. At the downstream end of the test section the water issued into the atmosphere as a free jet aimed into the drain pipe.

The fact that the water exits from the test section as a free jet fixes the pressure at the end of the tube very accurately as atmospheric pressure. Knowing this reference pressure, it is possible to calculate the pressure upstream in the fully developed region based on the well-known correlation for turbulent flow in a smooth tube. This calculated pressure may be compared with a measured pressure at the same point. The error is thus determined and a curve may be plotted.

A straight tube test section identical to the one shown in Figure 13 was constructed from transparent acrylic plastic (plexiglas). Attempts to calibrate the pressure taps in this test section were completely unsuccessful. It was impossible to obtain data which could be repeated on successive days. Tap #2 for example gave readings about 10 psi above the calculated pressure when the first tests were run. Other tests run on the next day produced readings 20 psi below the calculated pressure under the same test conditions. Data from all other pressure taps including the 0.0135 inch diameter and 0.0292 inch diameter taps showed similar trends.

Shaw (1) has shown that very small burrs at the intersection of the tap hole and the tube strongly affect the pressure tap error. An inspection of the test section showed considerable surface cracking. On this basis it was postulated that some sort of geometry change was occuring near the pressure tap hole which was causing the reading to change from day to day. It must be noted that the attempts to calibrate this plastic test section were made using water which presumably does not attack arcylic plastic. Pressure and temperature changes associated with starting up and shutting down probably did contribute

to the cracking, however. The cracking could also have been caused by the stresses introduced by the machining of the test section.

The assumption that the non-repeatability of the data for the plastic test section was caused by deterioration of the plastic made it necessary to use a metal tube. Stainless steel was chosen as the material least likely to rust or corrode. The stainless steel has a disadvantage, however, in not being transparent.

The straight tube test section shown in Figure 14 was constructed and tested as described above using water to calibrate the pressure taps. The data from three different runs on three different days were in very good agreement. The spread in this data was of the order of 1 psi. Each pressure tap had its own calibration curve. Errors ranged from 30 to 50 psi at various taps when the dynamic pressure was about 400 psi. (The pressure error is defined as being the measured pressure minus the "true" pressure.) This successful calibration of the stainless steel test section seems to confirm the assumption that calibration was not possible in the plastic test section due to small geometry changes. It also indicates that the use of acrylic plastic test sections under conditions of high dynamic pressure may not be advisable under circumstances where accurate pressure measurement is desired.

Using a stainless steel test section to solve the pressure measurement problem introduced a problem in viewing the two-phase flow. Two variables of particular interest may be obtained by viewing the flow. The first is the location of the start of the two-phase region relative to the measured pressure distribution and the second is the overall length of the two-phase flow region.

In order to be able to view the flow, a 90° acrylic sector was constructed and carefully fitted into the stainless steel test section. (See Figure 15.) The pressure taps all entered the test section in the 270° sector made of stainless steel so that any changes in the plastic would not affect the readings of the pressure taps. After the plastic plug was inserted into the stainless steel, the whole tube was carefully lapped. It was realized that even if the fit was perfect at room temperature there would be some misalignment at the higher operating temperatures due to differential thermal expansion. For this reason the "window" was made considerably longer than the length of the two-phase region. From preliminary observations made using the straight tube plastic test section discussed earlier, the length of the two-phase region in Freon 114 was known to be less than 1/2 inch. The "window" starts 2 3/8 inches from the sudden expansion, allowing an L/D of about 8 for any disturbance caused by a step at the upstream edge of the "window" to damp out.

Calibration runs were made using the free jet water technique described above. Measured pressures ranged from about 15 to 30 psi above the true pressure and were repeatable for runs on two successive days. Runs made on a third day deviated from the earlier data but the reason for this was quite obvious. During this third run considerable cavitation was evident. Many bubbles were generated at the upstream edge of the "window" and were observed throughout the rest of the tube. This was apparently caused by some stress relaxation in the plastic "window", as this cavitation was observed at all operating temperatures.

The test section was removed from the flow loop. The stainless steel section with the "window" in place was placed in boiling water in order to completely stress relieve the plastic sector. While the test section was still hot it was carefully lapped by the author in order to attain a smooth tube at temperatures more nearly typical of the desired operating conditions.

Heating of the test section as described above seems to have completely solved the problem caused by the "window" expanding into the test section. This stainless steel-tube plastic "window" combination was used for all succeeding tests in this project and at no time was severe cavitation noted. At some operating conditions a slight fringe of a white bubbly mixture about 1/16 inch long was observed at the upstream edge of the "window". No cavitation any more severe than this has been observed under any operating condition.

Final calibration of this test section was made using the free water jet technique and the calibration curve for each pressure tap was repeatable to within 1 or 2 psi as before. However, the error itself was found to vary from about -10 psi to +10 psi. This is almost an order of magnitude improvement over some of the earlier pressure tap errors observed. There are two possible explanations for this improvement. First consider the history of the test section. The test section without the "window" was manufactured by drilling the pressure tap holes into the unfinished tube. The tube was then hand lapped by a very competent machinist for two or three days, producing a surface with no visible scratches. Experimental data obtained at this point gave pressure tap errors of about 50 psi. The test section was returned to the machine shop and the same machinist fitted the

"window" into the test section. The final phase of this operation consisted of lapping the test section with the plastic "window" in place. Most of the material removed in this operation was taken off the plastic "window" which was made to project very slightly into the tube at the start. Tests run at this point gave errors of about 30 psi. Expansion of the plastic made a third lapping necessary. This was done by the author after some instruction by the machinist who had done the rest of the work. Again most of the material removed was from the plastic piece. The tests at this point produced errors between -10 and +10 psi. Data presented by Shaw (1) seem to indicate that a burr projecting 0.0001 inches into the stream at the tap hole could produce sizeable errors with the geometry considered here. Possibily a burr caused by drilling the tap hole was present and the three separate lappings were required to remove it. This seems unlikely since the first lapping required days, while the second and third required only an hour or so. A more likely explanation is the method used to clean the lapping compound out of the pressure tap holes. The process of lapping requires an abrasive compound which wears away the surface of the tube being lapped. This compound tends to plug up the tap holes during the lapping operation and they must be cleaned out before the test section can be used. The machinist used a drill or fine wire to clean out these holes, while the author reinstalled the test section into the flow loop and cleaned out each hole with high pressure water. It is suggested that the act of pushing a drill through the pressure tap hole could produce a burr of a large enough size to alter significantly the tap error. Other explanations could perhaps

be developed, but the main point of this discussion is to show just how much care is required to obtain accurate pressure measurements with flows having such high dynamic pressures.

Figures 16 through 19 show the calibration curves for four of the thirteen taps in the straight tube portion of the test section. The results are presented in the dimensionless form which Shaw (1) shows to be appropriate for fully developed flow. τ for these curves is about 1 psi. A curve has been fitted to the data by eye. The extrapolated calibration curve is assumed to fall between the horizontal dotted line and the straight line extension from the last data points. This extrapolation is necessary because it was not possible to overlap the entire Reynolds number test range of the Freon 114 with the water calibration runs. This difference in Reynolds number range obtained with the two fluids is due primarily to the difference in viscosity of the two fluids. (The viscosity of Freon 114 (14) is less than that of water at the same temperature). As shown later, the fact that the free water jet calibration did not completely overlap the Freon 114 data range was not too serious a problem.

As noted above, the calibration technique is only a valid technique in the region of fully developed turbulent flow. Deissler (15) gives an analytic solution based on the integral method which indicated that for pipe Reynolds numbers ($\rho_\ell V_o D/\mu$) greater than 10^5 the local friction factor reaches its fully developed value in less than 8 diameters. (A typical pipe Reynolds number for these tests is 10^6.) His experimental results and also those of Harnett (16) were in agreement with this prediction. Experiments show that the velocity profile may take 50 or more diameters to become fully developed.

On the basis of the above, the first pressure tap in the tube (tap #2) was placed a nominal 8 diameters from the termination of the bell-mounted entry.

Curves for the pressure tap error for taps #4, #6, and #7 were very similar to that of tap #2 shown in Figure 16. These taps showed a linear curve for the error over the test range. The slope and range of the data were about the same as that shown in Figure 16. Taps #3, #4, and #5 were all located at the same position but had three different diameters. (#3, d = 0.0135 inches; #4, d = 0.020 inches; #5, d = 0.0292 inches). At any given flow condition the error for these three taps was very nearly the same. Thus on the basis of this limited test it was not possible to draw any conclusions as to the most desirable tap size. (As noted earlier, however, a diameter of 0.020 inches seemed to be the best size for the pressure tap holes in the plastic test section.) Pressure Taps #8, #9, #10 and #11 were found to have calibration curves very similar to those shown in Figures 17, 18, and 19 for taps #12, #13, and #14. These curves start out very near to the line of zero error and then curve upward at a higher value of the Reynolds number.

It is also convenient to consider the pressure measurements obtained at tap #1. Tap #1 is located upstream of the bellmouth. Measurements obtained at this tap are useful because there is little or no error associated with the pressure measurement here. The pressure error, as shown above, is some fraction of the dynamic pressure. From continuity it is found that the dynamic pressure at tap #1 is 6.3×10^{-4} times the dynamic pressure in the straight tube. Thus, not only is the measurement error unimportant, but the dynamic pressure itself may be neglected in computing the stagnation pressure. Since tap #1 has no

error associated with it, it is convenient to relate the pressure measured here to that in the tube. In order to do this it is convenient to define a pressure coefficient, C_p, as follows.

$$C_p = \frac{\left[P_1 - \rho_\ell V_o^2/2\right] - \left[4 f \frac{L_T}{D} \frac{\rho_\ell V_o^2}{2} + P_{atm}\right]}{\rho_\ell V_o^2/2} \tag{22}$$

Where L_T is the total length of the straight tube (L_T = 9 1/2 inches). This pressure coefficient is the pressure at the start of the straight tube, assuming no losses in the bellmouth entrance, minus the pressure at the start of the straight tube, assuming fully developed flow through the <u>whole</u> tube, divided by the dynamic pressure. Thus the pressure coefficient is a stagnation pressure loss coefficient which adds the flow losses in the bellmouth to the flow losses in the straight tube entrance region in excess of the fully developed losses. This pressure loss coefficient is a function only of the pipe Reynolds number $\frac{\rho_\ell V_o D}{\mu}$ and may be determined experimentally. If C_p is known for a flow then it may be used along with the measured value of P_1 and the dynamic pressure to calculate an artificial pressure, P_i, which should fall on the fully developed pressure drop curve extrapolated to zero length.

$$C_p = \frac{\left[P_1 - \rho_\ell V_o^2/2\right] - P_i}{\rho_\ell V_o^2/2} \tag{23}$$

This operation might be termed an artificial calibration of tap #1, as compared to the actual calibration of the other pressure taps. This artificial calibration has an advantage over the other calibrations: C_p is a stagnation pressure loss coefficient and therefore should be a weak function of Reynolds number at high values of the Reynolds

number. This is an advantage here since it is desirable to extrapolate some of the present data to higher Reynolds numbers for use in conjunction with the Freon data.

Figure 20 shows the experimental data obtained using the free water jet. These data determine C_p as a function of the pipe Reynolds number. Most of the data points obtained for C_p are negative. Since C_p is a loss coefficient it seems that negative values are impossible. In fact there is a very good explanation for this behavior. When the straight tube portion of the test section was lapped, the tool was started from the bellmouth end of the test section. Taking the tool in and out caused the tube to become slightly oversize at this point. Thus the bellmouth nozzle ends slightly further downstream and the value of L_T used in Equation (22) should be decreased. Equation (22) is only a definition which it is convenient to retain since the negative values of the pressure coefficient have been explained. The experimental data in Figure 20 have been curve fitted by eye and this curve extrapolated as with the calibration curves.

The results obtained from the free water jet calibration technique may now be applied to data obtained for Freon 114 and used to correct for pressure tap errors. Figure 21 shows typical corrected Freon 114 data for a Reynolds number which lies in the calibration range. The data point at L = 0 was obtained from a measurement of the stagnation pressure, P_1, and from the appropriate value of C_p from Figure 20 Data points for taps #2 through #14 were corrected based on the appropriate calibration curve. The data point at L = 9 1/2 inches, corresponding to the end of the tube, is a measured back pressure. The location of this back pressure measurement is discussed later in this chapter. The

theoretical curve was obtained from the slip model below the saturation pressure and the theory for the pressure drop in fully developed turbulent flow at pressures above the saturation pressure. Thus the theoretical curve is calculated from the end of the test section to the inlet of the test section. The agreement between the theory and the experimental data is excellent.

Figure 22 shows a similar curve at a high Reynolds number. For this case it is necessary to use the extrapolated calibration curves to correct the measured pressure. The limits of the extrapolation give rise to the finite uncertainty in the computed result. This is indicated in Figure 22 by the bars above and below the data points. There is good agreement between the data and the theory.

It is concluded that: (1) with a stainless steel test section pressure tap error is repeatable. (2) it is possible to determine a non-dimensional curve of this error using the free jet calibration technique. (3) it is possible to use the non-dimensional curve as a calibration curve to correct pressure measurement errors obtained under different experimental conditions. (4) the non-dimensional pressure curve may be extrapolated to higher Reynolds numbers with some small loss in accuracy.

Experimental Study of Two-Phase Flow

It was assumed that once the pressure measurement problem was solved, it would be a relatively simple matter to place pressure taps in the two-phase region and measure the pressure distribution. As may be seen from the data in Figures 21 and 22, the real situation is

not quite so simple. The last tap, tap #14, is 0.125 inches from the end of the tube. To within the accuracy of the experimental data, there is no deviation of the measured pressure at this point from the linear curve of the single-phase region. Of course it would be possible to add one or two taps downstream of tap #14 but there is a limit to how close to the end of the tube a finite sized tap may be placed. Thus it would never be possible to place a tap right at the end of the tube. (A movable sting placed down the center of the tube could be placed with a pressure tap in the exit plane. This possibility was rejected because of the difficulties that would have been encountered in building it into the existing system). Furthermore, pressure taps placed downstream of tap #14 would be measuring pressures in a region in which the pressure gradient is extremely high.

It was noted that the two-phase region became much longer, extending the full length of the 2 3/8 inch "window", when only the first stage pump in the system was operating. Under these circumstances the stagnation pressure, P_1, was about 150 psig. Assuming that the dynamic pressure was about 100 psi then V_o was close to 100 ft/sec. This is noted here even though no data were recorded under these conditions because this lengthening of the two-phase region may cause the assumptions of the model to become invalid. The minimum velocity at which data were recorded was 170 ft/sec. In Chapter 2 a conservative statement was made to the effect that the model may not be valid at velocities below 150 ft/sec. On the other hand, the above evidence does not preclude the possibility that the model is valid at

or below velocities of 100 ft/sec. Only more extensive experimental data can conclusively answer this question.

From Figures 21 and 22 it is obvious that for many practical purposes a knowledge of the two-phase region is unimportant. For example, consider a flow situation similar to that in Figure 21 in which the upstream stagnation pressure and the pressure at the exit of the tube are given and the flow is to be caluclated. If the back pressure is below the saturation pressure, the assumption of single-phase flow and a back pressure equal to the saturation pressure yields very good results as may be seen by inspection of Figure 21.

There are circumstances when a knowledge of the two-phase region is useful. Any situation in which it is necessary to know what exit pressures correspond to unchoked flow or what the choked pressure is, requires some knowledge of the two-phase flow.

One way of defining a choked flow is the following. Choked flow exists when variations in the back pressure have no steady flow effect upstream. Following this line of reasoning it may be asserted that for unchoked flow back pressure variations do produce measurable changes in the upstream flow. This statement forms the basis for the rest of the experimental work performed in this project.

Assume there exists for the test section a unique pressure versus length curve. This curve consists of a linear single-phase portion followed by a two-phase curve. Referring to Figure 22, it is clear that a change in the back pressure, from the choked pressure to a higher pressure with the flow held constant, implies a shift of this unique pressure distribution downstream. This shift must be just that

required for the pressure distribution to match the back pressure at the end of the tube. The net result of this shift is a rise in pressure at each point along the tube. Stated another way, an increase in the back pressure causes all other pressures to rise. Furthermore, the way in which the pressure at tap #14, for example, varies as tha back pressure changes is controlled by the pressure distribution between these two points. Thus the pressure distribution in the two-phase region has been studied indirectly by looking at changes in the pressure measured at tap #14 as the back pressure is changed. This avoids the problem of putting instrumentation in the very short two-phase region.

A very crucial assumption in the above argument is that of a unique pressure distribution regardless of back pressure. It is easy to conceive of a situation in which this is not true. Consider for example flow in a very smooth walled tube with only one pressure tap. If this pressure tap were located in the flow at a point where the liquid was slightly superheated it would very likely produce sufficient disturbance to cause nucleation. If the back pressure were changed slightly, resulting in upstream changes, the nucleation point could easily remain at the pressure tap. Under these conditions the same form of the pressure distribution has not been preserved. The nucleation is occuring at a different pressure and, as shown above, the nucleation pressure is the point at which the two very different flow regimes connect. If this could be the case for the flow situation with just one pressure tap, the situation certainly could be compounded by the numerous pressure taps that are present in the test section used for this investigation. This possibility is rejected and the assumption

made that in all the data obtained in this investigation the nucleation pressure was equal to the saturation pressure. This assumption is based on the following experimental observations. At all test conditions considered herein a stream of bubbles was observed coming from tap #11. Tap #11 is 0.500 inches from the end of the tube. It was concluded that the bubbles formed at tap #11 and also at some of the subsequent taps were the result of localized pressure disturbances caused by the tap hole, i.e. cavitation, and that this process was occuring at pressures well above the saturation pressure. That this cavitation takes place at pressures above the saturation pressure may be seen from the data in Figures 21 and 22 and similar data not shown here. This is also supported by the fact that these bubbles do not appear to grow until they have been swept downstream a substantial distance. The presence of these vapor bubbles forms the basis for the assumption stated above, that is the two-phase flow region starts at the saturation pressure. Bubbles from tap #11 and other taps provide a substitute for wall nucleation conditions. The tube wall condition has no effect on the two-phase flow as long as the vapor phase grows from those bubbles produced upstream of the region of interest. Thus these observations justify the assumption of the existance of a unique curve of pressure distribution and also the related assumption of nucleation at the saturation pressure.

The experimental data were obtained in the following manner. The flow and temperature were set at the desired test condition. It was necessary to hold these two quantities as nearly constant as possible over the duration of a run. The flow was fairly easy to hold constant since the positive displacement pump driven by a very much overpowered

D.C. motor acted very much like a flow source. The temperature control presented some problems because fluctuations in steam and cooling water flow strongly affected the temperature of the Freon 114 in the test loop. Temperature changes are very important because a temperature change implies a change in the saturation pressure. Since the two-phase region starts at the saturation pressure, a change in this pressure obviously implies a new pressure distribution in the two-phase region. Eventually the technique of setting the temperature at some nominal value and then holding at this temperature to within $\pm$ 1°F was evolved.

The basic measurement for these tests was a pressure change at the last tap, tap #14. It was necessary to first establish a reference level for tap #14. This reference pressure is a function of the temperature (or saturation pressure) and therefore it is necessary to obtain experimentally a curve of this reference pressure versus temperature. This curve is generated with the flow at or near choking by varying the temperature over a range somewhat greater than the nominal test range of $\pm$ 1°F. A typical set of data used to establish this reference level is shown in Figure 23.

The back pressure was then raised in steps to a pressure slightly below the saturation pressure. The liquid temperature, the pressure at tap #14, the back pressure, and the flow rate were recorded at each of the steps. Lowering the back pressure back down to its minimum produced further data. Temperature corrections were made whenever necessary to maintain the liquid temperature in the desired test range.

The back pressure was measured at two different locations. One of these measurements was made at tap #15, which is placed in the stainless steel test section just after the sudden expansion to a diameter

of 1 inch. (See Figure 14) Downstream of the test section there was a further expansion into a 4 inch diameter pipe which serves as a plenum chamber. The second measurement of the back pressure, P_{16}, was made 3 inches from the end of the test section in this chamber. Table 6 summarizes the experimental values of these two pressures for a typical test run.

Table 6

Comparison of the Measured Back Pressure from Two Different Pressure Taps for Run #46-B

P_{15}, psia	P_{16}, psia
30.0	33.3
29.8	37.3
30.5	38.8
31.1	42.1
32.3	44.4
33.3	47.3
34.6	50.1
35.7	51.7
43.0	54.9
54.9	56.8
58.0	59.5
61.1*	62.1*

*All pressure measurements at higher values were in agreement to within 2 psi.

At or near the theoretical choking pressure the readings obtained at the two taps were in good agreement. As the back pressure was increased the difference became quite significant and then decreased to the order of the experimental accuracy. Based on the following observations, P_{16}, was eventually chosen as the correct value of the back pressure. Over the pressure range where there was a large difference between the pressure readings, the one inch diameter section beyond the end of the straight tube was observed to be filled with two-phase flow. As the pressure was increased a vapor "space" opened up around the two-phase region, which increased as the pressure was increased. This space was first observed at about the same pressure as that at which the difference in readings between the two taps became small. The variation of P_{16} with position of the back pressure control valve was much more continuous than that of P_{15}, which seemed to show a very rapid rise over a short region. Also it was noted, during runs to obtain the reference value of P_{14} as a function of temperature, that P_{15} would increase slightly with temperature while no similar change was noted at tap #16. Based on these observations it was postulated that when the pressure was low enough to cause the two-phase flow to expand and fill all of the one inch diameter section there was sufficient interaction of the flow with the walls to cause the pressure at P_{15} to be other than the actual back pressure. (Note that the flow out of the test section was not in equilibrium and therefore expanded upon leaving the straight tube due to the flashing of the liquid. This is in contrast to a gas jet which would only expand upon leaving a tube if the back pressure were below that required to choke the flow.)

The existance of this interaction was supported by the simultaneous occurance of the rapid rate of rise of P_{15} as a function of valve position, to a value equal to that of P_{16}, and the appearance of the vapor "space" around the two-phase jet. The fact that P_{16} could be held quite constant at low back pressures with small temperature variations, while P_{15} was affected by the upstream temperature variations seems to indicate that the flow near tap #15 is controlled by upstream rather than downstream conditions. Despite this rather lengthy discussion regarding which measured pressure is the "correct" back pressure it should be stressed that for all the data presented in this report the use of the "incorrect" back pressure would have little effect. This is true because the quantity ΔP_{14} is nearly constant in the experimental range in which there is a large difference between the two measured pressures. This may be seem by comparing the data in Table 6 with the corresponding data plotted in Figure 33.

Data reduction consisted of plotting a curve similar to Figure 23 to establish the reference pressure as a function of temperature. Then all P_{14} data, including that used to establish the reference pressure curve, has the reference pressure at that temperature subtracted from it. The resulting quantity, ΔP_{14} is then plotted versus the back pressure.

There is of course some uncertainty associated with all of these measurements. It has been shown that there is a known and repeatable single-phase pressure measurement error associated with each pressure tap. The above mentioned data reduction method involves taking the difference of two different pressures measured at the same tap under slightly different flow conditions. Implicit in this technique is

the assumption of constant error at these two conditions. If these two conditions both correspond to single-phase flow then the assumption has been shown by experiment to be correct. If one flow condition is single-phase and the other two-phase or if both are two-phase then no such statement can be made. However, it must be noted that the existance of pressure measurement errors was first noted in the two-phase region. This is evidence of positive errors under both flow conditions. A second point is that the measured error at tap #14 is small (about 5 psi). It is therefore reasonable to assume that changes in the error would be even smaller. These agruments are not strong enough to conclusively state that no error is introduced by this effect, but, lacking direct evidence to the contrary, it has been assumed that pressure tap error remains constant or changes a negligible amount under both single-phase and two-phase flow conditions.

Consider now the uncertainty associated with the actual experimental measurements. The back pressure was measured on a calibrated 100 psi full scale pressure gauge with 1/4% accuracy. This accuracy is very satisfactory. More important are the measurements of temperature and pressure at tap #14. The temperature was measured using a Copper-Constantan thermocouple. Using an accurate Leeds and Northrup potentiometer it was possible to observe voltage changes of 0.005 millivolts, corresponding to temperature changes of 0.2°F. Absolute uncertainty was somewhat greater, being of the order of 0.4°F. Using a 100 psi gauge with an 8 1/2 inch diameter dial it was possible to read pressure changes to an accuracy of 0.1 psi while the absolute accuracy was probably more nearly the 0.25 psi rated by the manufacturer. It should be stressed that all instruments were periodically calibrated.

The pressure gauges were calibrated on a dead weight tester and the thermocouple unit was calibrated against a precision thermometer. As may be seen from Figure 23, an uncertainty of 0.2°F in the temperature measurement corresponds to an uncertainty of about 0.2 psi in the reference value of P_{14}. The quantity of interest in this study is the change in pressure at tap #14, ΔP_{14}. Both quantities involved in the calculation of ΔP_{14} should have the same uncertainty (0.3 psi) so the uncertainty in ΔP_{14} should be double this or about 0.5 psi.

Comparison of Experimental and Theoretical Results

Figure 24 shows the experimental data corresponding to the physical situation considered in some detail from a theoretical point of view in Chapter 2. The agreement between the theoretical and the experimental results is excellent. The theoretical curve shown in Figure 24 may be obtained directly from the solid curve in Figure 12. Pick some value of the back pressure and use this value to obtain y/D from Figure 12. At the location of tap #14 (y/D = 0.483) move up the curve the distance y/D which has been obtained above. The pressure change over this distance is ΔP_{14}. Note that the theoretical curve in Figure 24 becomes linear with a slope of unity corresponding to all single-phase flow at pressures above the saturation pressure.

In the theory used in Figure 24 a constant value of the heat transfer coefficient, h, was ultimately used. This conclusion was reached after a rather lengthy process of elimination. It was originally felt that the two-phase region might best be modeled as a liquid region containing fairly uniformly dispersed bubbles. As a result of this

thinking a no slip model was developed which assumed infinite friction between the phases. It was assumed that the slip and no slip models would represent the two limiting cases with the actual physical situation somewhere in between. For the no slip model the equations presented in Chapter 2 still apply except for the two momentum equations which must be replaced by the following equations.

$$V_g = V_\ell \tag{24}$$

$$P_o - P = \rho_\ell V_o (V_\ell - V_o) \tag{25}$$

The no slip model predicts a choking pressure as a result of calculations similar to those performed in Chapter 2. The no slip model predicts a pressure which is higher than that obtained from the slip model. For the physical situations considered in this report the choked pressure obtained from the no slip model exceeded that of the slip model by about 10 psi. For the specific case considered theoretically in Chapter 2 and experimentally in Figure 24 the critical pressure obtained from the no slip model was 32.5 psia as compared to the 22.4 psia for the slip model.

An inspection of the experimental data shown in Figure 24, in conjunction with the two choked pressure predictions, seemed to indicate that the no slip model was more nearly correct. Certainly to within the accuracy of the data, the value of ΔP_{14} is zero at 32.5 psia. As a result of this reasoning an attempt was made to find some reasonable variation of the parameter $h(dA_h/dx)$ which would explain the experimental data in Figure 24. If the no slip model is valid then the vapor phase must consist of a distribution of very small bubbles to provide sufficient interphase drag. Therefore as a start it was assumed that

the gas phase was made up of bubbles which could be characterized by some mean radius R. This assumption was used to obtain the following expression for dA_h/dx.

$$\frac{dA_h}{dx} = \frac{3A_g}{R} \tag{26}$$

R and h were assumed to be constant. Thus the functional form of $h(dA_h/dx)$ was determined. Once the functional form of this parameter is known, only the length of the two-phase region is required to determine its scale. Based on both visual observations and pressure measurements, the length of the two-phase region was known to be about 1/4 inch. $h(dA_h/dx)$ was scaled (by trial and error) to give solutions with about the correct length of the two-phase region. Predictions for ΔP_{14} did not agree at all with the experimental data. The predicted values of ΔP_{14} were essentially zero up to a back pressure of 55 psia on the scale plotted in Figure 24.

An analysis predicting the growth of a vapor bubble in a liquid with a time varying pressure was performed. (For the details of this analysis see Appendix A.) On the basis of this analysis it was concluded that the assumption of a constant h was incorrect. Even if the average bubble radius remained constant as assumed, the analysis in Appendix A indicated that h should vary as $T_\ell - T_g$. (This means that the heat transfer to the liquid vapor interface varies as $(T_\ell - T_g)^2$.) Using this assumption and Equation (26) for dA_h/dx a new prediction for ΔP_{14} was obtained. The results obtained were in even poorer agreement with the experimental data than the first attempt. The values of ΔP_{14} obtained from this model were less than

the much too small values obtained from the previous model.

In the first try considered above, $h(dA_h/dx)$ increases through the two-phase region as A_g. In the second try, $h(dh_h/dx)$ increases as $A_g(T_\ell - T_g)$ which is a faster increase than the first. Since the results obtained from the second try were worse than the first, it was concluded that what was needed was an $h(dA_h/dx)$ which varies less than A_g. One possible assumption is to assume this whole parameter to be constant. This assumption was made---still using the no slip model---and predictions for ΔP_{14} obtained. These results were encouraging in that they at least gave values of ΔP_{14} of the correct order of magnitude. The resulting theoretical curve which started from 32.5 psia with zero slope did not have the same shape as the experimental data.

At this point the no slip model was abandoned in favor of the slip model. A bubble model was also tried with this model, where Equation (26) was again assumed to be correct. A value of $h\,D/R = 3.6 \times 10^7$ Btu/(hr ft^2°F) gave 0.350 inches as the length of the two-phase region. The value of ΔP_{14} at 50 psia obtained from this solution was 0.0624 psi. On the basis of the data in Figure 24, this solution was discarded. A second try with this model using the value $hD/R = 1.8 \times 10^7$ Btu/(hr ft^2°F) resulted in $y_{max} = 0.492$ inches and $\Delta P_{14} = 0.19$ psi at a back pressure of 50 psia. From these results it was concluded that this model was not the correct one for the actual physical situation.

It was known on the basis of the calculations made with the no slip model that agreement with the data could be improved by allowing

less variation of h. It was assumed that $h(dA_h/dx)$ was a constant and the calculations were made using the slip model. As shown in Figures 24 through 33, this assumption gives excellent agreement with the experimental data. The question still remained as to why a constant value of $h(dA_h/dx)$ worked so well. A possible answer to this is that the effective area is nearly constant because the vapor phase remains in a very thin layer near the tube wall. This is supported by visual observations. Looking as much down the axis of the flow as possible, one can see that there exists a large core of liquid, containing no visible bubbles, beyond the start of the two phase region. Furthermore, it is possible that the heat transfer coefficient from the central liquid core to the thin region at the wall is constant. (A detailed model for this heat transfer process is considered in Appendix B.)

Having determined that the "slip" model with a constant value of $h(dA_h/dx)$ gave the best agreement with experimental data, it was necessary to run over a variety of cases in an attempt to learn how this interphase heat transfer coefficient varied with the flow parameters. As mentioned above, it is possible, at least in principle, to determine the magnitude of h solely from a measurement of the length of the two-phase region. However, it was not possible to determine experimentally this two-phase length accurately enough by visual observation. The first visible sign of the two-phase region is a jagged line running around the tube. Because of this the heat transfer coefficient was obtained by picking the value which gave the best fit with the experimental data. The heat transfer coefficient

was varied in steps of 18,000 Btu/(hr ft^2°F). An increase in h shifts the theoretical curve in Figure 24 downward to lower values of P_{14}.

Figures 25 and 26 show data for runs in which the upstream liquid velocity has been increased. The heat transfer coefficient for these runs shows the rather interesting behavior of decreasing with an increasing velocity. This is contrary to the behavior of most heat transfer coefficients in flow situations. A simple model was developed to predict the heat-transfer coefficient but it predicted an increase in h with the velocity and a decrease with temperature. Despite this incorrect result in the predicted functional form of the heat transfer coefficient, the model did produce numerical values of the correct order of magnitude and is presented in Appendix B.

Figures 27, 28, and 29 show the data obtained at an increased temperature, T = 139°F. Again the heat transfer coefficient decreases with increasing velocity. It also should be noted that h is increasing with the liquid temperature. The scatter of the data in some of these Figures is somewhat greater than the previous Figures but most of the points fall within the $\pm$ 0.5 psi accuracy estimate.

Figures 30, 31, 32, and 33 constitute a third set of data taken at another temperature (154°F). Again the velocity is varied over a range of values. A further increase of h with temperature may be noted. Although Figures 31 and 32 are best fitted with the same h, this is probably due to experimental error. The overall trend for these four curves is still a decreasing h as the velocity increases.

Figure 34 summarizes the values of the heat transfer coefficient determined experimentally from the various sets of data. There is obviously some uncertainty in the value of h but this is not too surprising in view of the 0.5 psi uncertainty in ΔP_{14}. As mentioned

previously, integral steps of 18,000 Btu/(hr ft^2°F) in the value of h were used to determine the best theoretical fit to the data. This value, therefore represents a minimum uncertainty. On Figures 24 and 30 the variation of the theoretical curve with the value of h is shown. These two Figures represent a high and a low value of h. It is concluded from these Figures the uncertainty in h is about ± 10%. This is very good considering the 0.5 psi uncertainty in ΔP_{14}.

The results of this section may be summarized as follows: The slip model together with the assumption of a constant heat transfer coefficient has been used in conjunction with experimental data to determine h. The results are self-consistent in that they predicted the correct length of the two-phase region which was measured independently. Also the assumption of constant h is consistent with the observed flow, which was made up of a liquid core surrounded by a vapor phase region. Although the data are not sufficiently accurate to conclude that $h(dA_h/dx)$ does not vary at all throughout the two-phase region, calculations with other possible models indicated that order of magnitude variations in h were inconsistent with experimental results. The constant heat transfer coefficient which gave the best fit has been determined from the experimental data to an accuracy of about 10%. This experimentally determined h was found to increase with upstream liquid temperature and decrease with upstream liquid velocity over the experimental range. The main result of the slip model without including the variable, x, was a prediction of the critical pressure, P_c. Although this pressure has not been measured directly the experimental data tend to support

the predicted value. Consider the data in Figures 24 through 33. Obviously the point at which ΔP_{14} no longer changes with back pressure is, on the basis of the data alone, no more than 20 psi higher than the line marked "Slip Model Choked Pressure". Even if the predicted choking pressure were in error by 20 psi it would still be a better approximation than just using the saturation pressure. However, the overall consistency of the theoretical model and the data provide further confidence in the model as a whole. Thus it would seem that the prediction of the critical pressure has been justified to within 20 psi by the data alone and to a value considerably less than that by the good agreement between the data and the rest of the theoretical predictions.

Chapter 4

COMMENTS ON OTHER DATA AND MODELS

Although there has been much work done in two-phase flow in recent years with no small amount of concentration on two-phase choking, there has been little or no concentration on the specific type of two-phase flow considered here. Much of the recent work in two-phase choked flow has been motivated by an interest in reactor safety. In particular, the goal has been to predict the flow of the cooling fluid out of a nuclear reactor should an accident occur. Thus most of the theoretical and experimental work that has been done has considered the choking of a two-phase mixture which initially is a two-phase mixture or a slightly subcooled liquid. In this study Run #43-B (Figure 29) had the minimum liquid dynamic pressure of 255 psi. This gave a stagnation pressure of 357 psia at the point of flashing. If the liquid had been accelerated isentropically to the saturation pressure there would have had to have been 112°F of subcooling. In the actual case there was considerable stagnation pressure loss in the long tube so that the actual subcooling was 136°F. All other tests reported were subcooled more than this 136°F.

Smith (17) published, in 1963, an extensive literature summary on choking two-phase flow in which he referenced 79 other works. None of these papers considered flashing and two-phase flow of a liquid with more than a few degrees of subcooling. The only work to come to the

attention of this author in which the problem of high velocity flashing flow has been treated is that of Brown (18). His work was largely experimental and consisted of taking pressure measurements in a convergent-divergent nozzle. Due to the differences in geometry between his experiments and those presented here, no quantitative comparisons are possible. He did observe flashing upstream of the throat with subsequent choking at the throat and a pressure drop in the divergent section. This is in agreement with the qualitative observations noted in Chapter 1 of this work.

Despite the fact that such a comparison is probably unfair to both models because of the different physical situations being modeled, some of the more common two-phase choking models are contrasted with the present model. The models in the literature which give the best agreement with the experimental data are those in which critical flow is modeled in terms of the local properties at the critical point. The problem remains of predicting critical pressure, etc., in terms of the upstream flow conditions.

One common way of predicting choking is to attempt to use the well known relation from gas dynamics as a starting point.

$$G^2 = -\left(\frac{\partial P}{\partial v}\right)_s \tag{27}$$

G is the mass flow per unit area and v the specific volume. A similar expression may be obtained from Equation(5) by writing it in the following form.

$$-dP = G^2 d\left[\frac{\rho_g V_g^2 A_g}{G^2 A} + \frac{\rho_\ell V_\ell^2 A_\ell}{G^2 A}\right] \tag{28}$$

If the expression in brackets is defined as being equal to the specific volume then Equation (28) is similar to Equation (27). The specific volume so defined is somewhat artificial in that it does not have any physical significance. Fauske (19) in an early paper took the derivative in Equation (28) at constant entropy to complete the analogy with gas dynamics. To evaluate this derivative he assumed thermal equilibrium between the phases and that the pressure gradient has a finite maximum at the choking point. The latter assumption leads to an expression for the velocity ratio in terms of the density ratio.

$$\left(\frac{V_g}{V_\ell}\right) = \left(\frac{\rho_\ell}{\rho_g}\right)^{1/2} \tag{29}$$

This expression minimized the momentum flux at the choking point.

Another development has been given by Moody (20). He assumes thermal equilibrium between the phases and constant energy and entropy flux at any section. This allows him to write the expression

$$G = G\,(h_o,\ s_o,\ K,\ P) \tag{30}$$

Where h_o and s_o are respectively the stagnation enthalpy and entropy and K is the so-called slip ratio (V_g/V_ℓ). He maximizes G by setting

$$\left(\frac{\partial G}{\partial K}\right)_P = 0 \tag{31}$$

and

$$\left(\frac{\partial G}{\partial P}\right)_K = 0 \tag{32}$$

The result of this operation is an expression similar to that of Fauske for the velocity ratio at choked conditions.

$$\left(\frac{V_g}{V_\ell}\right) = \left(\frac{\rho_\ell}{\rho_g}\right)^{1/3} \tag{33}$$

This model minimizes the kinetic energy flux.

The two models presented are typical of some of the models found in the literature in that they (1) contain somewhat arbitrary assumptions, (2) are not necessarily in argeement with each other, and (3) seem to work quite well. Typical data are presented with the mass flow per unit area plotted versus the critical pressure with the quality at the critical point as a parameter.

Using the present model and the typical case considered in Chapter 2, with $P_s = P_o = 69.6$ psia and $V_o = 180$ ft/sec, the slip ratio at choking obtained from Figure 6 is

$$V_g/V_\ell = 2.54 \tag{34}$$

Under these conditions the density ratio is 118. Equations (29) and (33) give

$$V_g/V_\ell = 10.85 \tag{35}$$

and

$$V_g/V_\ell = 4.91 \tag{36}$$

Thus there seems to be no agreement between these models and the model developed herein.

Lavoie (21) has developed a generalized one dimensional model for two-phase flow and has written conservation equations similar to those presented in Chapter 2. He defines the choking point to be that point at which a mathematical solution no longer exists. (That is derivatives with respect to x become infinite.) He assumes that

$d\frac{(\rho_g V_g A_g)}{dx}$ is not an explicit function of any derivative. This seems to be an invalid assumption. Using this assumption he obtained a fairly simple expression relating conditions at the choked point. It was felt that this technique might produce another simple expression using the equations in Chapter 2 and not making the assumption made by Lavoie. The calculation was carried out and the resulting expression was practically useless due to its algebraic complexity. Needless to say the agreement between the choked conditions predicted by Lavoie and the model presented here was poor.

Fauske (22) has recently developed a new model for two-phase choking based on emperical data obtained by measuring the void fraction and pressure of choking air-water flow. The semi-empirical equation that he suggested using to predict the slip ratio at choking is

$$K = 0.17X^{.18} \left(\frac{\rho_\ell}{\rho_g}\right)^{1/2} \tag{37}$$

Where X is the mass flow fraction of the vapor (quality). He stated that if Equation (37) gave values less than unity, then a slip ratio of one should be used. A value less than unity is obtained when conditions from Chapter 2 are substituted into Equation (35). Even though this value does not equal 2.54 it is closer than any of the earlier estimates. This is an empirical result and it is perhaps not surprising that it does not work well with Freon 114. More important than the specific result are the general conclusions which Fauske draws from his experimental data. He suggested that the high values of the slip ratio used in the earlier calculations coupled with the assumption of thermal equilibrium were both incorrect but that the effects canceled. Based

on the slip ratios which he calculated from measured void fractions, he concluded that the slip ratio must be smaller than previously used. To compensate for the lowered slip ratio he was forced to assume non-equilibrium conditions existed at the point of choking.

These conclusions which Fauske came to experimentally are in good agreement with the model developed in Chapter 2 in which thermal equilibrium was not assumed and calculated values of the slip ratio were much smaller than used in many models

Chapter 5

CONCLUSIONS

The test facility and the apparatus designed and constructed for this two-phase research operated in a satisfactory manner. A stainless steel test section with a plastic "window" was designed and constructed. This test section was shown to be very satisfactory in that it allowed simultaneous visual observation of the flow and accurate pressure measurements. Acrylic plastic was shown to be a poor substance in which to attempt accurate pressure measurements under conditions of high dynamic pressure. Pressure tap holes drilled through the plastic caused errors as large as 50 psi and these errors were not repeatable from day to day but changed significantly.

Stainless steel was demonstrated to be a good material from which to manufacture a test section containing pressure tap holes. With careful machining the pressure tap error in stainless steel was shown to be small and repeatable. A free jet technique was developed for calibration of pressure taps in a straight tube test section and all pressure taps were calibrated to an accuracy of about 1 psi.

The flow of high velocity flashing Freon 114 ($Cl_2F_4C_2$) in a straight tube has been studied. Particular emphasis has been placed on the two-phase pressure distribution and the choking of the flow. Based on the observation that the length of the two-phase region is very short (about one L/D in a 1/4 inch diameter tube) a model has been

developed which predicts the choking pressure with the upstream single-phase flow parameters as the only inputs. This model has been used to predict critical pressures over a wide range of conditions. Some approximations are made to simplify the thermodynamic state equations and are shown to give results in good agreement with results obtained using the much more complicated state equations. Some theoretical results for water are presented using these approximations.

The model was extended to include a relation between static pressure and length along the tube in terms of an interphase heat transfer coefficient. It was concluded that the two-phase region was too short and the pressure gradient too high to allow this region to be systematically studied with pressure taps directly in the region. To get around this problem a new technique was developed for studying the two-phase region. This technique allowed the pressure distribution in the two-phase region to be studied indirectly by varying the back pressure and looking at pressure changes upstream. It was concluded that a constant heat transfer coefficient gave the best agreement with experimental pressure measurements and simultaneously predicted the correct length for the two-phase region. The heat transfer coefficient was found experimentally to decrease with velocity and increase with temperature. The heat transfer coefficient was found to have a very high value, a typical value being 200,000 Btu/(hr ft^2°F). A simple model for predicting this heat transfer coefficient gave values in this same general range and therefore increased the level of confidence in the experimental results. This model is not useful for <u>accurate</u> calculations of the heat transfer coefficient. On the basis of visual

observations and also the fact that a constant heat transfer coefficient worked best, it was concluded that the gas phase may be confined to a very thin region near the tube wall.

The overall consistency of the data and the model provided a verification of the model proposed. Although it was impossible to measure the choking pressure directly, the data indicated that the predicted choking pressure did not differ from the actual choking pressure by more than a few psi.

Chapter 6

RECOMMENDATIONS FOR FUTURE WORK

One interesting follow-up to this work would be to run tests with fluids other than Freon 114. An interesting result of these tests would be the heat transfer coefficient as defined in this work. Experimental determination of this parameter using other fluids would perhaps lead to a clearer understanding of the basic nature of this heat transfer coefficient.

It would also be interesting to extend the liquid velocity range downward to determine the precise limits of the "slip" model proposed herein. If either of these suggested projects is undertaken and if the present method of data taking is used, it is suggested that more accurate values of the pressure change, ΔP_{14}, could be obtained by using two identical or nearly identical test sections in parallel. Very accurate differential pressure gauges are available commerically and could be used to measure ΔP_{14} directly by raising the back pressure at one test section and leaving the other choked. Flow variations from throttling one and not the other would be negligible.

It is also suggested that the results obtained here could be used as a logical starting point for studies of convergent-divergent nozzle flows. The heat transfer coefficients determined here could

be used in conjunction with the "slip" model to make an analytic study of the choked nozzle. This problem is more complicated than the straight tube problem because the total flow area, A, is now a function of length and therefore it is not possible to obtain any solution independent of length.

Appendix A

BUBBLE GROWTH IN A SUPERSATURATED LIQUID WITH A TIME VARYING PRESSURE

The problem of bubble growth in a superheated liquid subjected to a time varying external pressure is considered.

An asymptotic solution is obtained which covers most of the range of physical interest. The solution agrees very well with that obtained by other authors for the case of constant external pressure. The results should be useful in studying problems in which liquids are accelerated into the two-phase region.

Equilibrium thermodynamics predicts the amount of vapor present when a liquid near saturation is accelerated through a nozzle or an orifice. Experimentally, the predicted amount of vapor is not always present. This deviation from thermodynamic equilibrium is due to rate processes involved in the phase change from a liquid to a vapor.

Consider a small bubble which is growing in a superheated liquid. The vapor bubble has a finite radius which gives rise to a pressure drop across the bubble boundary due to surface tension. The bubble is growing and pushing the surrounding liquid out of the way. Thus, there is a radial pressure gradient, which balances the inertia forces in the liquid. Finally there must be heat transfer to the bubble. This increases the amount of vapor in the bubble, causing it to grow. These three things all cause the bubble to grow at a finite rate, and therefore depart from the equilibrium value.

The objective of this study was to investigate the bubble growth problem as a liquid is accelerated into a supersaturated state. It was hoped that this study would give a characteristic bubble growth time which could be compared to a characteristic flow time. The transition from single-phase flow to two-phase flow could then be more fully understood. The pressure variation with length may be transformed to the problem of bubble growth in a large sea of liquid in which the pressure is a function of time.

A number of people have investigated the growth of a bubble in a uniformly superheated liquid at constant pressure. Among these are Plesset and Zwick (3), Forster and Zuber (4), and Scriven (5). Each derivation is different, but all arrive at the same result for large time except for small differences in a numerical constant. These results are in excellent agreement with experimental data.

Isbin and Gavalas (23) treat the problem of bubble growth along a streamline of saturation liquid as it accelerates through an aperture. In their analysis the drop radius is neglected when writing the heat conduction equation. This approximation is shown by Zuber (24) to give an error of about 50% for the case of constant liquid pressure. They also introduce a power series which by their own admission is only accurate to within 15%. Because of these equations of accuracy, and also because their result could not be easily generalized to other pressure distributions, no attempt was made to modify the Isbin and Gavalas solution.

Bubble growth is assumed to occur in the following manner in a liquid accelerating the nozzle. The liquid contains small solid particles and/or non-condensible gas bubbles which serve as nucleation sites for the vapor bubbles to grow on. These particles are convected downstream until the liquid superheat is great enough to cause these particles to be in unstable equilibrium and begin to grow. Dergarabedian (6) has shown that this initial unstable radius must satisfy the following inequality:

$$\frac{4\,\sigma}{3(P_g - P_R)} \leq R_o \leq \frac{2\,\sigma}{P_g - P_R} \tag{A-1}$$

Once the bubble starts to grow the dynamics of the problem are controlled by the momentum and energy equations in the liquid with boundary conditions to be satisfied at the moving bubble surface. The momentum equation in the liquid is,

$$\frac{\partial u}{\partial t} + u\,\frac{\partial u}{\partial r} = -\frac{1}{\rho_\ell}\,\frac{\partial P}{\partial r} + \nu\left[\frac{1}{r}\,\frac{\partial^2 (ru)}{\partial r^2} - \frac{2u}{r^2}\right] \tag{A-2}$$

The continuity equation may be written in terms of the bubble radius as follows provided the density of the vapor phase is much smaller than the density of the liquid phase.

$$ur^2 = \text{constant} = \frac{dR}{dt}\,R^2 \tag{A-3}$$

Scriven (5) carries through the analysis for the case in which the liquid and vapor densities are of the same order or magnitude. A similar correction could be made to the results presented here.

Note that a combination of Eqns. (A-1) and (A-2) eliminates the viscous term entirely. Scriven (5) erroneously includes a viscous term by incorrectly operating on the stress tensor in spherical polar coordinates. This error is not serious since he later drops his viscous term by stating that it is small.

By using Eqn. (A-3) and integrating Eqn. (A-2) between R and infinity, the familiar Rayleigh equation results.

$$\frac{P_R - P_\infty}{\rho_\ell} = R\frac{d^2R}{dt^2} + 3/2\left(\frac{dR}{dt}\right)^2 \qquad \text{(A-4)}$$

Note that P_∞ may, in general, be a function of time.

Introducing the surface tension in Eqn. (A-4) gives

$$\frac{P_g - P_\infty}{\rho_\ell} = \frac{2\sigma}{\rho_\ell R} + R\frac{d^2R}{dt^2} + 3/2\left(\frac{dR}{dt}\right)^2 \qquad \text{(A-5)}$$

The energy equation in the liquid is

$$\frac{\partial T}{\partial t} + u\frac{\partial T}{\partial r} = \frac{\alpha}{r^2}\frac{\partial}{\partial r}\left(r^2\frac{\partial T}{\partial r}\right) \qquad \text{(A-6)}$$

Using Eqn. (A-3) the energy equation becomes

$$\frac{\partial T}{\partial t} + \frac{R^2}{r^2}\frac{dR}{dt}\frac{\partial T}{\partial r} = \frac{\alpha}{r^2}\frac{\partial}{\partial r}\left(r^2\frac{\partial T}{\partial r}\right) \qquad \text{(A-7)}$$

Using the first law of thermodynamics and the perfect gas law, for a control volume consisting of the vapor bubble, the following result is obtained.

$$4\pi R^2 k\left(\frac{\partial T}{\partial r}\right)_{r=R} = m_g c_{pg}\frac{dT_g}{dt} + h_{fg}\frac{dm_g}{dt} - V_g\frac{dP_g}{dt} \qquad \text{(A-8)}$$

This can be transformed, by using the perfect gas law, to the following:

$$4\pi R^2 k \left(\frac{\partial T}{\partial r}\right)_{r=R} = m_g \left(c_{pg} - \frac{h_{fg}}{T_g}\right) \frac{dT_g}{dt} + \overline{V}_g \left(\frac{h_{fg}}{RT_g} - 1\right) \frac{dP_g}{dt}$$

$$+ \frac{h_{fg}}{R_g T_g} \frac{d V_g}{dt} \qquad \text{(A-9)}$$

If the enthalpy of vaporization is much greater than $R\,T_g$ and $c_{pg}T_g$ then these terms may be dropped in the above equation. This assumption is consistant with the previous one, in which the vapor density was assumed to be small compared to the liquid density. Both of these assumptions are true only when the temperature and pressure are much below the critical temperature and pressure. Thus Eqn. (A-9) becomes,

$$4\pi R^2 k \left(\frac{\partial T}{\partial r}\right)_{r=R} = h_{fg} \frac{dm_g}{dt} \qquad \text{(A-10)}$$

The formulation of the problem is now complete except for the thermodynamic relation between the vapor pressure and the vapor temperature and the remaining boundary conditions. These boundary conditions are

$$t = 0 \quad R = R_o, \frac{dR}{dt} = 0 , \quad T = T_\infty$$

$$r \to \infty \quad T = T_\infty = \text{constant} \qquad \text{(A-11)}$$

Eqn. (A-7) is a non-linear partial differential equation. The rest of the equations are non-linear total differential equations. To reduce Eqn. (A-7) to a total differential equation an integral technique, similar to the boundary layer integral method in fluid mechanics, was used. A thermal boundary layer thickness, δ_t is assumed to exist in the liquid outside the vapor bubble. The temperature profile in the boundary layer is assumed to be

$$T - T_o = (T_\infty - T_o)\left[\frac{2\,(r - R)}{\delta} - \frac{(r - R)^2}{\delta}\right] \qquad \text{(A-12)}$$

It is convenient to define a new variable

$$\gamma = T_\infty - T_g \tag{A-13}$$

Combining Eqns. (A-7), (A-12), and (A-13) and integrating between R and R + δ gives

$$\frac{1}{\gamma}\frac{d\gamma}{dt}\left[1/3 + 1/6\,\frac{\delta}{R} + \frac{1}{30}\left(\frac{\delta}{R}\right)^2\right] + \frac{1}{\delta}\frac{d\delta}{dt}\left[1/3 + 1/3\left(\frac{\delta}{R}\right) + \frac{1}{10}\left(\frac{\delta}{R}\right)^2\right] + 1/R\,\frac{dR}{dt}\left[2/3 + 1/6\left(\frac{\delta}{R}\right)\right] = \frac{2\alpha}{\delta^2} \tag{A-14}$$

This can be simplified if $\delta < R$. This assumption will be justified later on in the paper.

$$\frac{2d\gamma}{\gamma} + \frac{2d\delta}{\delta} + \frac{4dR}{R} = \frac{12\alpha}{\delta^2}\,dt \tag{A-15}$$

Eqn. (A-15) can be integrated to give

$$\delta^2\,\gamma^2 R^4 = 12\,\alpha\,\int_0^t \gamma^2\,R^4 dt \tag{A-16}$$

Equations (A-4), (A-10), (A-12), (A-13), and (A-16) are now a set of non-linear total differential equations. Simple numerical techniques exist for solving this type of equations. However, further progress can be made by neglecting the derivatives of ρ_g compared with the derivative of R in Eqn. (A-10). This is physically reasonable since R changes by orders of magnitude while ρ_g changes only by a few percent. Eqn. (A-10) becomes

$$\rho_g\,h_{fg}\,\frac{dR}{dt} = k\left(\frac{\partial T}{\partial t}\right)_{r\,=\,R} = \frac{2k\gamma}{\delta} \tag{A-17}$$

Now Eqns. (A-16) and (A-17) may be combined and integrated to give an explicit expression for R in terms of γ. Combining these two equations and multiplying by R^2 gives

$$R^2\, dR = \frac{2k}{\rho_g\, h_{fg}\quad \sqrt{12\,\alpha}} \left[\frac{\gamma^2 R^4\, dt}{\int_0^t \gamma^2 R^4 dt}\right]^{1/2} \qquad \text{(A-18)}$$

The right hand side of Eqn. (A-18) is of the form $d\,u/u^{1/2}$ and may be integrated.

The final result is

$$R = \frac{2k}{\rho_g\, h_{fg}\, \sqrt{\alpha}} \left[\int_0^t \gamma^2\, dt\right]^{1/2} \qquad \text{(A-19)}$$

where the initial value of R has been neglected.

This result is valid only if the thermal boundary layer is less than the bubble radius. Mathematically, this condition is

$$\delta/R = \frac{\rho_g\, h_{fg}\alpha}{k\gamma} < 1 \qquad \text{(A-20)}$$

By making the above approximations, an explicit expression for the bubble radius as a function of the temperature difference (γ) has been obtained. To obtain this temperature difference, the vapor temperature T_g, must be related to P_g and Eqn. (A-5) solved for γ. Since T_g and P_g vary only slightly from the reference value, it would be convenient to use a relation similar to the Clapeyron relation. The Clapeyron relation is derived for a system in equilibrium in which surface tension effects are exactly zero. In this problem, surface tension forces may be a dominate term, so some modification seems to be necessary. However, Hatsopoulos and Keenan (25) show that the vapor pressure over a curved surface differs from that over a flat surface only by the difference in hydrostatic head of the vapor. The vapor density has already been

assumed small, so the ordinary Clapeyron relation for a system without surface tension effects may be applied to a system with surface tension to relate the pressure of the gas phase to the temperature. Plesset and Zwick (3) Forster and Zuber (4) and Scriven (5) all use the Clapeyron relation, but none of them adequately justify its use. The relation is

$$\Delta P = \frac{h_{fg}}{T_o (v_\ell - v_g)} \Delta T \approx \frac{\rho_{go} h_{fg}}{T_o} \Delta T \qquad \text{(A-21)}$$

Using the pressure at t = 0, P_o, and the saturation temperature at pressure P_o, T_o, as reference values, Eqn. (A-21) becomes,

$$P_o - P_g = \frac{\rho_{go} h_{fg}}{T_o} \left[T_o - T_g \right] \qquad \text{(A-22)}$$

Since P_∞ is a known function of time determined by the flow geometry, we may say,

$$P_\infty = P_o - F(t) \qquad \text{(A-23)}$$

A combination of Eqns. (A-5), (A-13), (A-22), and (A-23) gives the following:

$$\gamma = T - T_o - \frac{T_o \rho_\ell}{\rho_{go} h_{fg}} \left[- \frac{F(t)}{\rho_\ell} + \frac{2\sigma}{\rho_\ell R} + R \frac{d^2R}{dt^2} + 3/2 \left(\frac{dR}{dt}\right)^2 \right] \qquad \text{(A-24}$$

Forster and Zuber (4) have shown that the inertia forces in the above equation are so small as to be negligible over the whole range of bubble radii. The surface tension forces are important until R = 10 R_o, but are negligible after that. Thus in the limit for large time Eqns. (A-19) and (A-24) may be solved for R in terms of known quantities. The result is

$$R = \frac{2k}{\rho_{go}\, h_{fg} \sqrt{\alpha}} \left[\int_0^t \left(\frac{F(t)\, T_o}{\rho_{go}\, h_{fg}} + T_\infty - T_o \right)^2 dt \right]^{1/2} \qquad \text{(A-25)}$$

For the case of constant P_∞, F(t) is zero and Eqn. (A-25) becomes,

$$R = \frac{2k\, (T_\infty - T_o)\, t^{1/2}}{\rho_{go}\, h_{fg} \sqrt{\alpha}} \qquad \text{(A-26)}$$

This result is in excellent agreement with the results of Plesset and Zwick (3) and Scriven (5), who obtained

$$R = 2\sqrt{\frac{3}{\pi}}\, \frac{k\, (T_\infty - T_o)\, t^{1/2}}{\rho_{go}\, h_{fg} \sqrt{\alpha}} \qquad \text{(A-27)}$$

Forster and Zuber (4) obtained

$$R = \sqrt{\pi}\, \frac{k\, (T_\infty - T_o)\, t^{1/2}}{\rho_{go}\, h_{fg} \sqrt{\alpha}} \qquad \text{(A-28)}$$

A solution was also obtained by using a linear temperature profile in the thermal boundary layer. This result was:

$$R = 2 \sqrt{\frac{3}{4}}\, \frac{k}{\rho_{go}\, h_{fg} \sqrt{\alpha}} \left[\int_0^t \left(\frac{F(t)\, T_o}{\rho_{go}\, h_{fg}} + T_\infty - T_o \right)^2 dt \right]^{1/2} \qquad \text{(A-29)}$$

If Eqn. (A-27) is assumed to be the exact asymtotic solution for the constant pressure case, then Eqn. (A-26) is in error by 1.6% and Eqn. (A-29) is in error 12% (for F(t) equal to zero). The error is greater for the linear temperature profile, as might be expected, but is still not large enough to cast any doubts on the integral method of solution. Since the integral technique gives results very close to the solution for P_∞ a constant obtained by three different methods and authors, it is concluded that Eqn. (A-25) is a valid solution for F(t) non-zero. As stated earlier, Eqns. (A-27) and (A-28) are in excellent agreement with available data.

APPENDIX B

Approximate Model for Interphase Heat Transfer Coefficient

In order to theoretically justify the seemingly high value of the interphase heat transfer coefficient determined experimentally in the main body of this report, an approximate analysis is presented here. Assume that the flow consists of a circular core of liquid surrounded by a vapor annulus as shown in Figure 2. The shear at the liquid-vapor interface is assumed to be zero and the axial velocity is constant at any section in the liquid. There is an heat flow from the liquid core to the liquid-vapor interface. The temperature at the interface is assumed to be the local saturation temperature.

The continuity equation in the liquid is

$$\frac{\partial(rv)}{\partial r} + r\frac{dV_\ell}{dx} = 0 \qquad \text{(B-1)}$$

V_ℓ is the liquid velocity in the x-direction and is a function of x only and v is the radial velocity.

Neglecting axial heat conduction, the energy equation may be written as follows:

$$V_\ell \frac{\partial T}{\partial x} + v\frac{\partial T}{\partial r} = \frac{\alpha_{eff}}{r}\frac{\partial}{\partial r}\left(r\frac{\partial T}{\partial r}\right) \qquad \text{(B-2)}$$

α_{eff} is an effective turbulent thermal diffusivity.

To approximately solve the above equation, an integral method was used. The following secord order temperature profile was assumed

to exist in a thin thermal boundary layer in the liquid.

$$T = T_g - (T_o - T_g)\left[2\left(\frac{r - R_\ell}{\delta}\right) + \left(\frac{r - R_\ell}{\delta}\right)^2\right] \tag{B-3}$$

Equation (B-3) may be substituted into Equation (B-2) and, using Equation (B-1), integrated from $R_\ell - \delta$ to R_ℓ. After a considerable amount of algebraic manipulation, the following result is obtained.

$$(T_o - T_g)\frac{d}{dx}\left(\frac{V_\ell R_\ell^2}{2}\right) + \frac{d}{dx}\left[V_\ell T_g\left(1/3\, R_\ell\delta - \frac{\delta^2}{12}\right)\right] = -\frac{2\,\alpha_{eff}\, R_\ell (T_o - T_g)}{\delta} \tag{B-4}$$

The heat transfer dq shown in Figure 2 is given by

$$dq = -k_{eff}\left(\frac{\partial T}{\partial r}\right)_{r=R_\ell} 2\pi R_\ell dx = 4\, k_{eff}\frac{(T_o - T_g)}{\delta}\,\pi\, R_\ell dx \tag{B-5}$$

Using the control volume in Figure 2, a second expression for dq may be obtained.

$$dq = \rho_\ell V_\ell A_\ell h_\ell^o - \rho_\ell V_\ell A_\ell h_\ell^o - d(\rho_\ell V_\ell A_\ell h_\ell^o) + h_\ell^o(T_g)\, d\,(\rho_\ell V_\ell A_\ell)$$

$$= -\rho_\ell V_\ell A_\ell d(h_\ell^o) - C_\ell(T_\ell - T_g)\, d\,(\rho_\ell V_\ell A_\ell) \tag{B-6}$$

This differs from the expression obtained in Chapter 2 because, in this case, the liquid being evaporated leaves the control volume at temperature T_g. This difference is not important since this term is negligible compared to the first.

Combining Equations (B-4), (B-5), and (B-6) and neglecting δ/R_ℓ with respect to unity gives

$$(T_o - T_g)\ d\ (V_\ell A_\ell) + 2/3\ d(V_\ell A_\ell T_g \delta/R_\ell) = \frac{V_\ell A_\ell d(h_\ell^o)}{c_\ell}$$

$$+ (T_\ell - T_g)\ d\ (V_\ell A_\ell) \qquad \text{(B-7)}$$

The enthalpy change dh_ℓ^o may be approximated as $c_\ell dT_\ell$. Using this Equation (B-7) becomes

$$2/3\ d\ [V_\ell A_\ell (T_g - T_o)\delta/R_\ell] = d[V_\ell A_\ell (T_\ell - T_o)] \qquad \text{(B-8)}$$

This may be integrated to give

$$\frac{\delta}{R_\ell} = \frac{3(T_o - T_\ell)}{2(T_o - T_g)} \qquad \text{(B-9)}$$

Note that T_ℓ is the average liquid temperature obtained by averaging over the liquid core region, which is at temperature T_o, and the boundary layer region, with the temperature given by Equation (B-3).

From the definition of h and Equation (B-5) the following relation is obtained

$$dq = h(T_\ell - T_g)\pi D\ dx = 4\ k_{eff}\ \frac{(T_o - T_g)\pi R_\ell}{\delta}\ dx \qquad \text{(B-10)}$$

It may be assumed that $(T_\ell - T_g) = (T_o - T_g)$. Inspection of Figure 5 shows that this is a good assumption. Thus the value of h is obtained by combining Equations (B-9) and (B-10)

$$h = \frac{8\ k_{eff}\ (T_o - T_g)}{3\ D\ (T_o - T_\ell)} \qquad \text{(B-11)}$$

In Chapter 3 it was found that a constant value of h gave good agreement with experimental data. Equation (B-11) is in good agreement

with this observation. k_{eff} should remain constant as the central liquid core changes little throughout the two-phase region. The ratio of the two temperature differences is nearly constant, as may be seen from Figures 4 and 5. Both the numerator and the denominator are nearly straight lines, making the ratio nearly constant.

Since it is possible to calculate the temperature difference ratio appearing in Equation (B-11) from the slip model developed in Chapter 2, it is only necessary to determine the value of k_{eff} in order to predict the heat transfer coefficient, h. In order to get some numbers out of Equation (B-11), it was assumed that the ratio of k_{eff} to k was the same as the ratio of the Nusselt number for turbulent pipe flow to the Nusselt number for laminar flow. Rohsenow and Choi (2) give a value of 4.36 for the Nusselt number in fully developed laminar flow with a uniform heat flux. For the turbulent flow the McAdams correlation was used

$$Nu = 0.023\ (Rey)^{.8}\ (Pr)^{.4} \qquad (B\text{-}12)$$

The Reynolds number in this expression was evaluated in the single phase region ahead of the actual two-phase flow.

Thus the following expression was used to obtain k_{eff}

$$\frac{k_{eff}}{k} = \frac{Nu}{4.36} \qquad (B\text{-}13)$$

This expression used in conjunction with Equation (B-11) produced values of h which were of the same order of magnitude as

those found experimentally. However, the predicted values of h increased when the experimentally determined values decreased. Typical results are summarized in Table 7.

TABLE 7

Comparison of Predicted and Experimentally Determined Interphase Heat Transfer Coefficient

V_o, ft/sec	180	234	170	179	234
T_o, °F.	127	127	154.5	154.5	154.5
Figure Number	24	26	30	31	33
Reynolds Number x 10^{-6}	1.68	2.63	1.96	2.06	2.70
Prandtl Number	6.42	6.42	5.73	5.73	5.73
$(T_o - T_g)/(T_o - T_\ell)_{min}$	112	195	51.3	57.2	101
$(T_o - T_g)/(T_o - T_\ell)_{max}$	210	423	100.5	114.7	223
h_{exp}, Btu/(hr ft^2 °F) x 10^{-3}	180	126	378	306	252
h_{min}, Btu/(hr ft^2 °F) x 10^{-3}	416	1048	184	214	465
h_{max}, Btu/(hr ft^2 °F) x 10^{-3}	818	2275	360	429	1026

Since the theoretical model did not correctly predict the variation of h, further calculations were made to see where the model failed. Immediately suspect is the method used to determine k_{eff}. A possible approach is to calculate k_{eff} from the experimentally determined h and see if the resulting values make sense. This was done using the numerical values in Table 7. The non-dimensional parameter k_{eff}/k was found to decrease with increasing Reynolds number and also with increasing Prandtl number. This is opposite the behavior that was expected.

Because of this apparent inconsistency no further attempts were made to modify the theoretical model. It is possible that the model does not correspond to the actual physical situation closely enough to produce predictions in agreement with the data.

Thus a model has been developed which predicts values of h of the same order of magnitude as those found experimentally. This increases the level of confidence in the experimental heat transfer coefficient. The model is not sufficiently accurate to be used for actual predictions of the interphase heat transfer coefficient.

Appendix C

BIOGRAPHICAL SKETCH

The author, John W. Murdock, was born on 29 July 1941 and lived in Beaver, Utah, until 1957. He then moved to Southern California and he graduated from Redlands High School in June 1959.

He entered the Massachusetts Institute of Technology as a freshman in September 1959. During his undergraduate career he was elected to membership in Pi Tau Sigma, Sigma Xi, and Tau Beta Pi. He was a member of the Undergraduate Honors Course in Mechanical Engineering and received his Bachelor and Master of Science degrees in February 1964.

During 1963-64, he held a Visking Company fellowship in Mechanical Engineering. Since that time he has been a Research Assistant in Mechanical Engineering at the Massachusetts Institute of Technology. He received the Mechanical Engineer degree in June 1965.

BIBLIOGRAPHY

1. Shaw, R., "The Influence of Hole Dimensions on Static Pressure Measurements," Journal of Fluid Mechanics, 1960, 7, 550-60.

2. Rohsenow, W. M. and Choi, H. Y., Heat, Mass, and Momentum Transfer, Englewood Cliffs, N. J.: Prentice-Hall, Inc., 1961.

3. Plesset, M. S. and Zwick, S. A., "The Growth of Vapor Bubbles in Superheated Liquids," Journal of Applied Physics, 1954, 25, 493-500.

4. Forster, H. K. and Zuber, N., "Growth of a Vapor Bubble in a Superheated Liquid," Journal of Applied Physics, 1954, 25, 474-478.

5. Scriven, L. E., "On the Dynamics of Phase Growth," Chemical Engineering Science, 1959, 10, 1-13.

6. Dergarabedian, P., "Observations on Bubble Growth in Various Superheated Liquids," Journal of Fluid Mechanics, 1960, 9, 39-48.

7. Chao, B. T., "Motion of Spherical Gas Bubbles in a Viscous Liquid at Large Reynolds Numbers," The Physics of Fluids, 1962, 5, 69-79.

8. Schlichting, H., Boundary Layer Theory, New York, N. Y.: McGraw-Hill Book Company, Inc., 1962.

9. "New General Equations," Freon Products Division, E.I. du Pont de Nemours and Company, Wilmington, Delaware, Bulletin X-88B, March 1966.

10. "Thermodynamic Properties of Freon-114," Freon Products Division, E.I. du Pont de Nemours and Company, Wilmington, Delaware, Bulletin T-114D.

11. Bergles, A. E. and Rohsenow, W. M., "The Determination of Forced-Convection Surface-Boiling Heat Transfer," Transactions of the ASME, Journal of Heat Transfer, Paper No. 63-HT-22, 1963.

12. "Surface Tension of the Freon Compounds," Freon Products Division, E.I. du Pont de Nemours and Company, Wilmington, Delaware, Technical Bulletin D-27.

13. Crandall, S. H., Engineering Analysis -- A Survey of Numerical Procedures, New York, N. Y.: McGraw-Hill Book Comapny, Inc., 1956.

Bibliography (continued)

14. Downing, R. C., "Transport Properties of Freon Fluorocarbons," Freon Products Division, E.I. du Pont de Nemours and Company, Wilmington, Delaware, Technical Bulletin C-30, 1965.

15. Deissler, R. G., "Turbulent Heat Transfer and Friction in the Entrance Regions of Smooth Passages," Transactions of the ASME, 1955, 77, 1221-33; also NACA Tech. Note. 3016.

16. Hartnett, J. P., "Experimental Determination of the Thermal Entrance Length for the Flow of Water and Oil in Circular Pipes," Transactions of the ASME, 1955, 77, 1211-20.

17. Smith, R. V., "Choking Two-Phase Flow Literature Summary and Idealized Design Solutions for Hydrogen, Nitrogen, Oxygen, and Refrigerants 12 and 11," National Bureau of Standards Tech. Note 179, 1963.

18. Brown, R. A., "Flashing Expansion of Water Through A Converging-Diverging Nozzle," University of California, Lawrence Radiation Laboratory, UCRL-6665-T, 1961.

19. Fauske, H. K., "Critical Two-Phase Steam-Water Flows," Proc. Heat Transfer and Fluid Mech. Inst., Stanford University Press, Stanford, California, 1961.

20. Moody, F. J., "Maximum Two-Phase Vessel Blowdown from Pipes," Transactions of the ASME, Journal of Heat Transfer, Paper No. 65-WA/HT-1, 1965.

21. Lavoie, G. A., "One Dimensional, Non-Equilibrium, Compressible, Two Phase Gas-Liquid Flow," M.S. Thesis, Massachusetts Institute of Technology, 1965.

22. Fauske, H. K., "Two-Phase Two-and One-Component Critical Flow," Symposium on Two-Phase Flow, University of Exeter, England, 21-23 June 1965, Vol. I, pp. G101-14.

23. Isbin, H. S. and Gavalas, G. R., "Two-Phase Flow Through an Aperture," NSA 16-20615, 1962.

24. Zuber, N., "Hydrodynamic Aspects of Boiling Heat Transfer," AECU 4439, 1959.

25. Hatsopoulos, G. N. and Keenan, J. H., Principles of General Thermodynamics, New York, N. Y.: John Wiley and Sons, Inc., 1965.

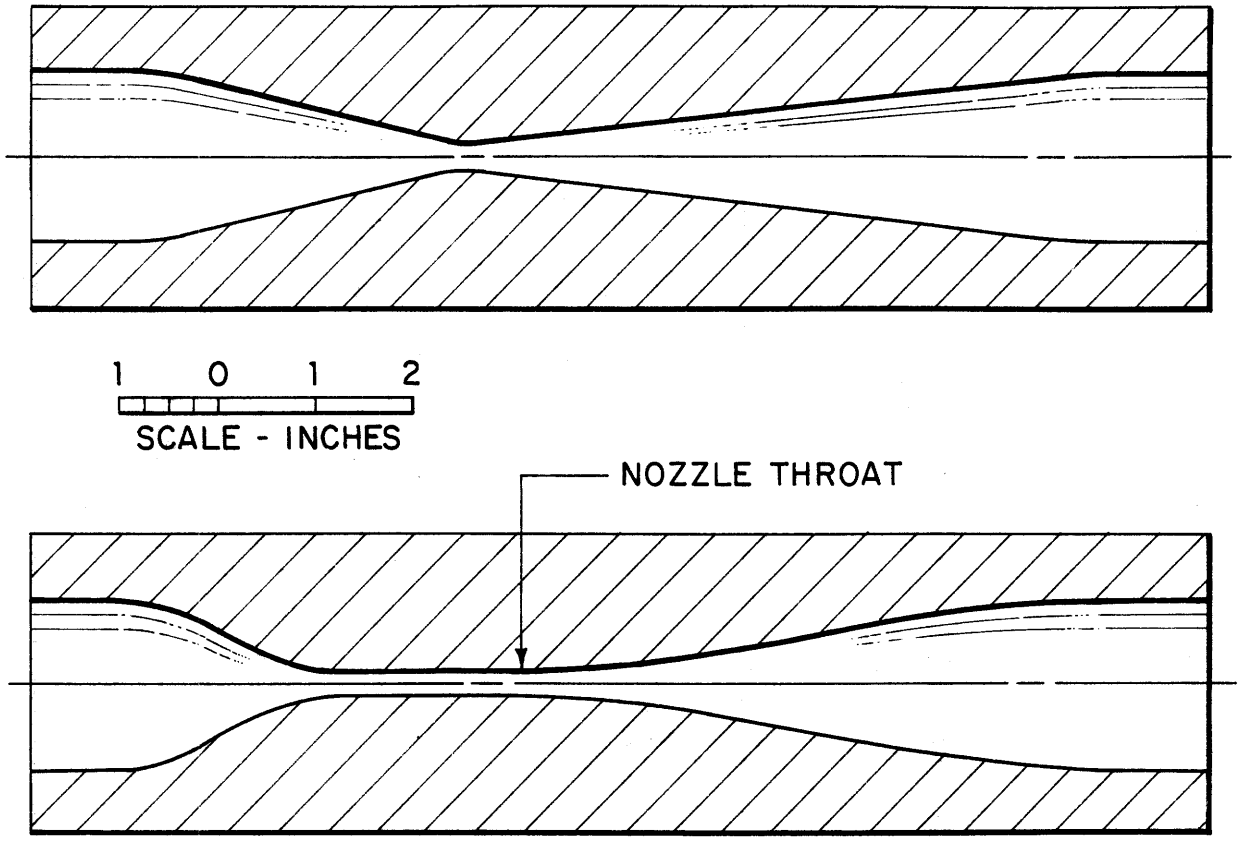

NOTE: FLOW DIRECTION FROM LEFT TO RIGHT

FIG. 1 CONVERGENT-DIVERGENT NOZZLES USED FOR PRELIMINARY TESTING

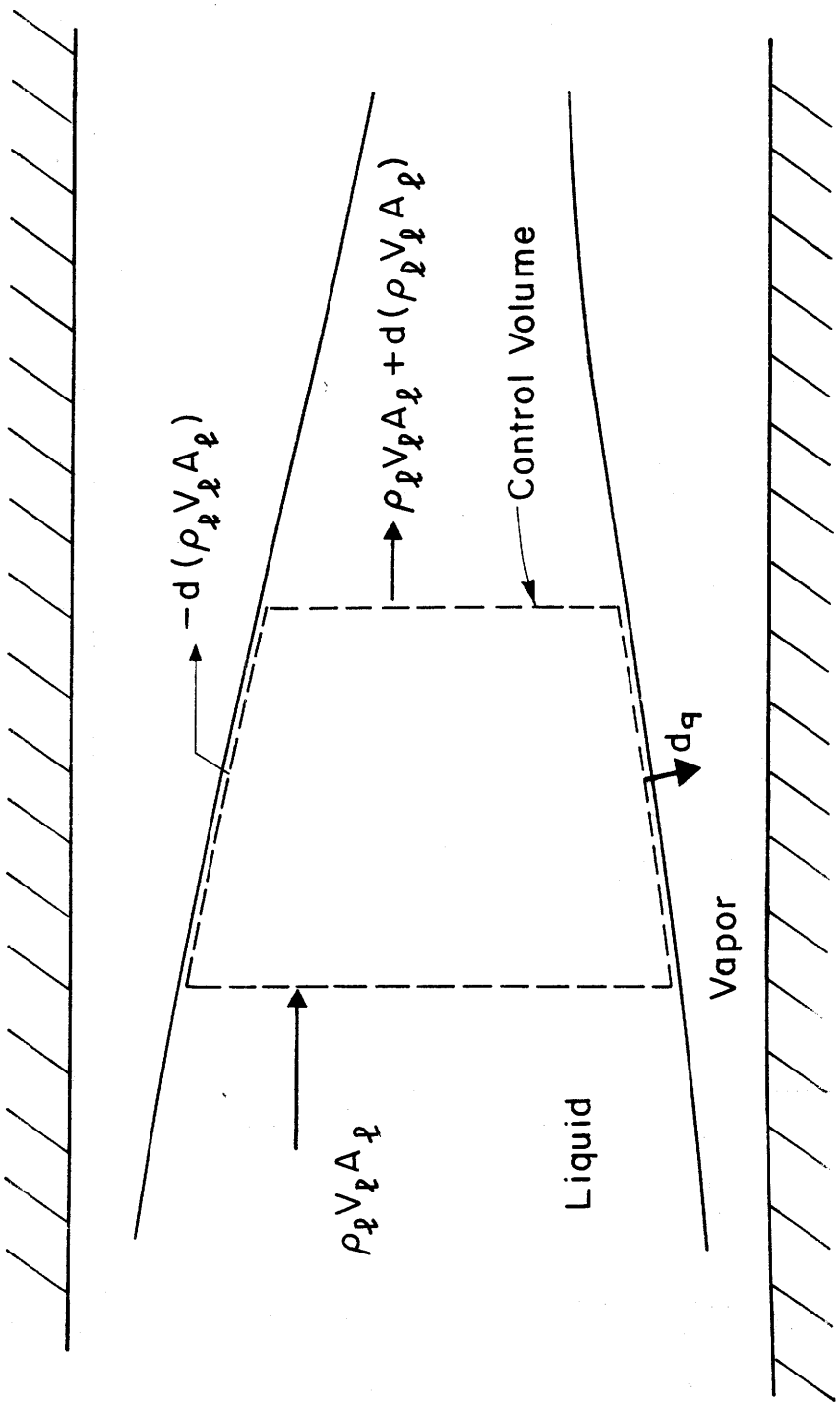

FIG. 2 CONTROL VOLUME FOR LIQUID PHASE

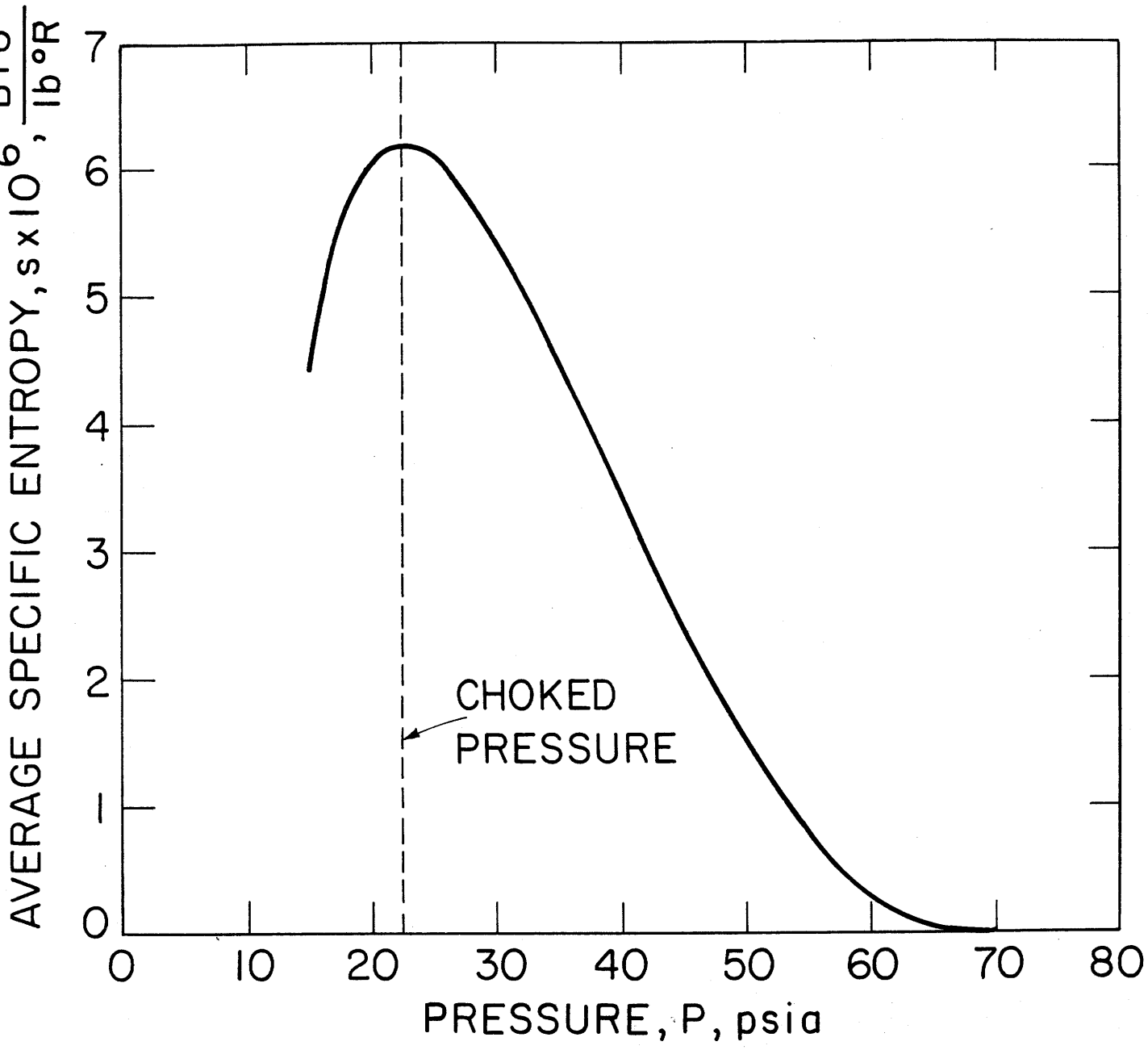

FIG. 3 AVERAGE SPECIFIC ENTROPY VERSUS ABSOLUTE PRESSURE

$P_s = P_0 = 69.6$ psia $\quad V_0 = 180$ ft/sec

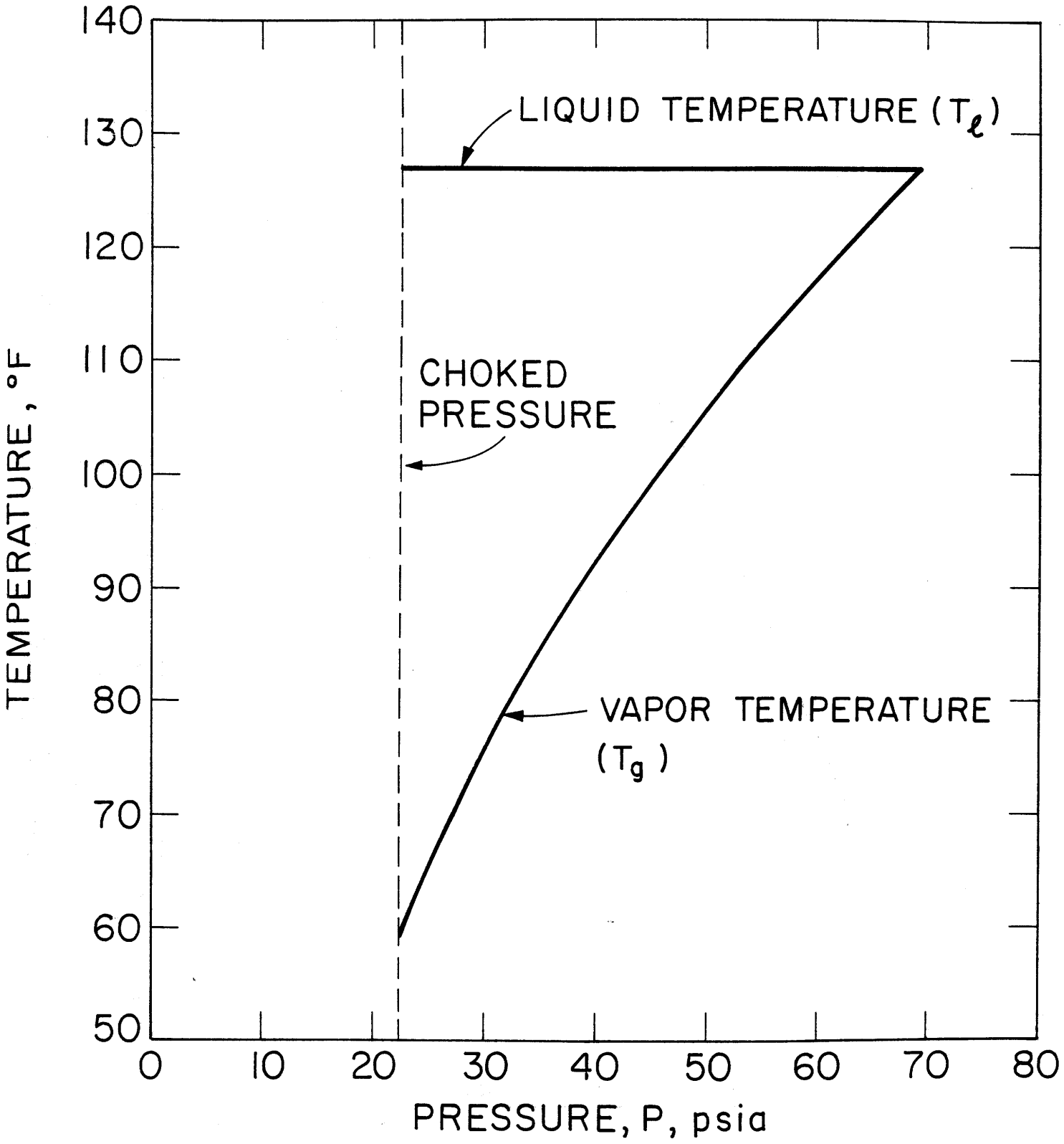

FIG. 4 TEMPERATURE VERSUS ABSOLUTE PRESSURE

$P_s = P_0 = 69.6$ psia $\quad V_0 = 180$ ft/sec

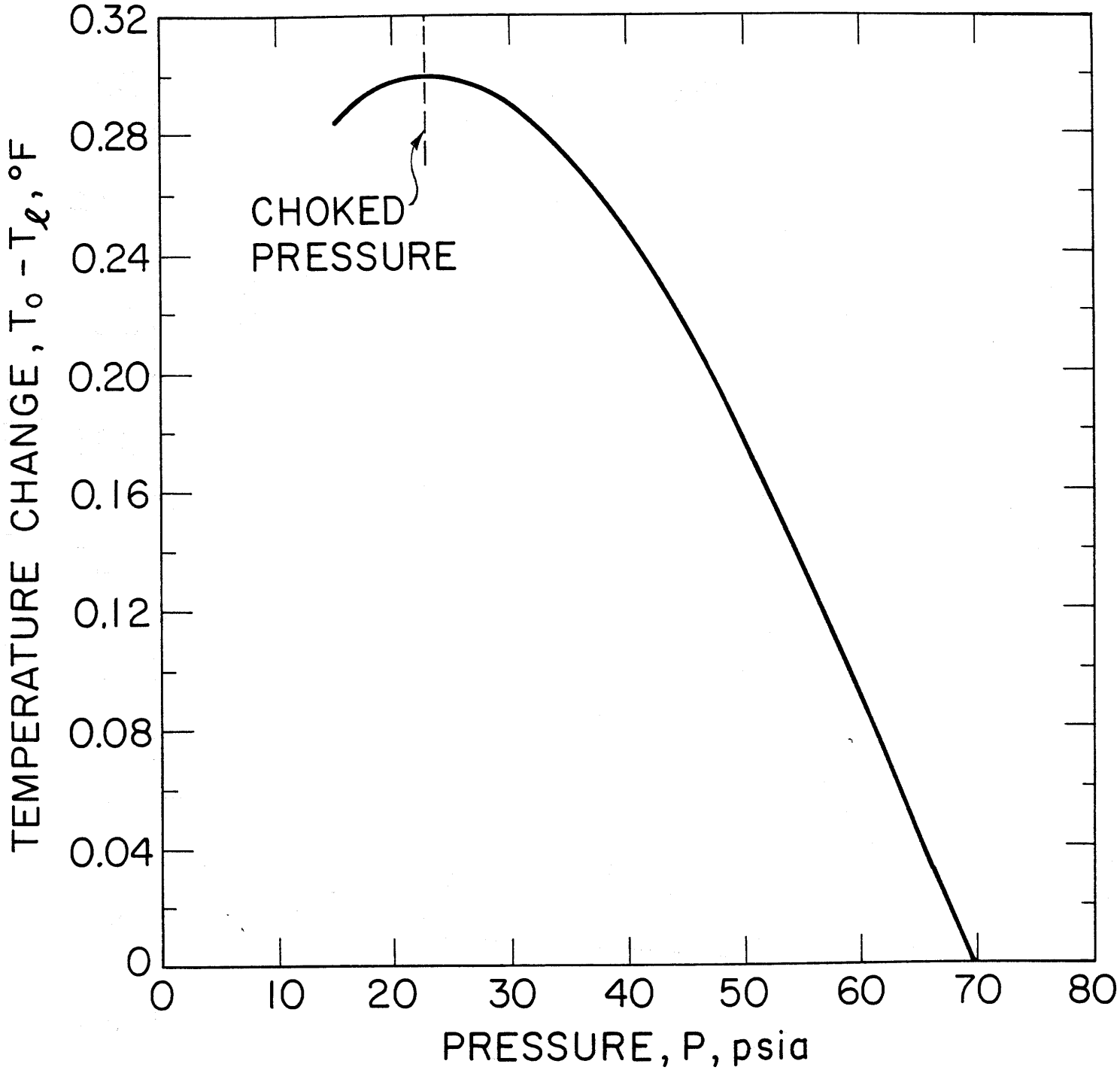

FIG. 5 LIQUID TEMPERATURE CHANGE VERSUS ABSOLUTE PRESSURE

$P_s = P_0 = 69.6$ psia $V_0 = 180$ ft/sec

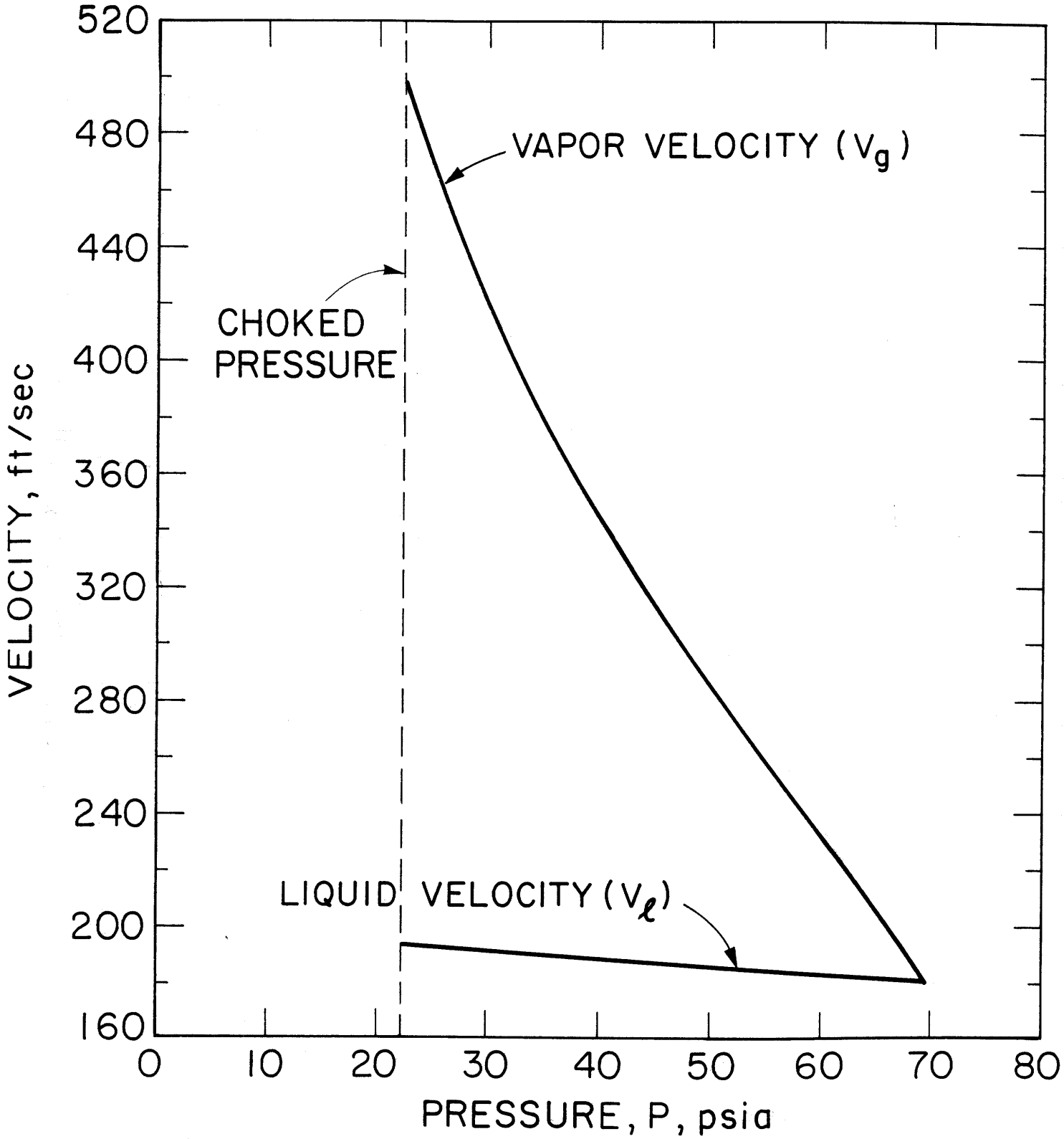

FIG. 6 VELOCITY VERSUS ABSOLUTE PRESSURE

$P_s = P_0 = 69.6$ psia $\qquad V_0 = 180$ ft/sec

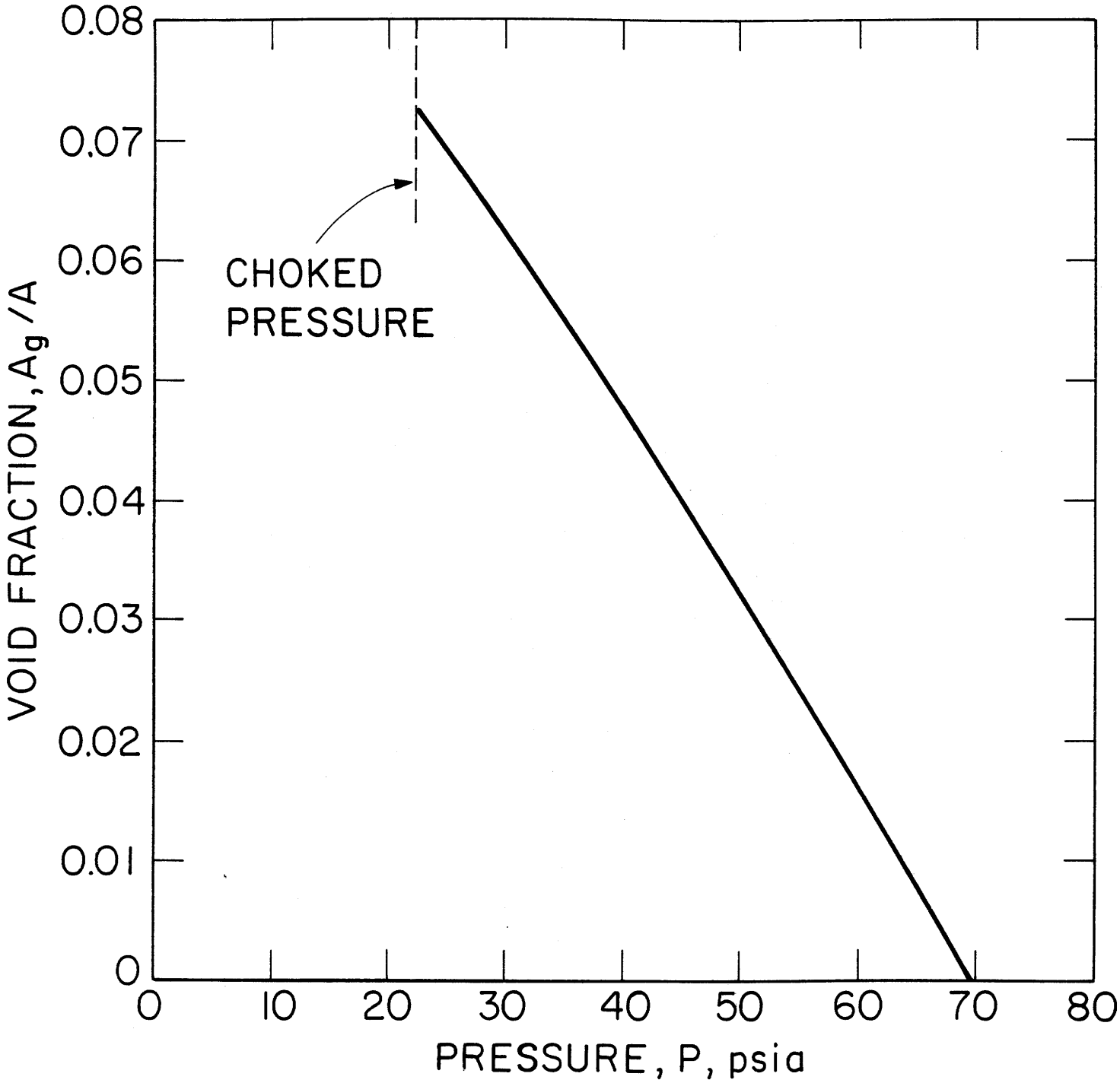

FIG. 7 VOID FRACTION VERSUS ABSOLUTE PRESSURE

$P_s = P_0 = 69.6$ psia $\quad V_0 = 180$ ft/sec

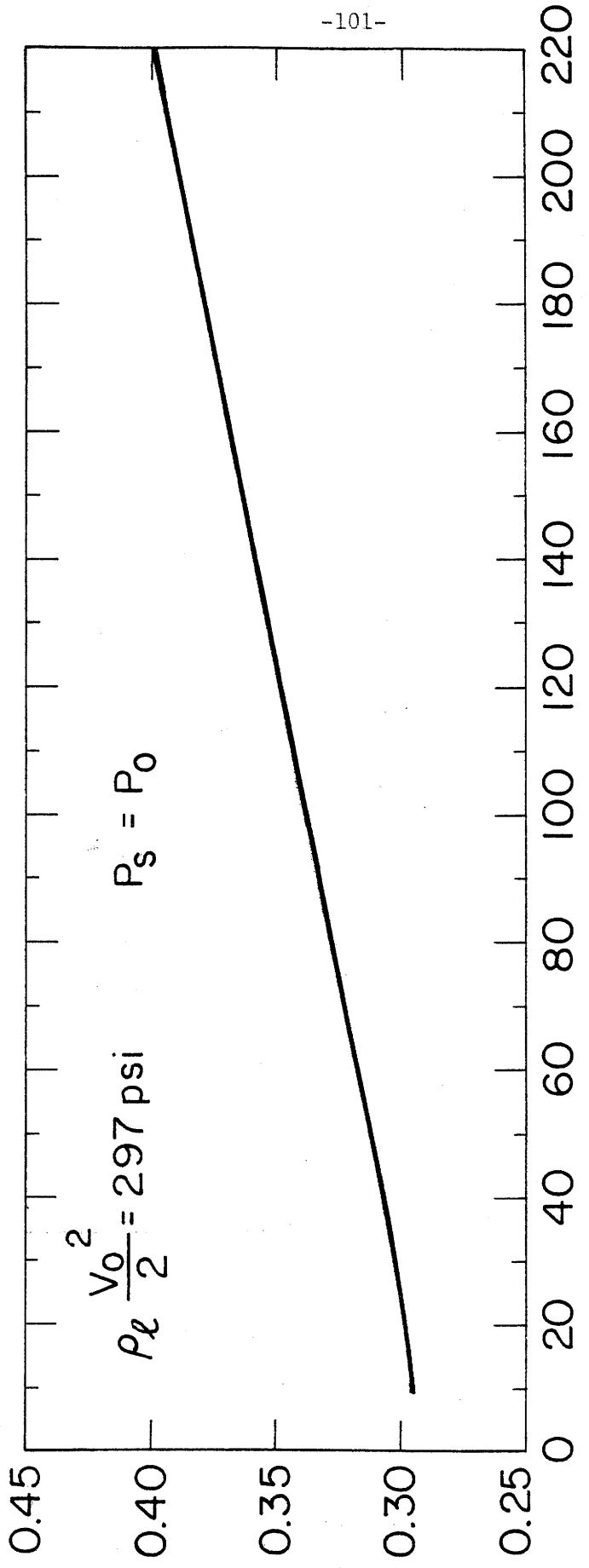

FIG. 8 VARIATION OF CRITICAL PRESSURE RATIO WITH SATURATION PRESSURE

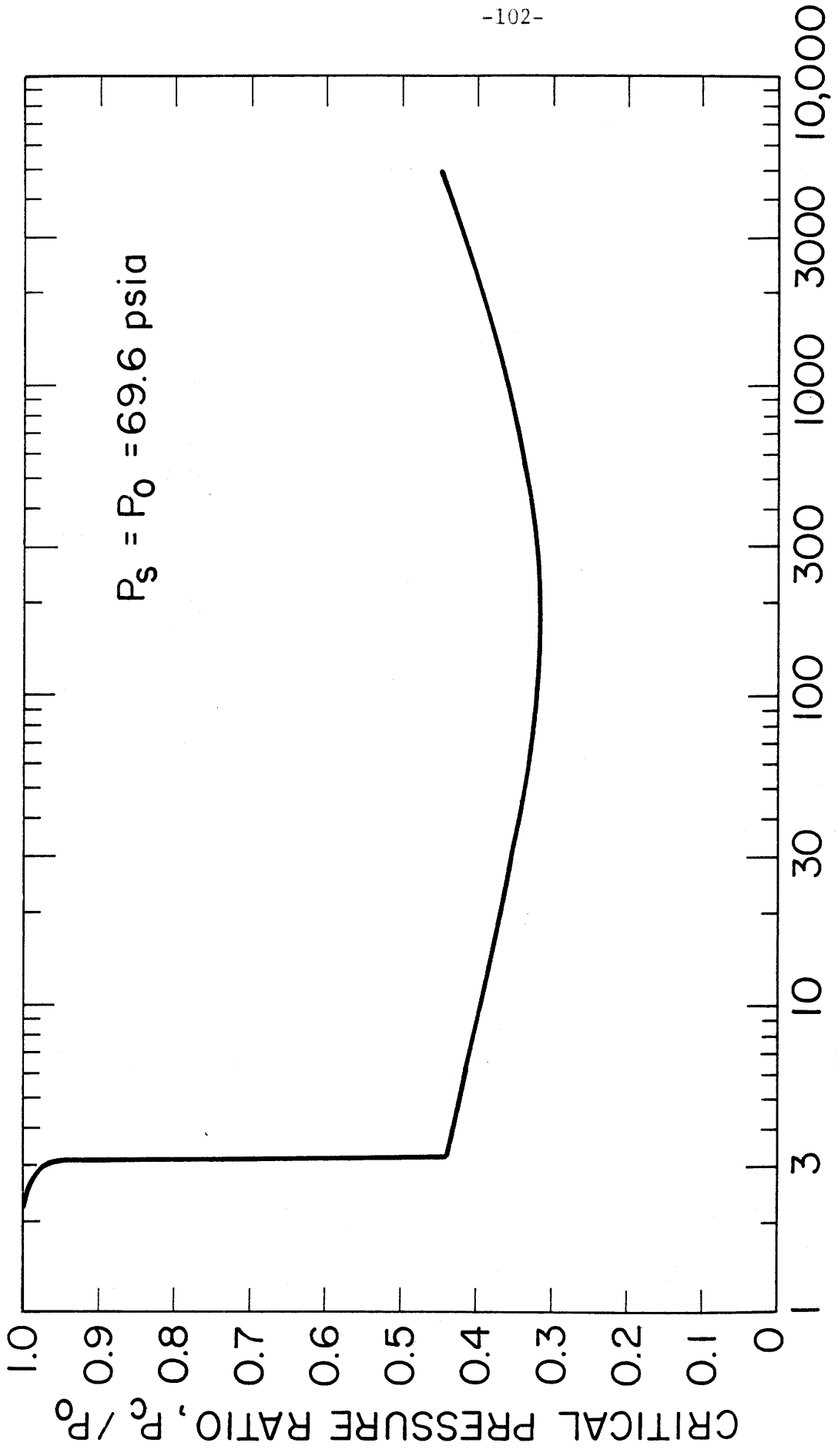

FIG. 9 VARIATION OF CRITICAL PRESSURE RATIO WITH LIQUID DYNAMIC PRESSURE

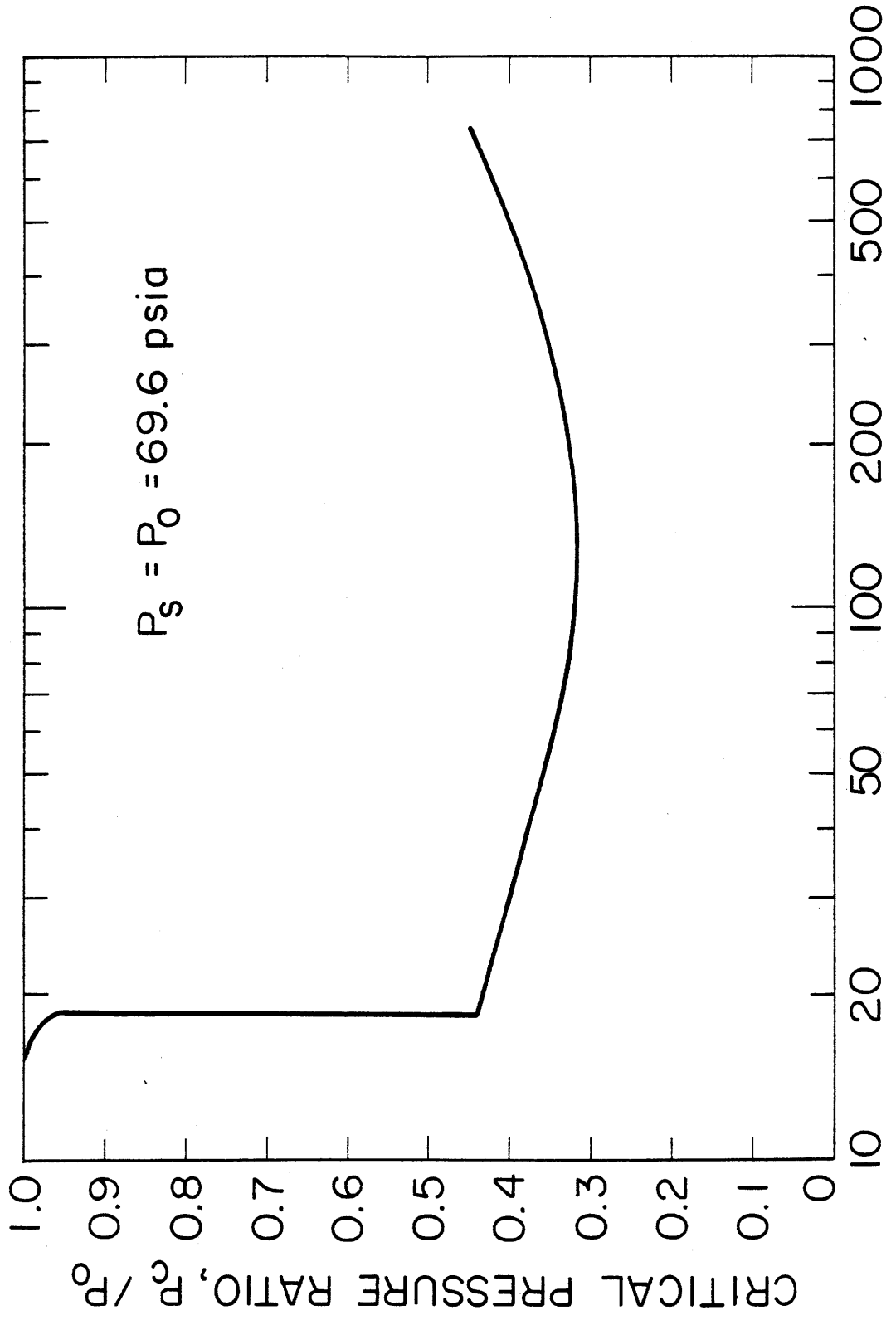

FIG. 10 VARIATION OF CRITICAL PRESSURE RATIO WITH LIQUID VELOCITY

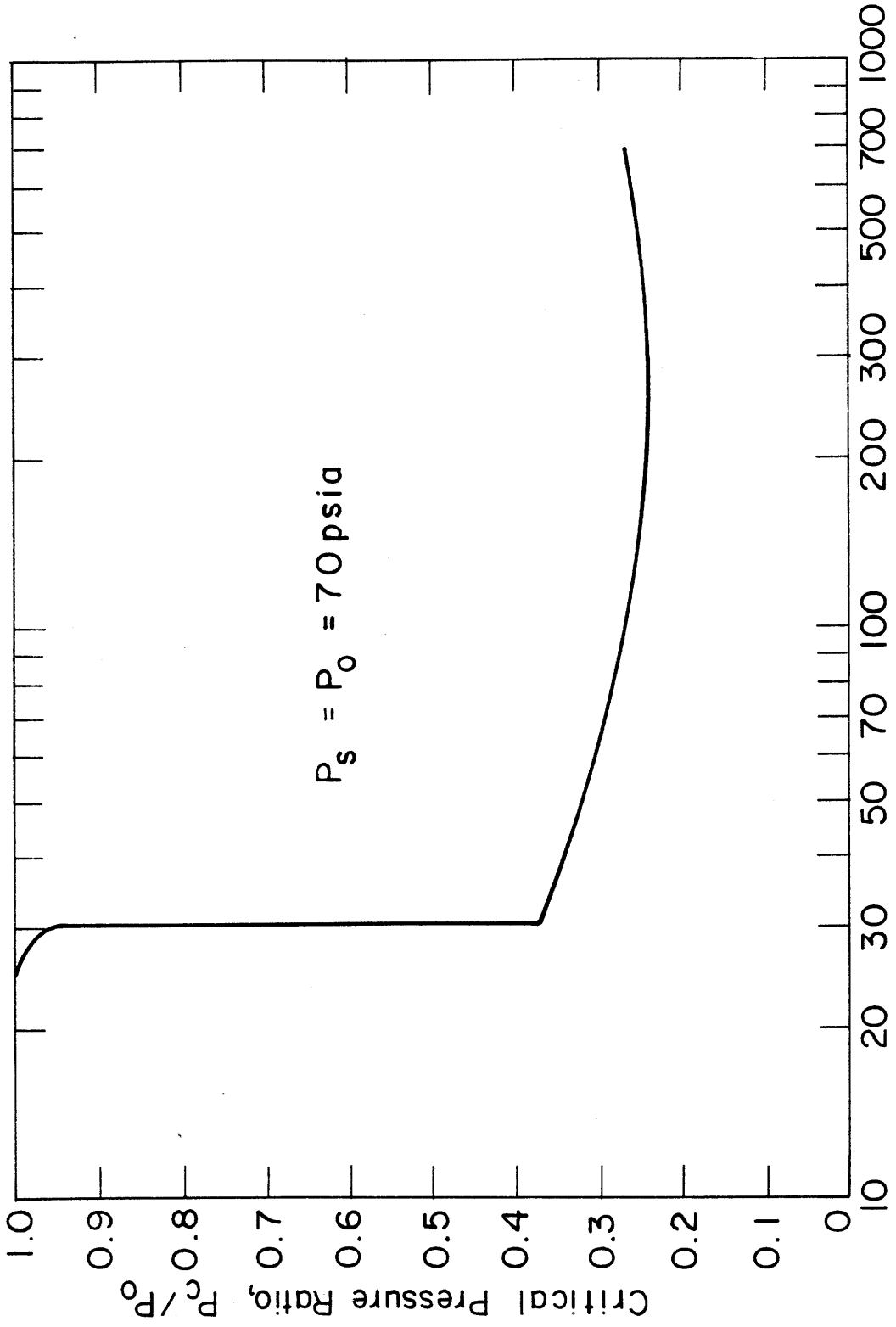

FIG. 11 VARIATION OF CRITICAL PRESSURE RATIO WITH LIQUID VELOCITY FOR STEAM-WATER TWO-PHASE FLOW

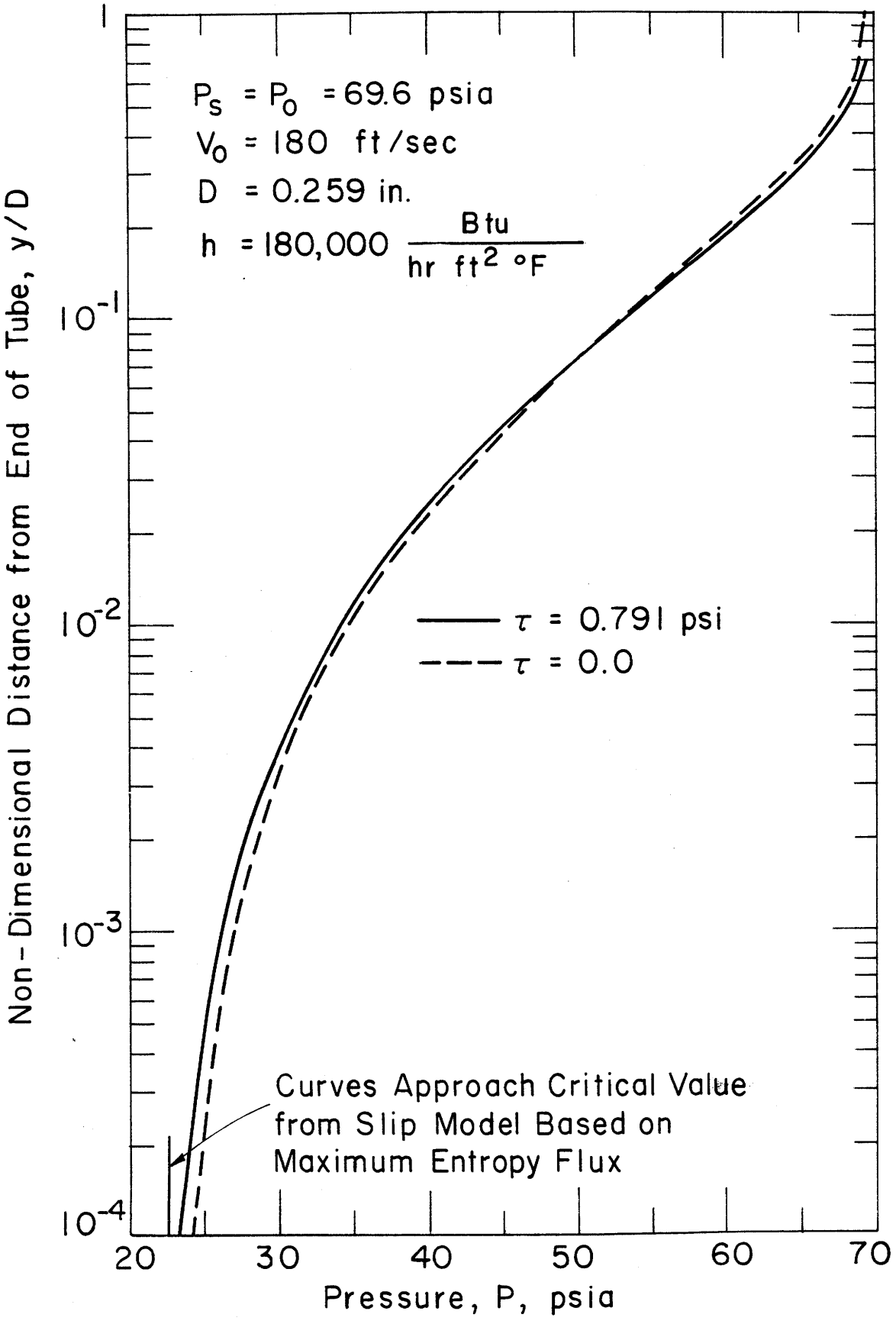

FIG. 12 NON-DIMENSIONAL DISTANCE VERSUS ABSOLUTE PRESSURE

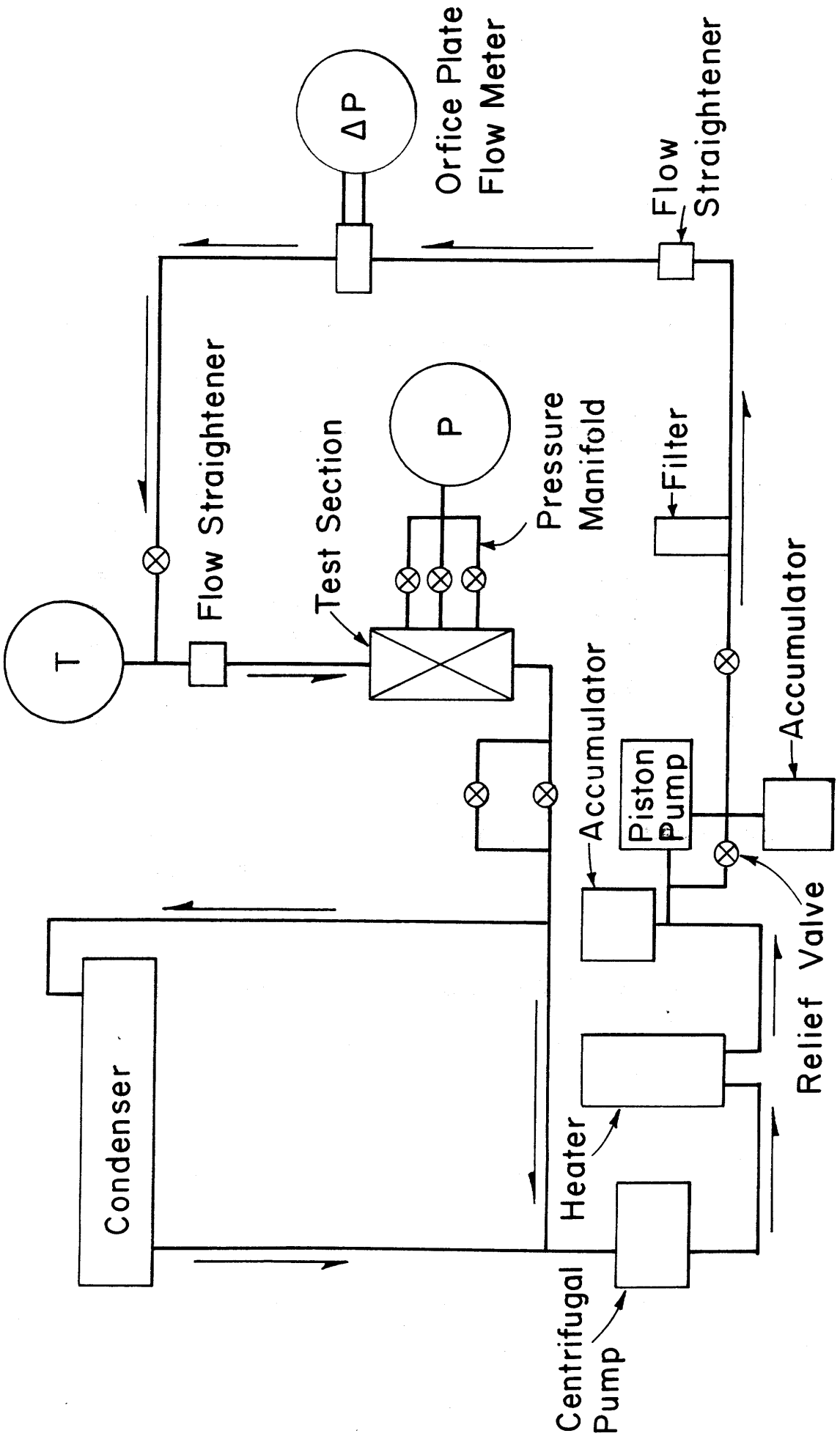

FIG. 13 TEST APPARATUS SCHEMATIC

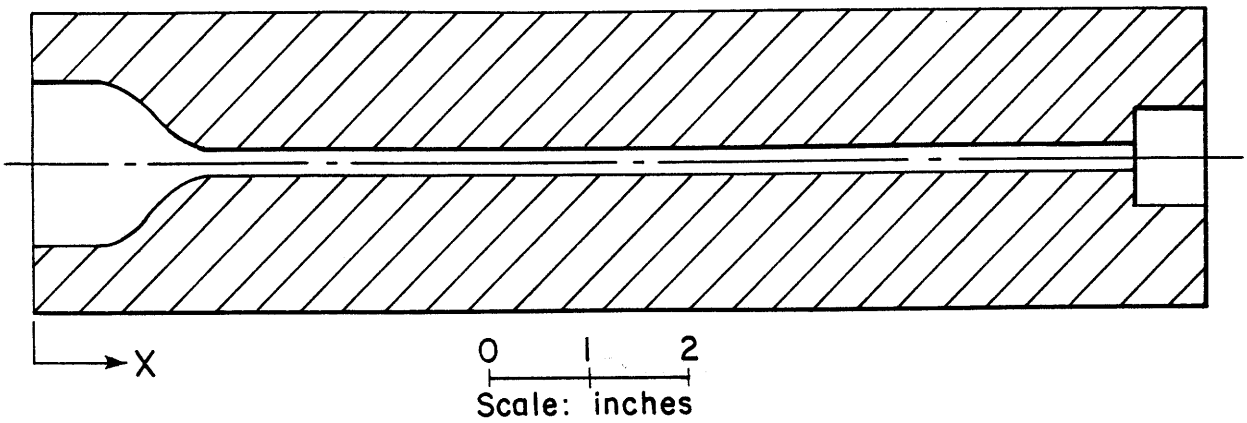

Position of Pressure Tap, x Inches

#1	0.625[a]	#9	10.500
#2	0.750	#10	10.625
#3	5.750[b]	#11	10.750
#4	5.750	#12	10.875
#5	5.750[b]	#13	11.000
#6	7.750	#14	11.125
#7	8.750	#15	11.281[c]
#8	9.750		

a Upstream of bellmouth

b All pressure tap holes are 0.020 inches in diameter except # 3 (0.0135) and # 5 (0.0292).

c Downstream of tube exit plane.

FIG. 14 STRAIGHT TUBE STAINLESS STEEL TEST SECTION

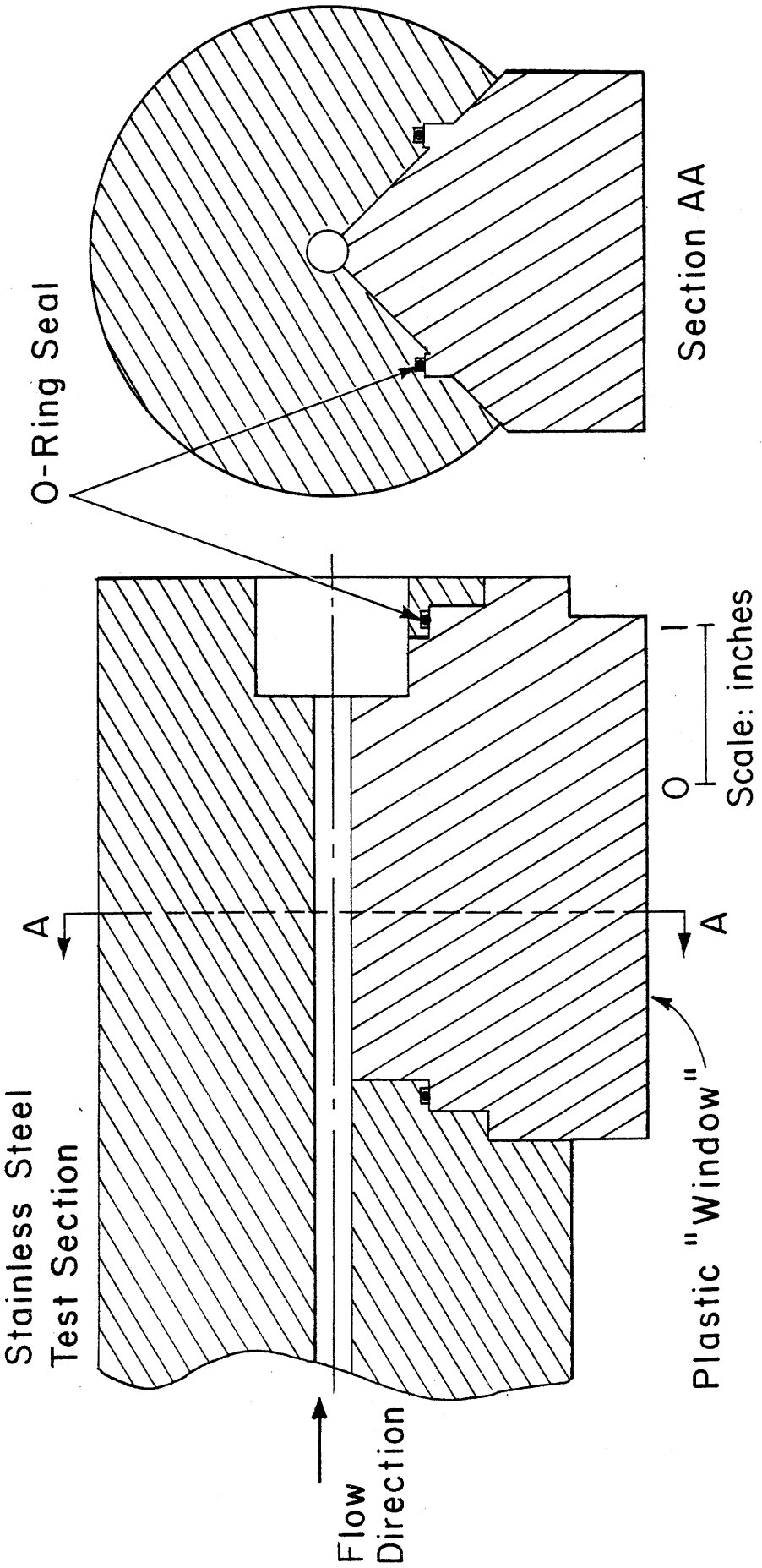

FIG. 15 DETAILS OF PLASTIC VIEWING SECTOR

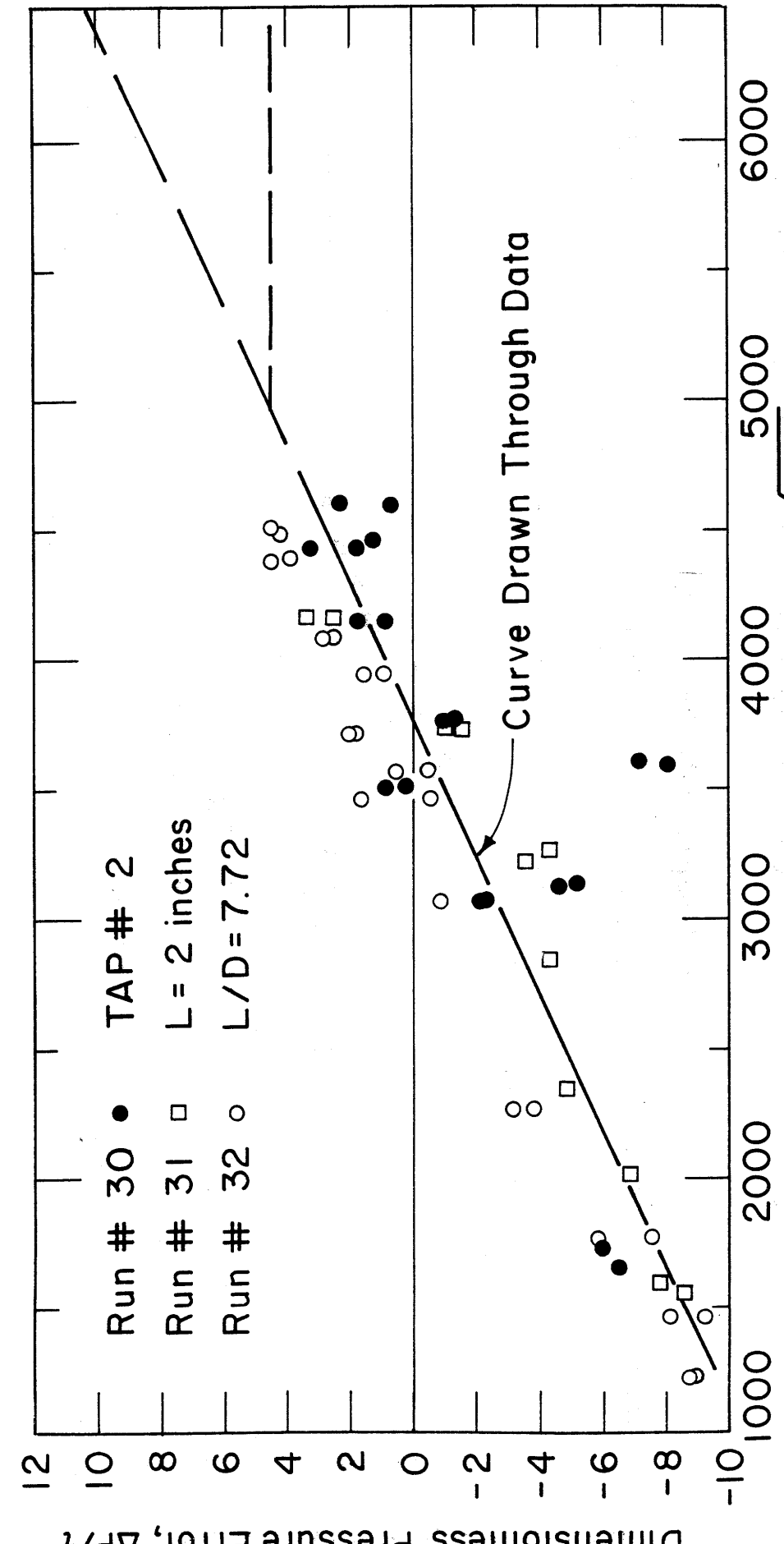

FIG. 16 PRESSURE TAP CALIBRATION USING FREE WATER JET

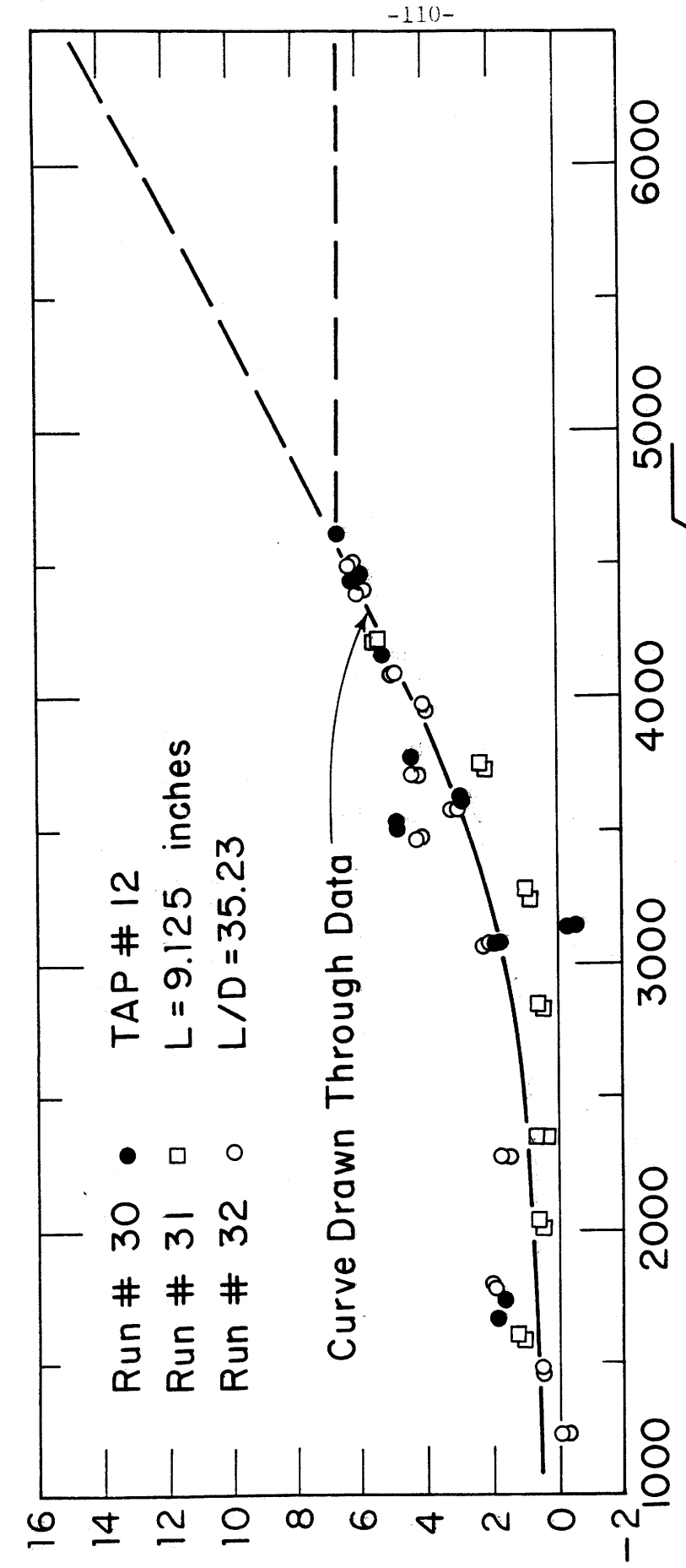

FIG. 17 PRESSURE TAP CALIBRATION USING FREE WATER JET

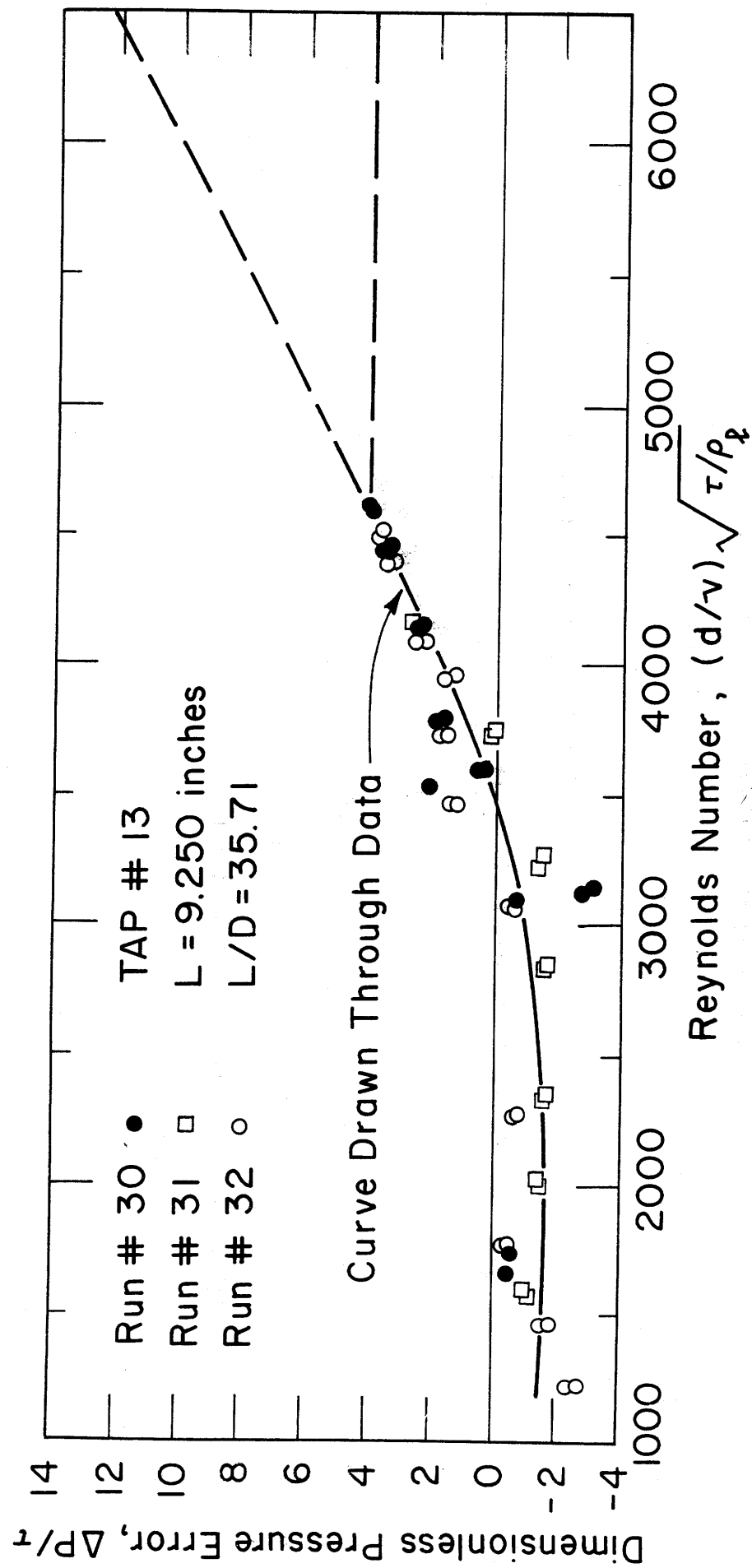

FIG. 18 PRESSURE TAP CALIBRATION USING FREE WATER JET

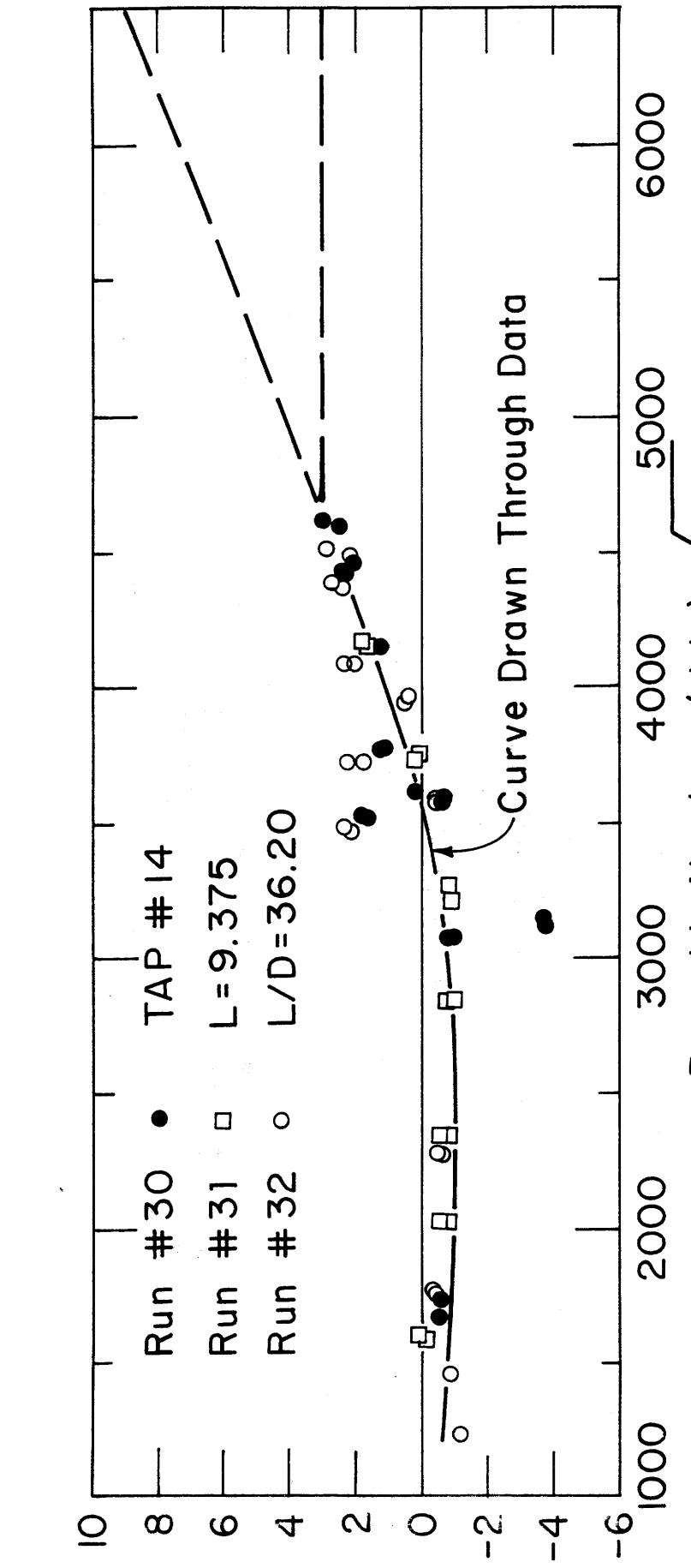

FIG. 19 PRESSURE TAP CALIBRATION USING FREE WATER JET

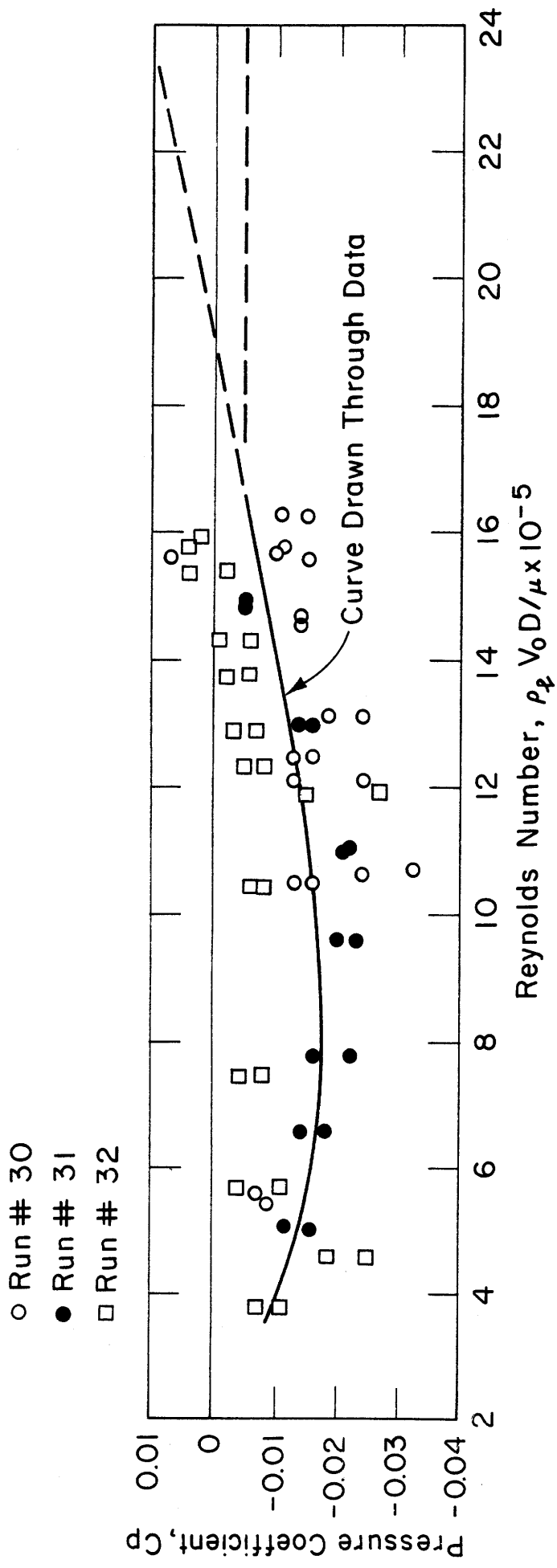

FIG. 20 PRESSURE COEFFICIENT VERSUS REYNOLDS NUMBER FOR TAP #1 FROM FREE WATER JET DATA

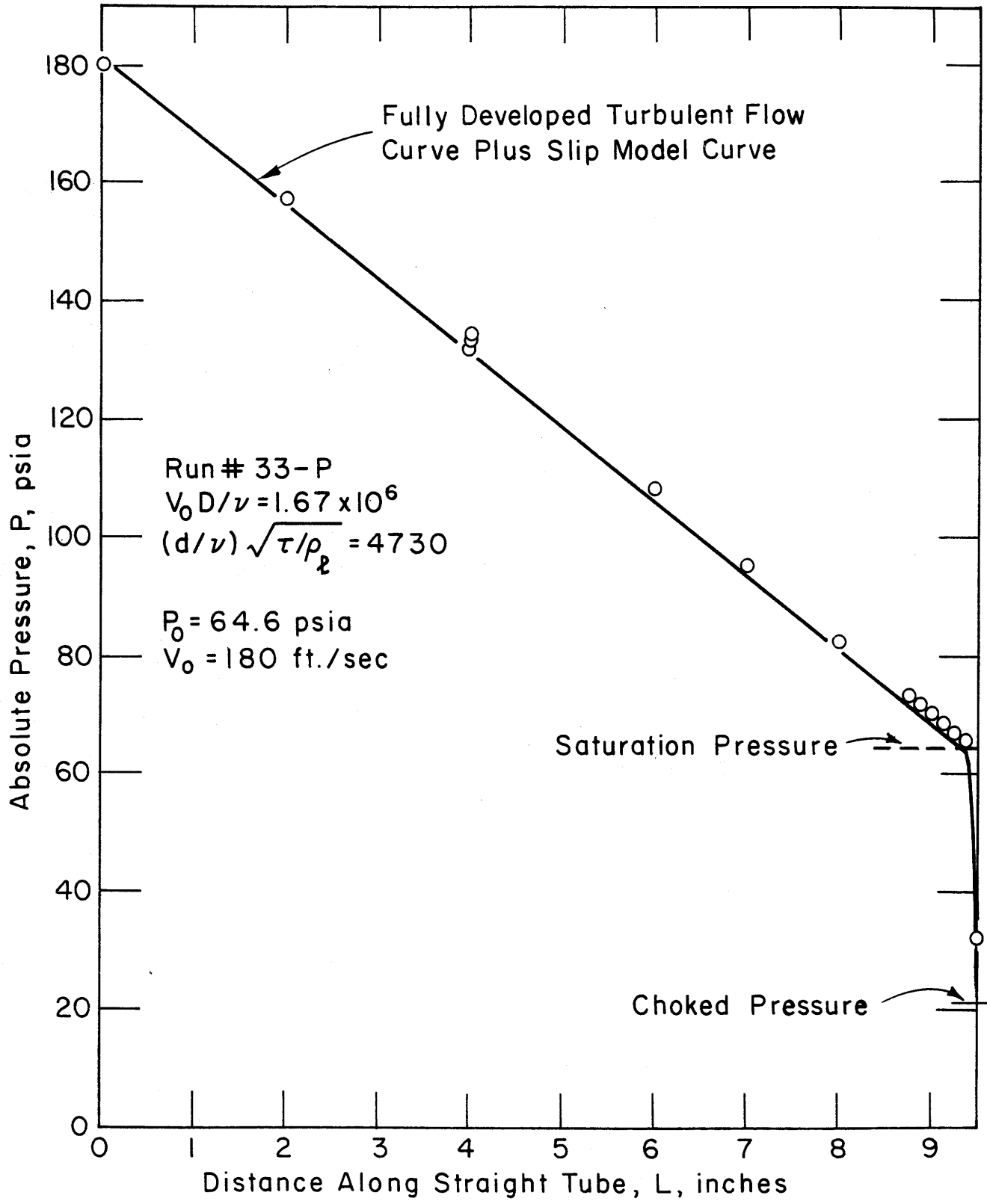

FIG. 21 PRESSURE VARIATION WITH LENGTH FOR FREON 114

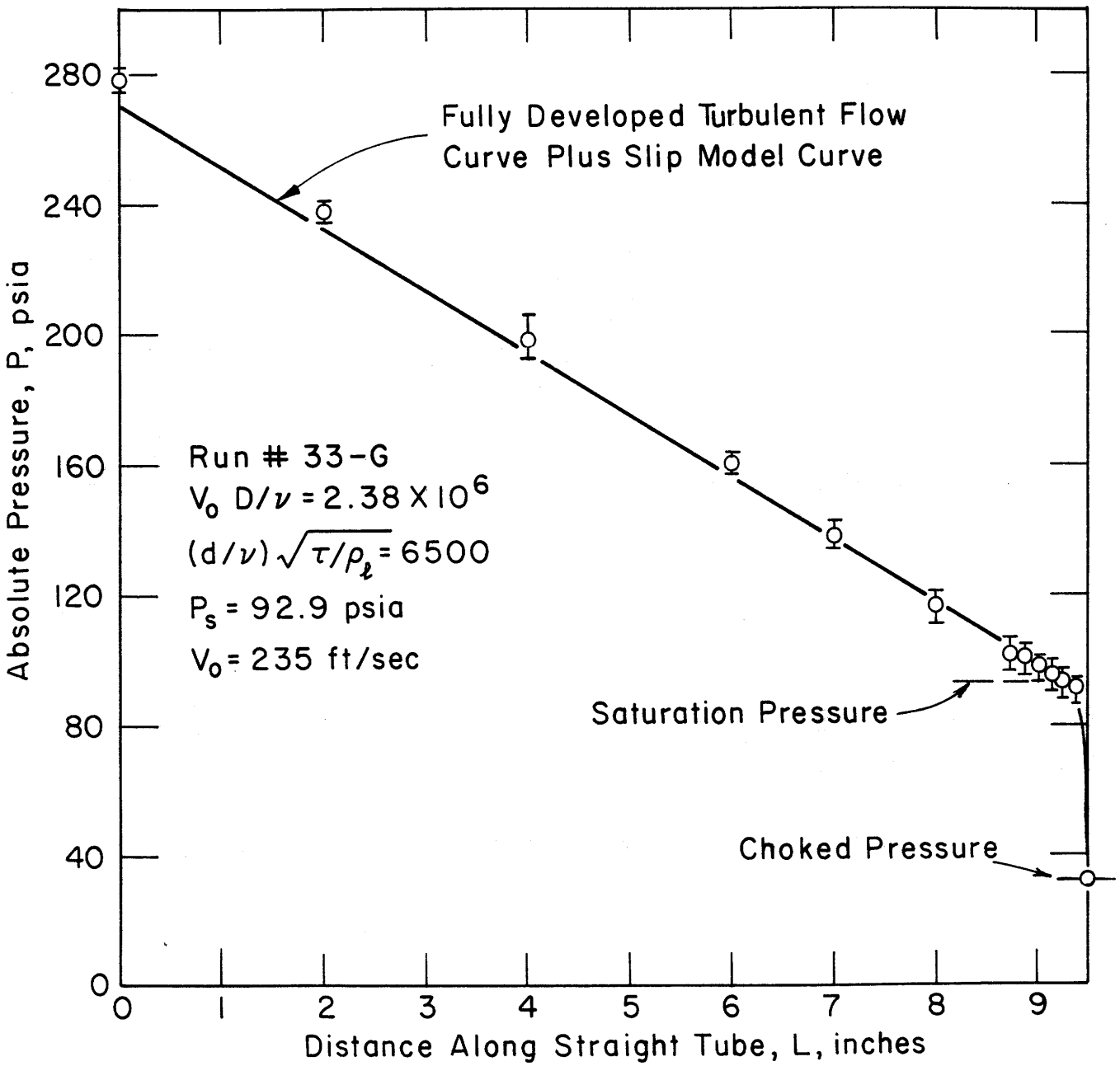

FIG. 22 PRESSURE VARIATION WITH LENGTH FOR FREON 114

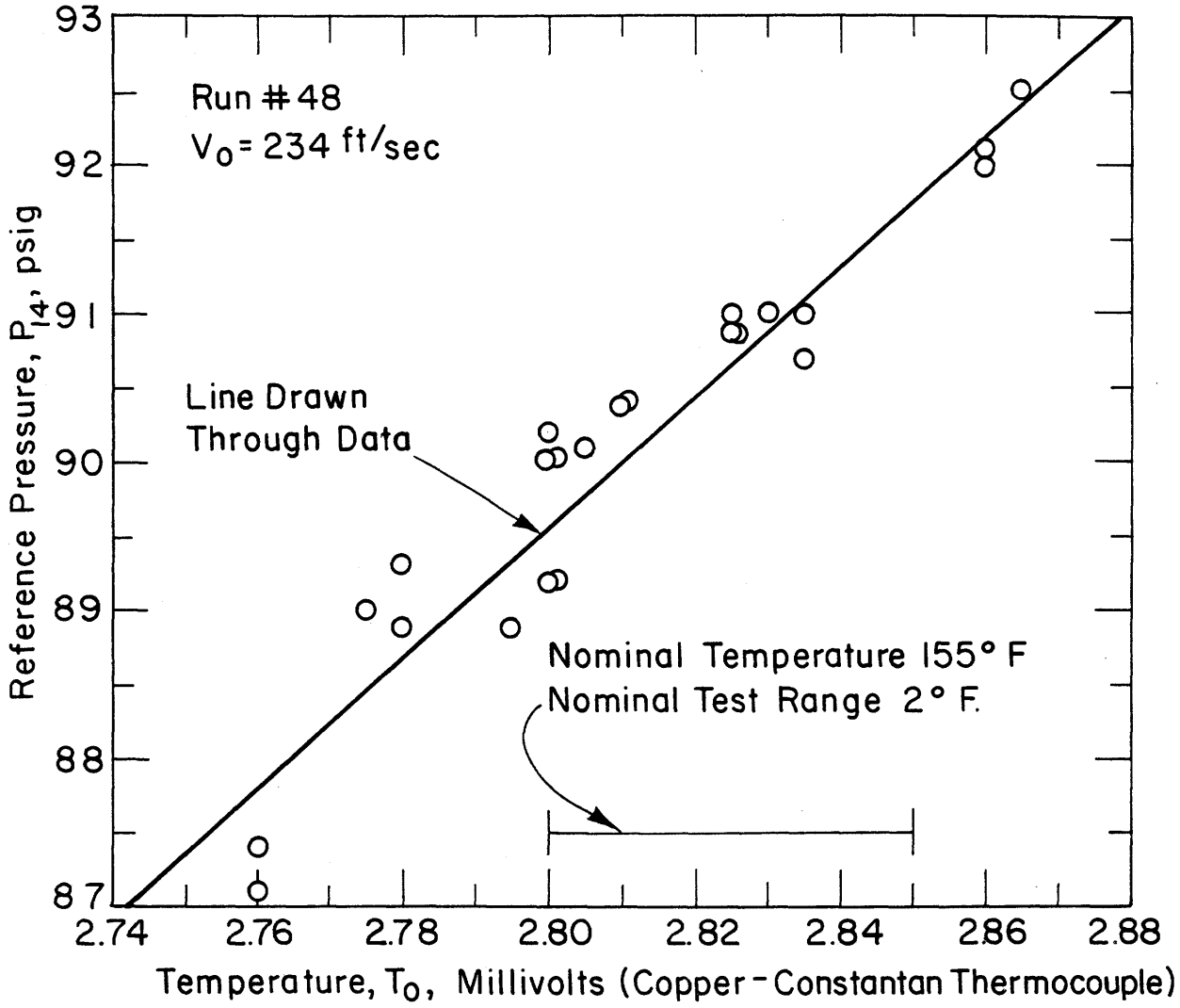

FIG. 23 VARIATION OF THE REFERENCE PRESSURE AT TAP # 14 WITH TEMPERATURE

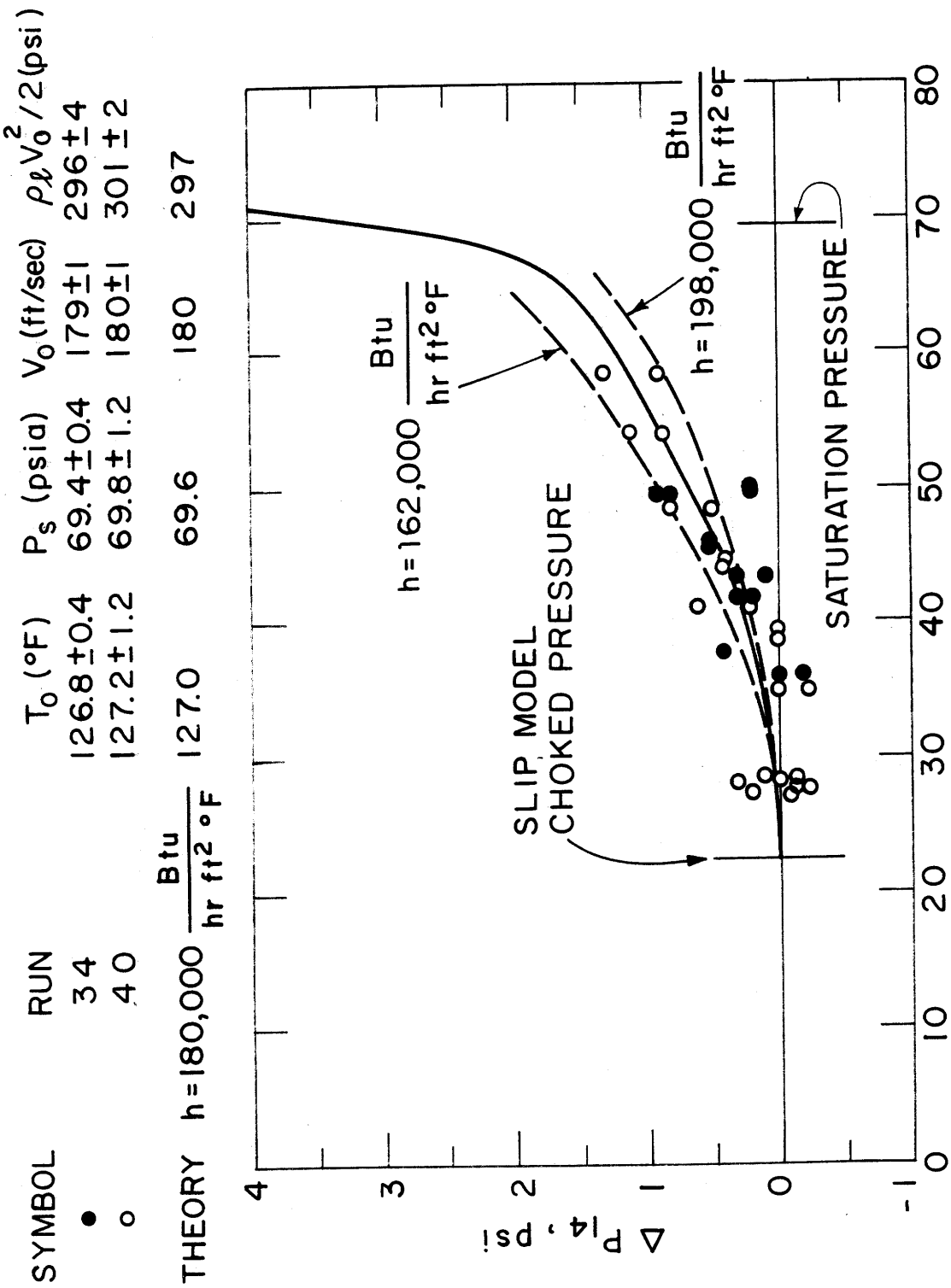

FIG. 24 VARIATION OF TEST SECTION PRESSURE FROM CHOKED VALUE

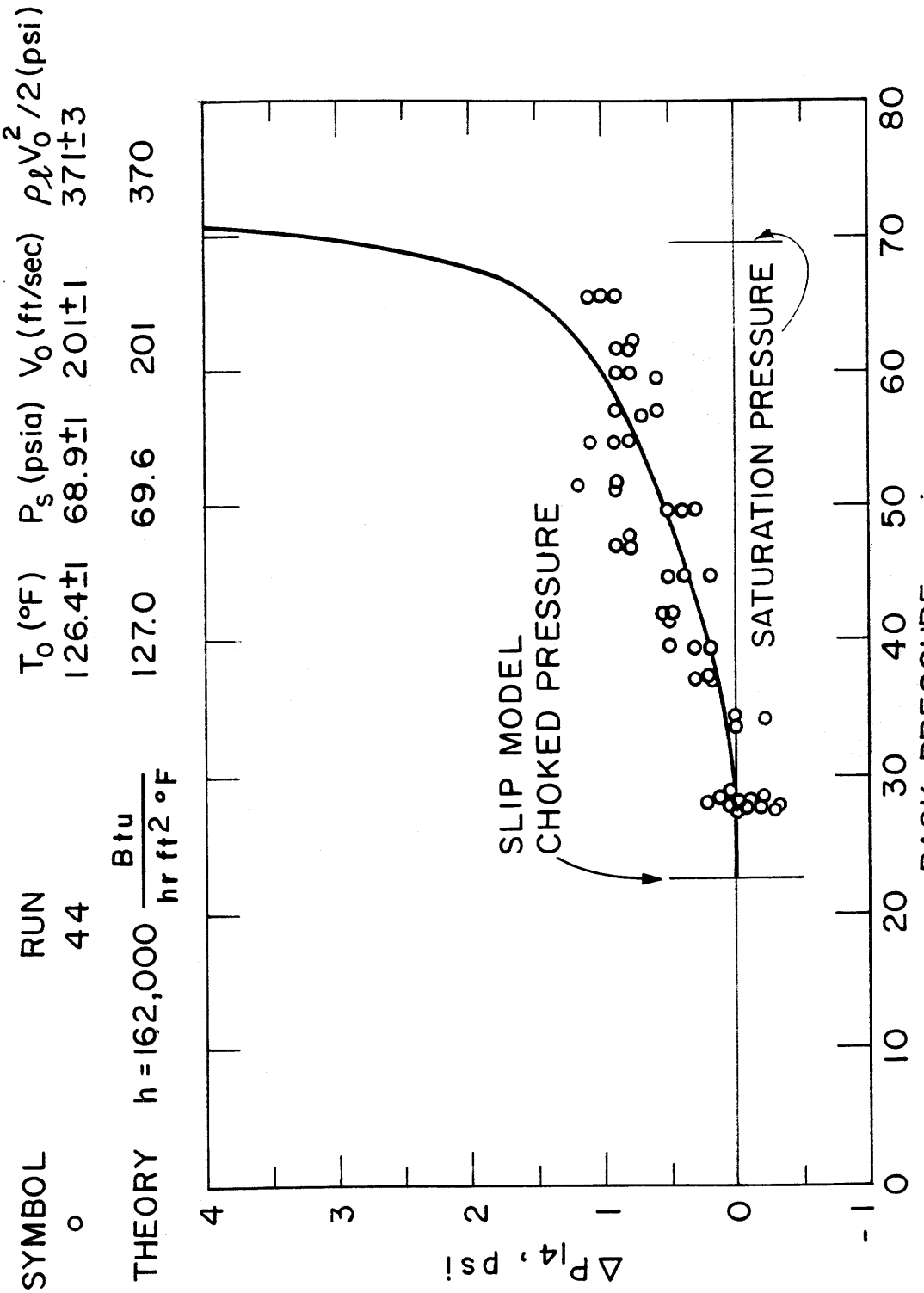

FIG. 25 VARIATION OF TEST SECTION PRESSURE FROM CHOKED VALUE

SYMBOL	RUN	T_0 (°F)	P_s (psia)	V_0 (ft/sec)	$\rho_\ell V_0^2/2$ (psi)
○	49 - A	126.8±1.0	69.4±1.0	234±1	504±5
●	50 - A	126.8±1.0	69.4±1.0	235±1	514±5
THEORY	$h = 126{,}000 \frac{Btu}{hr\ ft^2\ °F}$	127.0	69.6	234	503

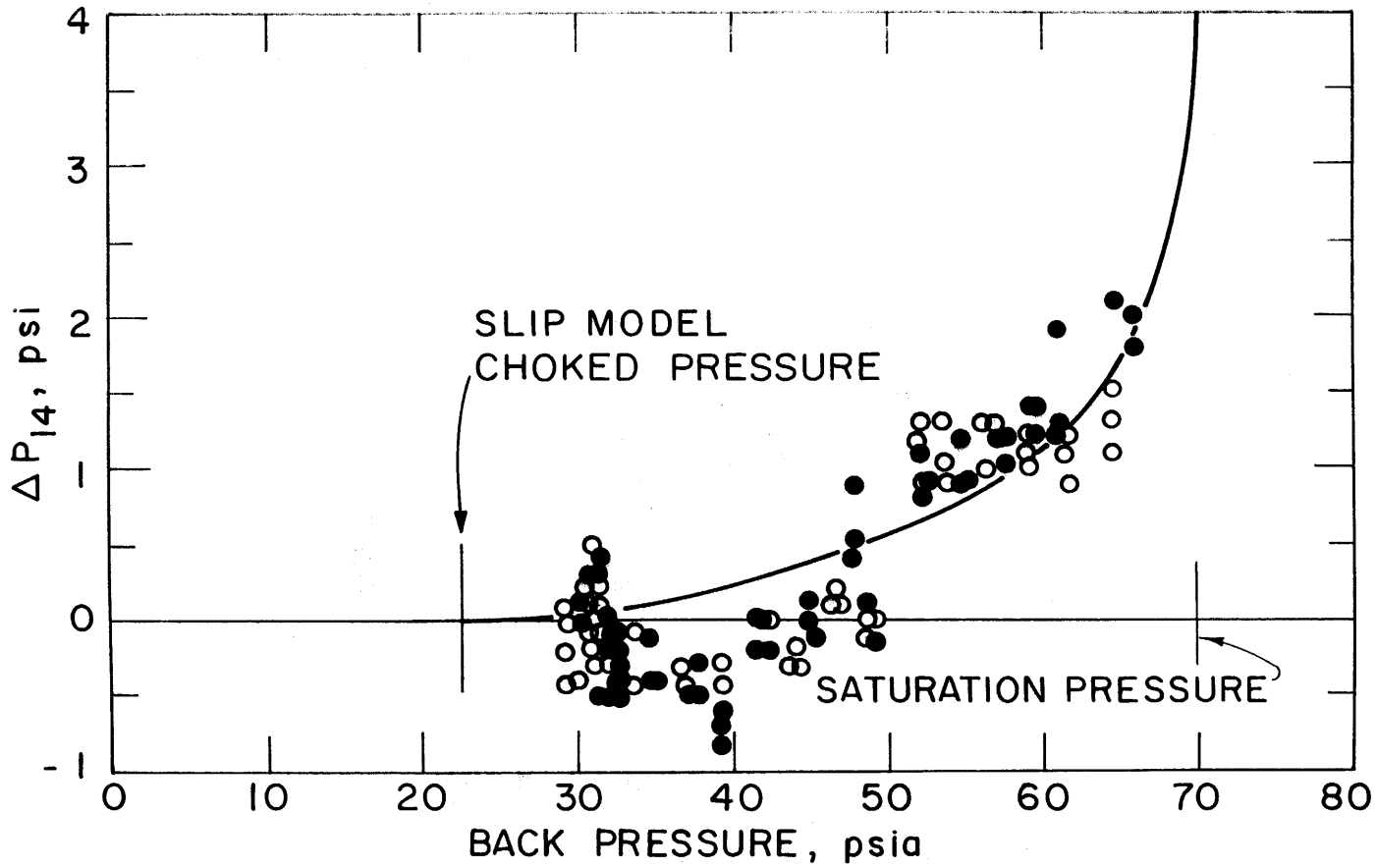

FIG. 26 VARIATION OF TEST SECTION PRESSURE FROM CHOKED VALUE

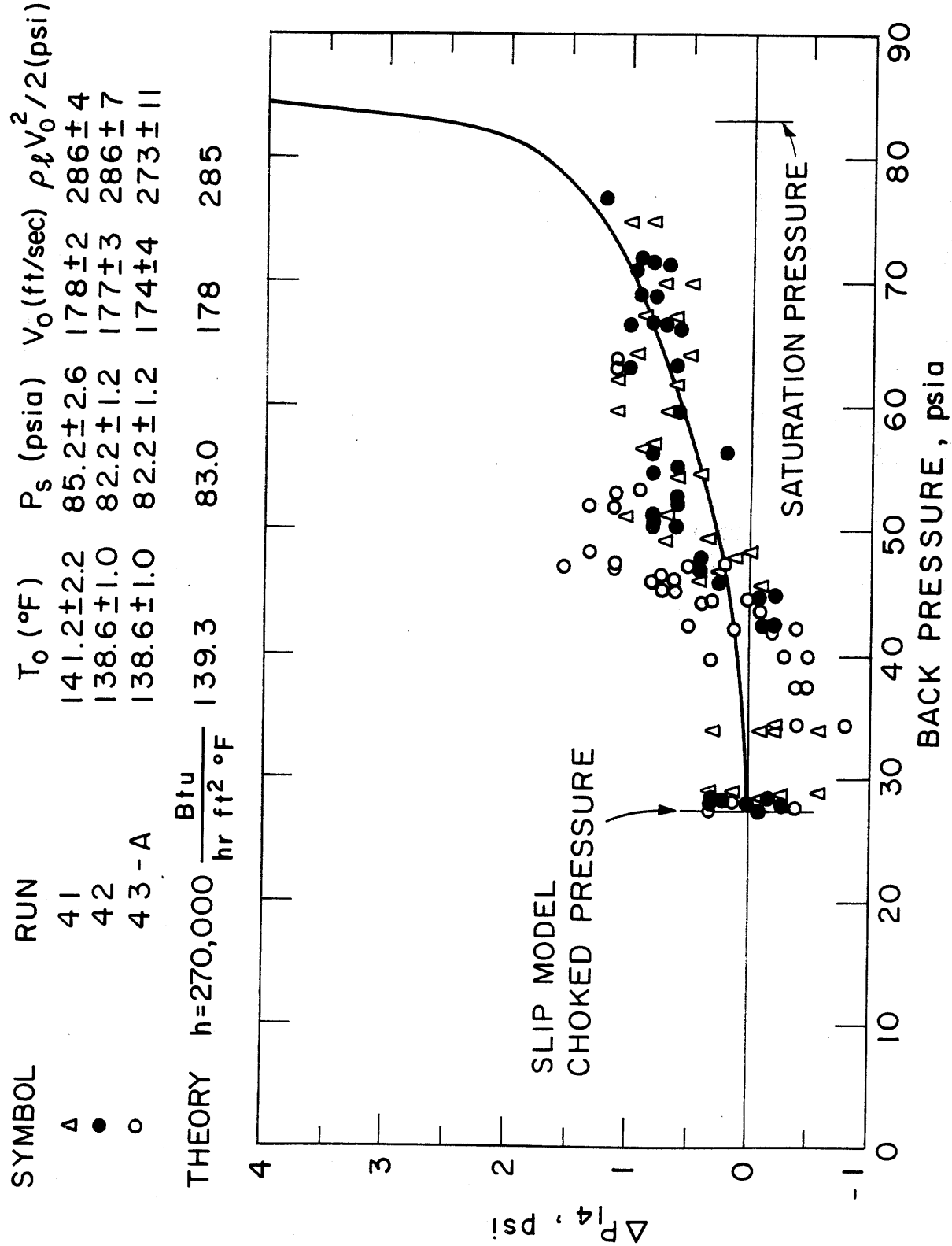

FIG. 27 VARIATION OF TEST SECTION PRESSURE FROM CHOKED VALUE

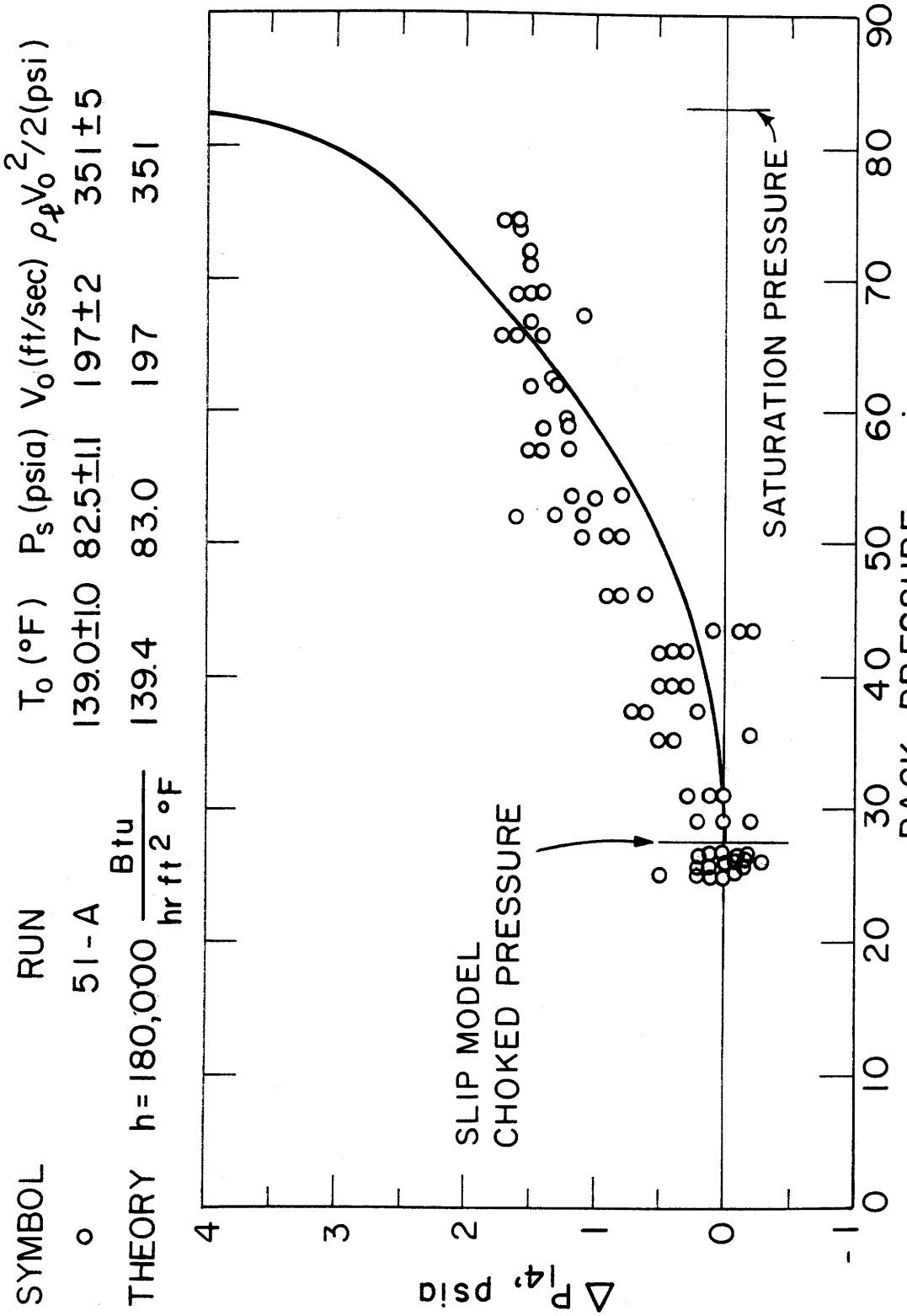

FIG. 28 VARIATION OF TEST SECTION PRESSURE FROM CHOKED VALUE

SYMBOL	RUN	T_0 (°F)	P_s (psia)	V_0 (ft/sec)	$\rho_\ell V_0^2/2$ (psi)
o	49-B	139.2±1.0	82.8±1.2	235±2	498±8
THEORY	$h = 144{,}000 \frac{Btu}{hr\ ft^2\ °F}$	139.4	83.0	235	498

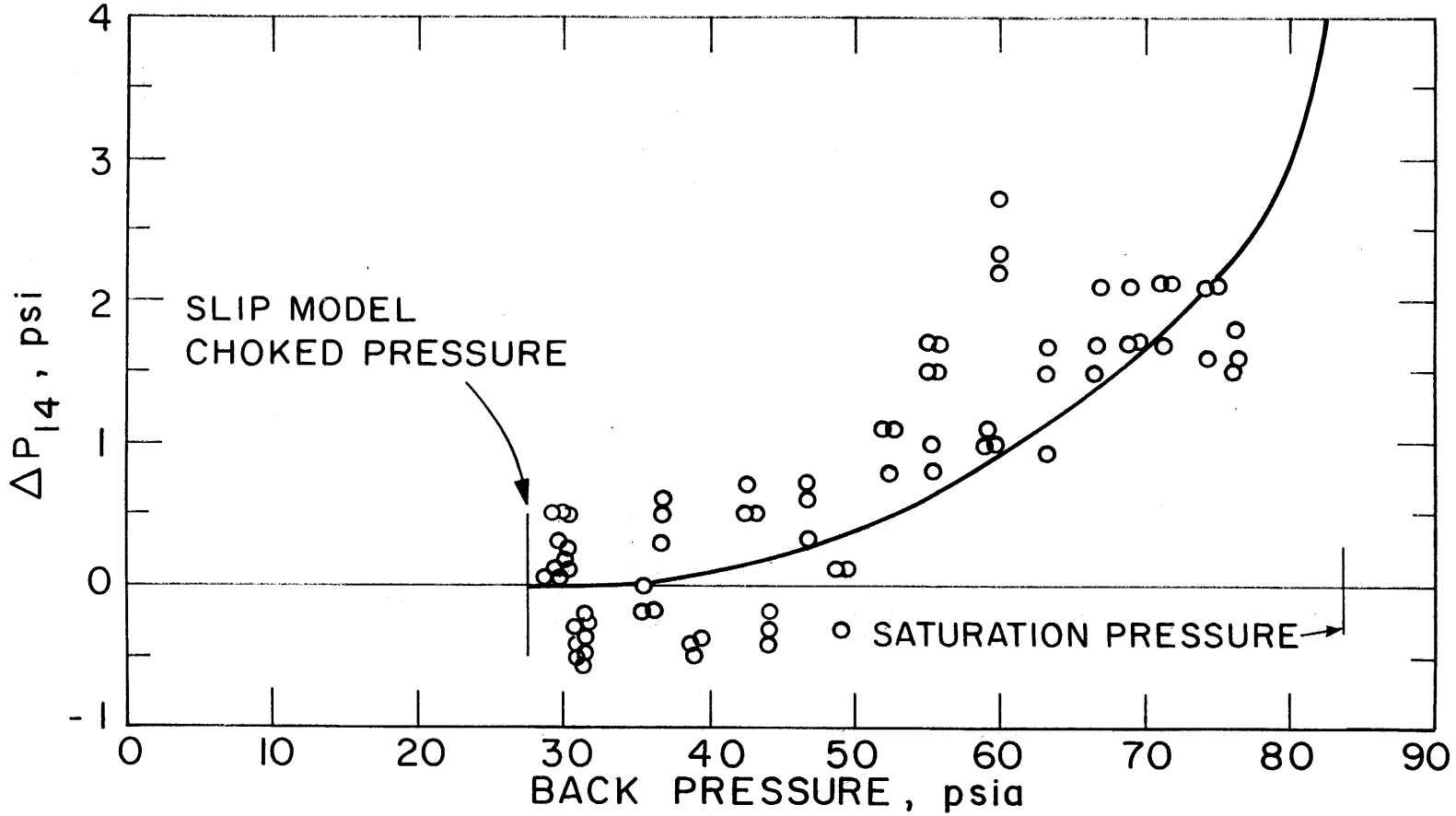

FIG. 29 VARIATION OF TEST SECTION PRESSURE FROM CHOKED VALUE

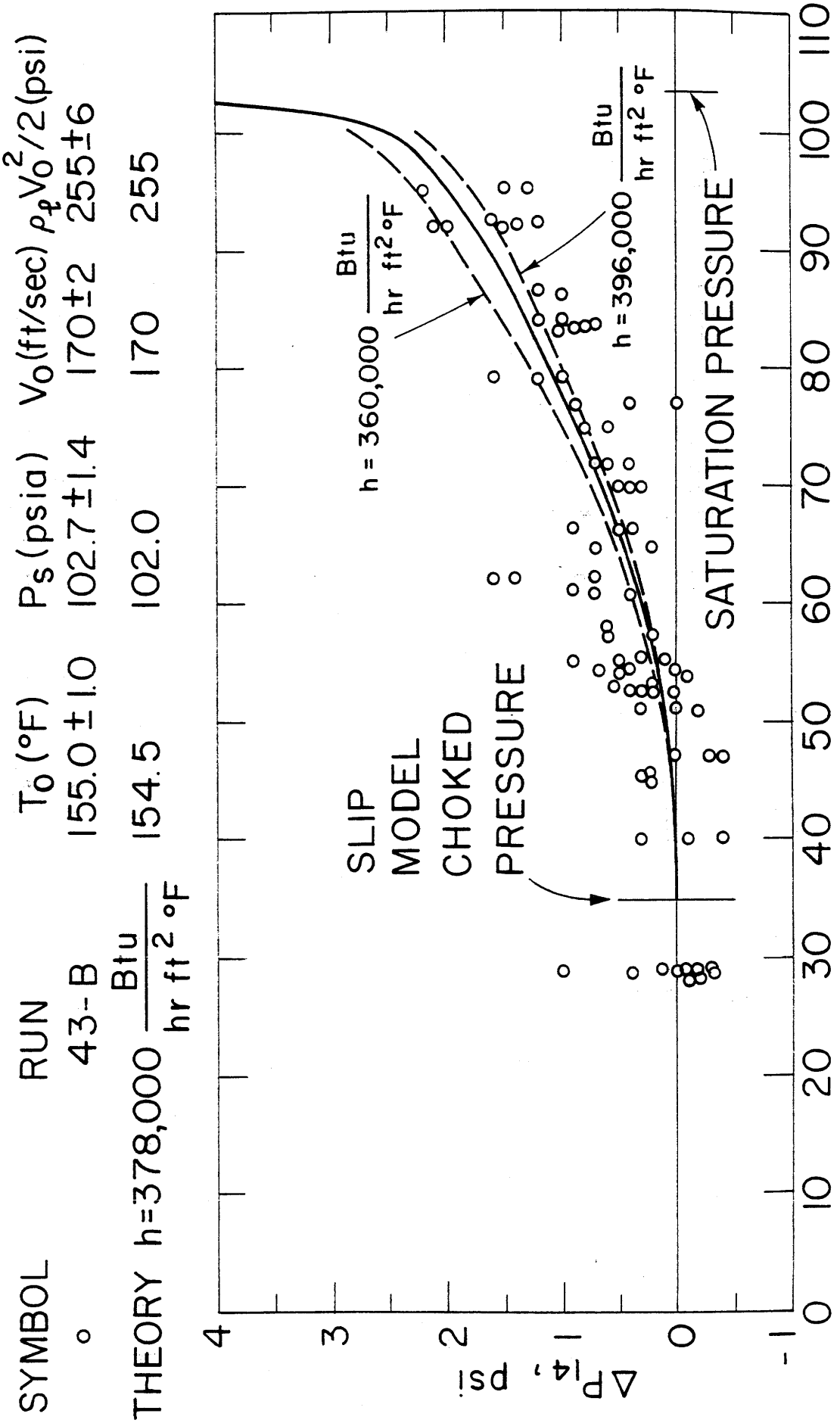

FIG. 30 VARIATION OF TEST SECTION PRESSURE FROM CHOKED VALUE

SYMBOL	RUN	T_0 (°F)	P_s (psia)	V_0 (ft/sec)	$\rho_\ell V_0^2/2$ (psi)
•	38	154.9 ± 1.6	102.6 ± 2.2	178 ± 1	280 ± 2
○	51-B	155.0 ± 1.0	102.7 ± 1.4	180 ± 1	287 ± 3
THEORY	$h = 306{,}000 \frac{\text{Btu}}{\text{hr ft}^2\,°\text{F}}$	154.5	102.0	179	283

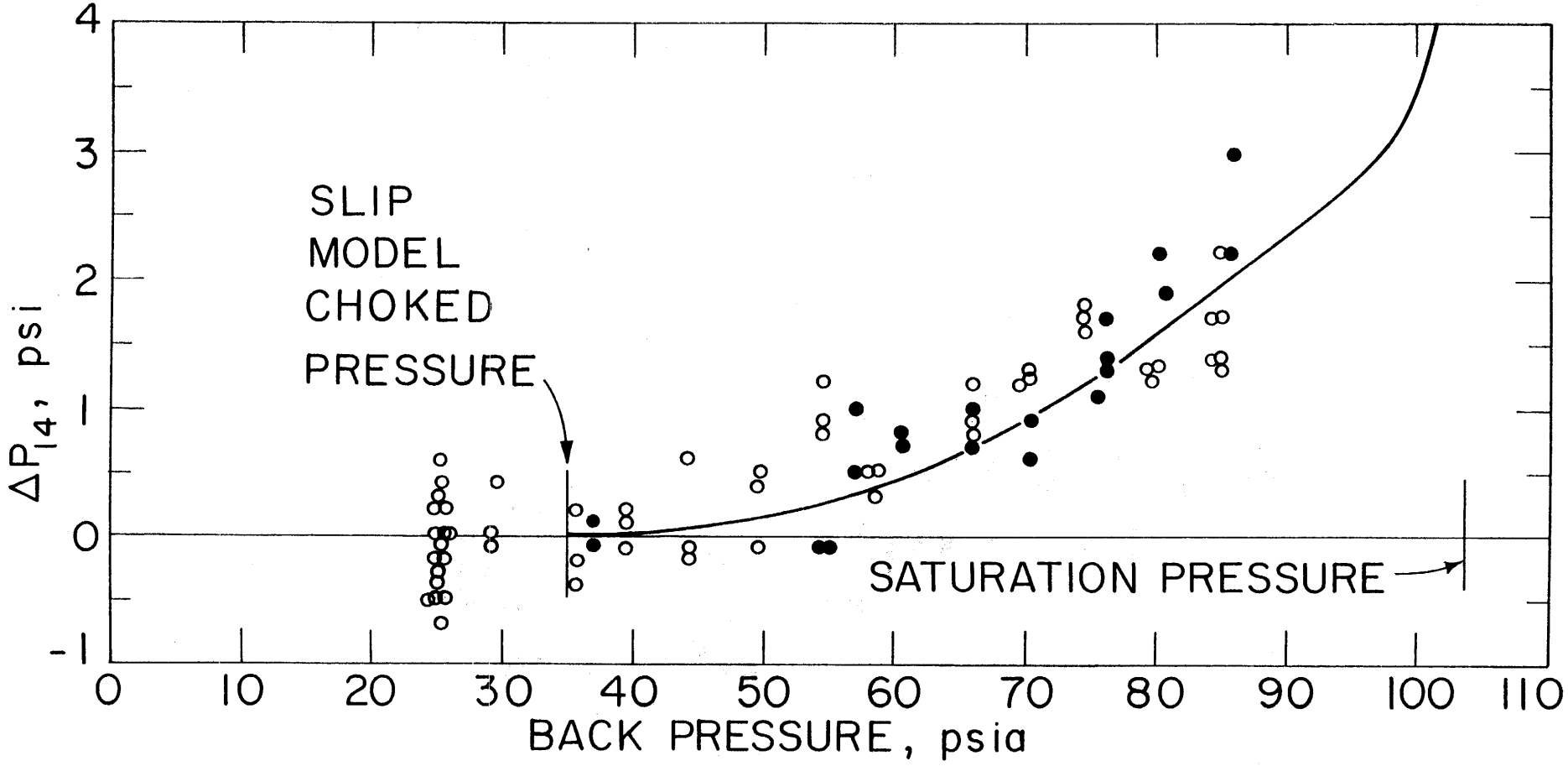

FIG. 31 VARIATION OF TEST SECTION PRESSURE FROM CHOKED VALUE

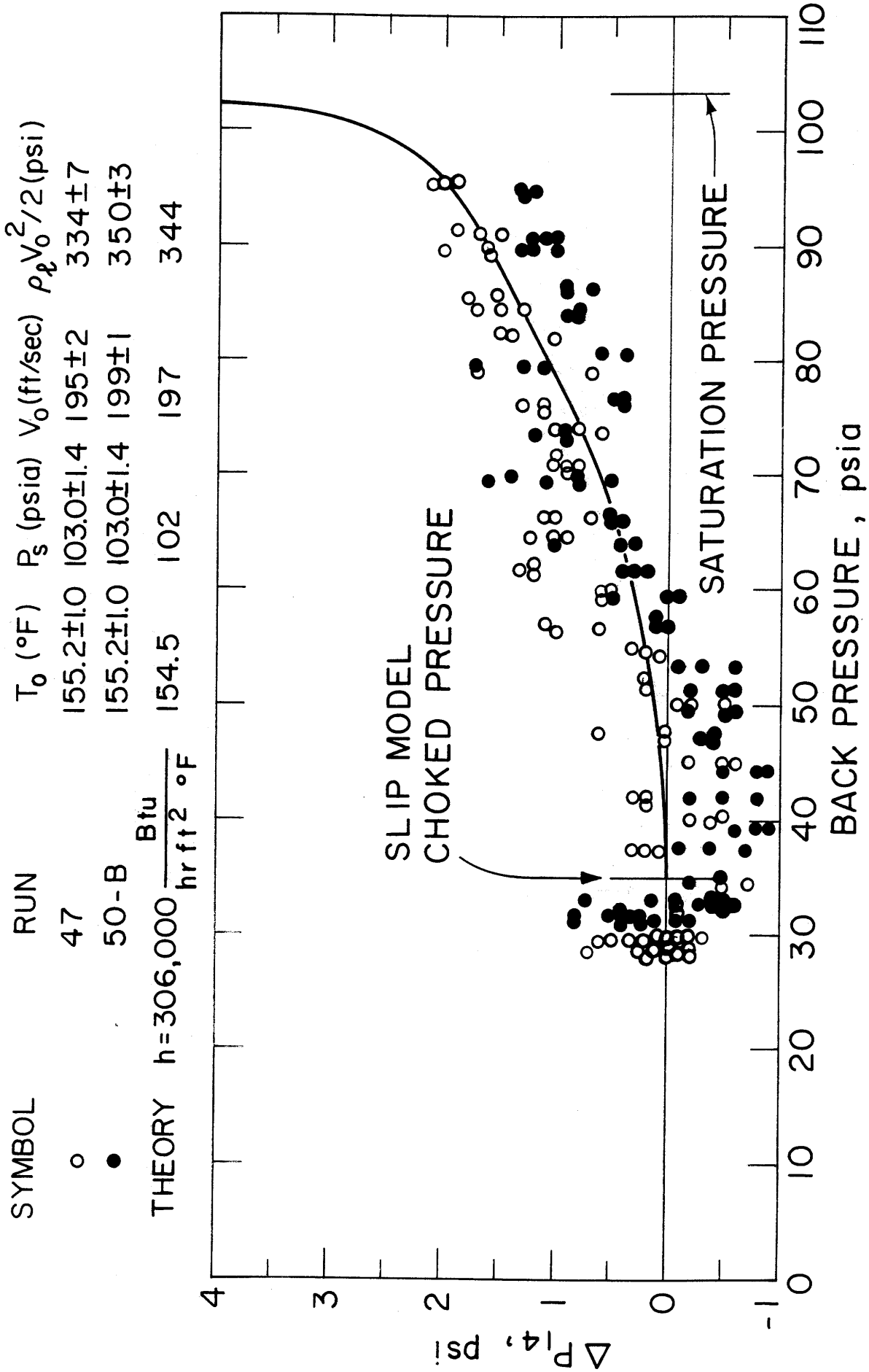

FIG. 32 VARIATION OF TEST SECTION PRESSURE FROM CHOKED VALUE

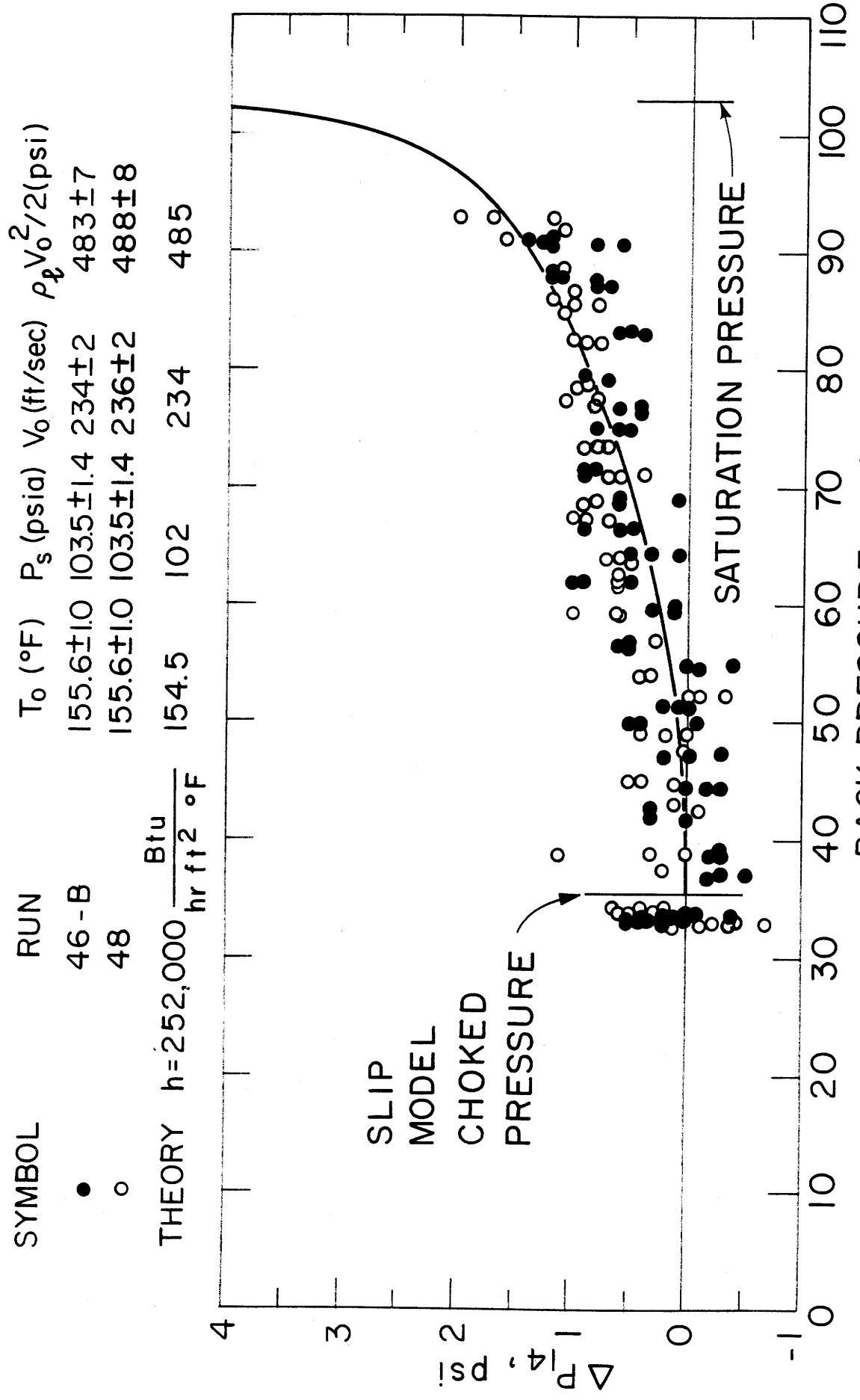

FIG. 33 VARIATION OF TEST SECTION PRESSURE FROM CHOKED VALUE

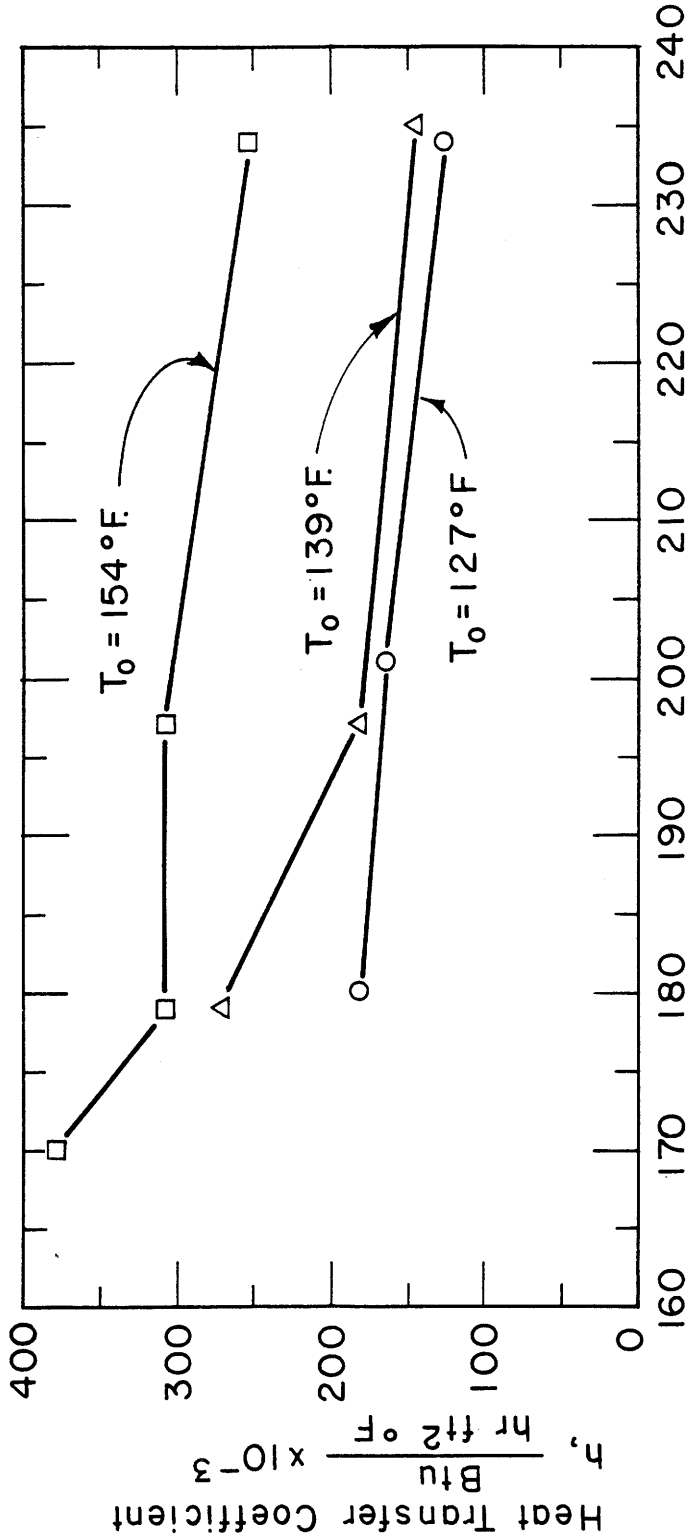

FIG. 34 VARIATION OF HEAT TRANSFER COEFFICIENT WITH VELOCITY AND TEMPERATURE